Region 2
UNIVERSITY TRANSPORTATION RESEARCH CENTER

Blast Load Effects on Highway Bridges

Prepared by
Anil K. Agrawal, Ph.D.
Department of Civil Engineering
The City College of New York

Zhihua Yi
Ph.D. Student
The City College of New York

April 2009

Disclaimer

The contents of this report reflect the views of the authors, who are responsible for the facts and the accuracy of the information presented herein. The contents do not necessarily reflect the official views or policies of the UTRC or the Federal Highway Administration. This report does not constitute a standard, specification or regulation. This document is disseminated under the sponsorship of the Department of Transportation, University Transportation Centers Program, in the interest of information exchange. The U.S. Government assumes no liability for the contents or use thereof.

TECHNICAL REPORT STANDARD TITLE PAGE

1. Report No.	2. Government Accession No.	3. Recipient's Catalog No.

4. Title and Subtitle	5. Report Date
High Precision Analysis of Blast Events on Highway Bridges	December 31, 2008.
	6. Performing Organization Code
7. Author(s)	8. Performing Organization Report No.
Anil K. Agrawal and Zhihua Yi, The City College of New York	
9. Performing Organization Name and Address	10. Work Unit No.
The City College of New York 160 Convent Avenue New York, NY 10031	11. Contract or Grant No. 49777-19-05
	13. Type of Report and Period Covered
12. Sponsoring Agency Name and Address	
University Transportation Research Center City College of New York New York, NY 10031	14. Sponsoring Agency Code

15. Supplementary Notes

16. Abstract

There has been increased awareness about safety of highway bridges from intentional/unintentional blast loads. This report focuses on the investigation of behavior of various bridge components during blast loads through a high fidelity finite element model of a typical highway bridge.

Computer programs, such as LS-DYNA offer detonation simulation capabilities to propagate blast loads through air medium. However, blast pressures generated by such programs are significantly different than those by ConWep, a computer program based on semi-empirical equations. In this report, we have presented a new approach to generate blast loads by ConWep and transmit it through air medium to structural components. In order to investigate effects of blast loads on bridge components, a very detailed finite element model of the bridge with approximately 1 million degrees of freedom has been developed. The bridge has been subjected to three levels of blast loads, designated as "Low", "Medium" and "Large". In order to investigate correlations between seismic detailing, concrete strength and blast load magnitude, the bridge model has been designed for three different seismic regions with concrete compressive strength varying from 3,000 to 10,000 psi. Based on simulation results, 14 damage mechanisms prominent during blast load effects on bridges have been identified and correlated with seismic damage mechanisms.

Simulation results show that seismic capacities and blast load effects are strongly correlated. Better seismic capacity directly implies better blast load resistance. However, several damage mechanisms are not present during seismic loadings and protection of bridge components from failure because of these mechanisms needs to be considered by improved detailing of components and optimization for multi-hazard seismic blast designs. We have also presented a framework for the performance based multi-hazard blast-seismic design approach. Different performance levels for bridge components subject to blast loads have been defined. Considering bridges designed for different seismic capacities, performance matrices have been developed to demonstrate the limitation of seismic detailing in dealing with blast loads. These performance matrices can be fully developed by considering different performance levels during multi-hazard seismic-blast loads in future research.

17. Key Words	18. Distribution Statement
Safety, Bridge, Blast, Seismic Capacity	

19. Security Classif (of this report)	20. Security Classif. (of this page)	21. No of Pages	22. Price
Unclassified	Unclassified		

Form DOT F 1700.7 (8-69)

UTRC Report: BLAST LOAD EFFECTS ON HIGHWAY BRIDGES

By

Anil K. Agrawal and Zhihua Yi

Department of Civil Engineering
The City College of New York
New York, NY 10031

University Transportation Research Center

Abstract

BLAST LOAD EFFECTS ON HIGHWAY BRIDGES

There has been increased awareness about safety of highway bridges from intentional/unintentional blast loads. This report focuses on the investigation of behavior of various bridge components during blast loads through a high fidelity finite element model of a typical highway bridge.

Computer programs, such as LS-DYNA offer detonation simulation capabilities to propagate blast loads through air medium. However, blast pressures generated by such programs are significantly different than those by ConWep, a computer program based on semi-empirical equations. In this report, we have presented a new approach to generate blast loads by ConWep and transmit it through air medium to structural components.

In order to investigate effects of blast loads on bridge components, a very detailed finite element model of the bridge with approximately 1 million degrees of freedom has been developed. The bridge has been subjected to three levels of blast loads, designated as “Low”, “Medium” and “Large”. In order to investigate correlations between seismic detailing, concrete strength and blast load magnitude, the bridge model has been designed for three different seismic regions with concrete compressive strength varying from 3,000 to 10,000 psi. Based on simulation results, 14 damage mechanisms prominent during blast load effects on bridges have been identified and correlated with seismic damage mechanisms.

Simulation results show that seismic capacities and blast load effects are strongly correlated. Better seismic capacity directly implies better blast load resistance. However, several damage mechanisms are not present during seismic loadings and protection of bridge components from failure because of these mechanisms needs to be considered by improved detailing of components and optimization for multi-hazard seismic blast designs.

We have also presented a framework for performance based multi-hazard blast-seismic design approach. Different performance levels for bridge components subject to blast loads have been defined. Considering bridges designed for different seismic capacities, performance matrices have been developed to demonstrate the limitation of seismic detailing in dealing with blast loads. These performance matrices can be fully developed by considering different performance levels during multi-hazard seismic-blast loads in future research.

ACKNOWLEDGEMENTS

The research presented in this report is partially sponsored by the Region 2 University Transportation Research Center at the City College of New York. The authors are very grateful for the support, participation feedback provided by Dr. Sreenivas Alampalli of the New York State Department of Transportation, Albany, New York and Dr. Mohammed Ettouney of Weidlinger Associates, New York. Research and opinion presented in this report are those of the authors and don't reflect opinion of the sponsoring agency.

TABLE OF CONTENTS

LIST OF FIGURES

LIST OF TABLES

CHAPTER 1. INTRODUCTION

1.1 BACKGROUND

The number and intensity of domestic and international terrorist activities, including the September 11, 2001 attack on World Trade Center towers in New York, have heightened our concerns towards the safety of our infrastructure systems. Terrorists attack targets where human casualties and economic consequences are likely to be substantial. Transportation infrastructures have been considered attractive targets because of their accessibility and potential impacts on human lives and economic activity. Duwadi from Federal Highway Administration (FHWA) realizes that bridge is vulnerable to physical, biological, chemical and radiological attack in addition to natural hazards and FHWA prepares for the next generation of bridges and tunnels that are redundant and resilient to withstand unforeseen events [Duwadi and Chase (2006); Duwadi and Lwin (2006)]. An Al Qaeda terrorist training manual captured in England contains goals that included missions for "gathering information about the enemy and blasting and destroying bridges leading into and out of cities."[TxDOT (2002)].

A Blue Ribbon Panel (BRP) consisting of bridge and tunnel experts from professional practice, academia, federal and state agencies, and toll authorities was convened in 2003 to examine bridge and tunnel security and to develop strategies and practices for deterring, disrupting, and mitigating potential attacks. The BRP, sponsored jointly by the Federal Highway Administration (FHWA) and the American Association of State Highway and Transportation Officials, acknowledged that the nation's bridges and tunnels are vulnerable to terrorist attacks. Among the 600,000 bridges in the United

States, preliminary studies indicate that there are approximately 1,000 where substantial casualties, economic disruption, and other societal ramifications would result from isolated attacks. The BRP believes that loss of a critical bridge or tunnel could exceed $10 billion [BRP (2003)]. Recent collapse of the I-35W bridge over the Mississippi in Minneapolis during rush hour on August 1, 2007 has clearly demonstrated the vulnerabilities in our highway bridge infrastructures, and its societal and economic impacts nationwide. Above observation shows that the highway system in our country may have serious vulnerabilities to blast damages that must be addressed urgently.

Bridges are very complex and varied systems. Decisions relating to blast threats (magnitude and location), affected bridge components by direct blasts, as well as existing redundancies of bridges can be daunting, even for the simplest of bridges. The Blue Ribbon Panel placed first priority on deterrence, denial and detection of blasts, second on defense with standoff and third on structural modifications through design and detailing. Highway bridges are readily accessible to vehicles that can carry explosives. Continuous monitoring of even critical bridges and inspection of vehicles approaching these bridges will require tremendous funds and other resources. Barrier standoffs may be effective in reducing the destructive effects of blast loads on bridge piers. The BRP has recommended minimum barrier standoffs for different vehicular threat types in terms of explosive weight (lbs TNT). However, for different reasons, it may not be possible to provide adequate standoff to protect bridge piers on busy highways. In such cases, strengthening of bridge components becomes the only viable protective option.

Loads imposed on highway bridge components during a blast loading event can exceed those for which bridge components are currently being designed. In some cases,

the loads can be in the opposite direction of the conventional design loads. Consequently, highway bridges designed using current design codes may suffer severe damages even from a relatively small sizes explosion. For example, Figure 1.1 shows a bridge in Iraq severely damaged by a relatively small amount of explosive placed by terrorists near piers of the bridge.

Figure 1.1 A bridge in Iraq damaged by a relatively small amount of explosives placed in a terrorist attack.

Although several guidelines to design blast resistant buildings exist, currently there is no guideline for the design of blast resistant design of highway bridges. In fact, there is very limited information available on widely acceptable analysis tools for analysis of blast effects on highway bridge components. Blast resistant design guidelines for highway bridges have been developed by U.S. Department of Army [USDOA (1969, 1990, 1992, 1998)], US Department of Defense [DOD (2003)], Defense Threat Reduction Agency [DTRA (1997)], U.S. General Services

Administration [GSA (2003), ISC (2001)], National Institute of Standards and Technology [NIST and USDOC (2006)], and American Society of Civil Engineer [ASCE (2005)]. Most of the research in the area of bridge safety has been focused on improving safety of highway bridges during extreme seismic events. The most significant research in the area of blast-resistant design guidelines for highway bridges is being conducted under the National Cooperative Highway Research Program (NCHRP) project number NCHRP 12-72. Outcome of this project is expected to present guidelines on improving blast resistance of highway bridge components. The objectives of research presented in this report are more focused on investigation of behavior of various bridge components during blast load events using high fidelity finite element model of a typical highway bridge in USA.

1.2 RESEARCH OBJECTIVES

The objectives of this report are to extensively investigate finite element tools for simulation of blast load effects on various bridge components, develop high-fidelity finite element model of a typical highway bridge in USA, investigate performance of different components during blast events, identify typical mechanisms responsible for causing damage/failure of typical components and develop seismic-blast correlations for multi-hazard design of bridge components.

Although experimental verification using scaled models is generally carried out in developing design guidelines for structures subject to hazards such as earthquakes, wind, etc., this is not practical in case of blast loads because of following three reasons.

i. It is very difficult to reproduce the same blast wave environment, even in the same

test field and using the same amount of explosive charge because of the temperature, humidity and dust condition of the air [Mays and Smith (1995)]. Consequently, it is very difficult to carry out systematic experimental study of different parameters affecting behavior of structures subject to blast loads, particularly of relatively complex structures.

ii. It is difficult to ensure reliability of sensors and data measurements, e.g., strain gauge, displacement sensors, etc., during explosion tests because of large deformation and fragmentation of the test structure. The sensors are likely to be destroyed during first few milliseconds of these types of experiments [Boyd (2000); John (2005)]. Most of the experimental data / results are inferred from videos or pictures obtained during the experiments.

iii. Experimental blast tests are also cost-prohibitive and can only be carried out at select facilities.

Because of reasons described above, analytical tools such as hydro-codes have significantly more reliability and accuracy in the simulation of blast load effects on structures. In this report, LS-DYNA, which is one of the most investigated and well-developed hydro-codes, is used for the simulation of blast load effects on highway bridges. In LS-DYNA, blast loads can be applied on the structure either by applying blast wave pressure load based on semi-experimental equations directly on structural surfaces or by simulating the detonation process of high explosive to automatically facilitate interaction between blast waves and the structure. In this report, these two methods will be investigated. However, in order to preserve the reliability of blast load simulations, blast loads generated by LS-DYNA must satisfy the following

requirements:

1. Blast loads simulated in LS-DYNA should be similar to those by experimental tests or standard semi-experimental data using ConWep program [USAE Engineer Research & Development Center (2005)]. Generally, blast loads vary drastically with standoff distance (distance of structure from the blast center) and are going to be significantly different on different components.

2. The times of arrival of blast waves at different components of the bridge should be similar to those by ConWep program so that the interaction between blast loads and structural components could be correlated with actual dynamic effects during a blast load event.

3. The blast load should be transferred to remaining portions of bridge components through surrounding air-structural interaction after a portion of bridge component is damaged because of spalling or rounding a barrier.

Once the explosive environment can be simulated correctly, we can apply the blast wave loads to selected structural systems by building its finite element model. In this report, our main objective has been to investigate blast load effects on a typical highway bridge in USA. Based on detailed review of national bridge inventory, we have selected a typical three-span reinforced concrete bridge located on a major highway. A detailed finite element model has been developed in LS-DYNA by considering very fine modeling of all structural components, including modeling of elastomers and steel plates in bridge bearings. In order to simulate blast load effects, a FEM mesh of air layer has also been built and the bridge model has been immersed in the air layer. Overall, the

bridge finite element model has over 1 million degrees of freedom. Specific attention has been paid on the following simulation issues during the finite element modeling: (i) finite element type for a particular bridge member/component, (ii) influence of mesh topology and mesh size (iii) influence of time step size control in the whole simulation, and, (iv) application and effects of gravity load and (v) simulation stability and reliability issues, such as hourglass numerical stability problem and contact problem.

Blast load effects on the bridge can be quantified in terms of failure mechanisms of different bridge components through simulation of the whole bridge system in LS-DYNA. Through extensive numerical simulation of the finite element model of the bridge, we have identified all possible damage mechanisms and their extent of severity in terms of bridge safety. By the knowledge of these mechanisms, an engineer can design a particular component to resist formation of mechanisms that have been observed to form in that member. Quantitative displacement and stress time history information obtained from finite element simulations can be used to develop more understand effects parametric study by varying bridge pier sizes and unconfined concrete strength. Utilizing seismic design guidelines for bridges, we have also investigated correlations between seismic ductility and blast load effects.

Multi-hazard seismic-blast ductility and strength correlations have been investigated by designing three hypothetical bridges with different levels of seismic resistance and subjected to varying levels of blast loads. Comparison of results clearly demonstrates that bridge components with higher seismic resistance can withstand higher levels of blast loads. However, several failure mechanisms that are present in blast load effects are not present in bridges subject to seismic loads. This observation

can be used as a fundamental aspect in developing multi-hazard design guidelines for highway bridges.

Although this report addresses high-fidelity simulation of blast load effects on bridge components and identifies important failure modes, there is need for continued and extensive research in the subject area. Some of the important issues that need to be addresses through future research efforts are (i) reliability of material behavior models, (ii) optimum size of finite element mesh for different components, (iii) simplified model for bridge components and (iv) fragility of bridge components to blast load effects. Investigation of above issues requires calibration of finite element model and material models using blast test data. In this report, the issue of simplified design model has been addressed by proposing a simplified pier-bent model that can simulate blast load effects similar to that of the whole bridge model. Further development and detailed verification of this simplified model is needed in future research. Development of this simplified model will enable engineers to study performance of different detailing / retrofit options using relatively lesser computation efforts.

1.3 OUTLINES OF THE REPORT

This report presents research work carried out towards objectives mentioned above. The entire report consists of seven chapters. Each of these chapters deals with separate but inherently integrated tasks. The outline of this report is as follows:

Chapter 1, which is this chapter, presents the problem statement and the objectives of this research.

Chapter 2 presents a detailed literature review on blast load effects. The

state-of-the-art and the state-of-the-practice on the blast analysis, design and practice in civil engineering are reviewed critically. Recent progress on multi-hazard research has also been presented.

Chapter 3 investigates the characteristics of blast loads and approaches for the simulation of blast loads. Traditionally, blast loads are either applied directly on structural surfaces or are generated by detonation simulation. Both these approaches have limitations. We have proposed a new approach of blast load simulation that can overcome shortcomings of traditional methods. Blast wave loads generated by the proposed method can satisfy requirements for the simulation of blast load effects on Highway Bridges.

Chapter 4 describes hypothetic target bridge and the development of finite element model. This chapter discuss in detail material properties and constitutive equations for different materials, the finite element modeling of the whole bridge and modeling issues such as application of gravity loads, hourglass numerical stability problem and contact problems. A comprehensive study of elastomeric bridge bearings, including literature review, bearing performance under static and blast loads, is also carried out.

Chapter 5 presents on identification of finite element model parameters, such as simulation time step size and mesh size, based on selected experimental data on blast tests on beams and columns available in the literature.

Chapter 6 presents results of the whole bridge blast load simulation. Three bridges with increasing levels of seismic resistance are designed and are subjected to

different levels of blast loads. Failure mechanisms during different blast load levels are identified and are populated into multi-hazard (seismic and blast threats) bridge matrices. Preliminary development of performance-based blast resistant design guidelines are also developed.

Chapter 7 presents conclusions of the research and recommendations on future research in the subject area.

CHAPTER 2. LITERATURE REVIEW ON BLAST LOAD EFFECTS

2.1 INTRODUCTION

This chapter presents a detailed review of the state-of-the-art on blast effects, mitigation and protective design technologies, blast simulation using hydro-codes and current state-of-the-art on blast-resistant bridge design.

Section 2.1 of this chapter discusses the historical development of the existing knowledge base on blast loads, the nature of explosions, and the induced physical behavior of materials. Section 2.2 presents a critical review of "progressive collapse" phenomenon, which causes global failure of a structural system because of some localized damages. Section 2.3 discusses various design codes applicable to blast-resistant design of structures. In Section 2.4, a detailed review of various methodologies to analyze blast load effects on structures is presented. Although a majority of design guidelines are based on semi-empirical relationships, much of the existing knowledge on blast environments and the effects of high-intensity, short-duration loadings on the behavior of structures, systems, and components is embodied in sophisticated "first-principle" computer programs, such as LS-DYNA. Section 2.5 presents a detailed review of current research on simulation of blast load effects on structures using LS-DYNA. Finally, Section 2.6 presents a critical literature view on blast load effects on highway bridges and their components.

2.1 Historical Background on Blast Loads

Explosive devices have been used for hundreds of years, yet comprehensive treatment of blast-effects and their mitigation appeared in the Western Hemisphere only

during and after World War II. Following the war, the Office of Scientific Research and Development [NDRC (1946)] produced the seminal, unclassified document on weapons and penetration capabilities. This report remains of value even today. While the document is difficult to locate, some of the information it contains has been republished [Bangash (1993)]. Of special interest in the latter publication is information that permits estimates on the penetration resistance of structural elements of various materials by projectiles of many forms.

World War II was the first international conflict that resulted in massive destruction of cities, mostly with high powered explosives, which also inflicted enormous casualties. In the latter stages of the war, the use of two nuclear weapons demonstrated the destructive capability of such weapons [Glasstone and Dolan (1977)].

In the United States, a comprehensive research program during the past half century was undertaken to increase the blast resistance of military structures such as weapons storage facilities and command, control, and communication facilities. Much of this research was in response to deployment of ballistic and guided missile systems. A number of widely used manuals on protective structures were developed to address both the nuclear threat and the threat of conventional weapons. These manuals reflect the improvements in engineering practice that occurred over the years [ASCE (1985); Crawford et al. (1974); Newmark and Haltiwanger (1962)]. This progression of manuals concentrated on techniques for estimating the loading from nuclear weapons explosions, attenuation of pressure effects in the air and on the ground, simple analytical techniques for the design and proportioning of structural elements, guidelines for designing and analyzing equipment, and many other related topics.

Although nuclear weapons effects was the primary focus of protective design through the 1970s, related work was ongoing to develop quantitative procedures for the design of structures subject to accidental explosions. Extensive research and development programs, including numerous full- and small-scale structural response and explosive effects tests, formed the empirical basis for the development of guidelines on resistance of structures to the effects of accidental explosions [USDOA (1990)]. Several other manuals dealing with blast effects and the design of protective structures have also been developed for use by the military services during last two decades [Drake et al. (1989); USDOA (1990), (1992), (1998)].

Increased terrorist activity during last two decades has also led to a number of design guidelines for building structures in recent years [ASCE (1999), (2005); DOD (2003); GSA (2003); ISC (2001)]. These efforts have been put into practice by National Institute of Standards and Technology through draft manuals in 2006 [NIST and USDOC (2006)]. According to Lew (2006), current goal in blast-resistant design of buildings is to find an analytical tool to evaluate the performance of structures during blast loads. Although none of these manuals address the issue of blast load effects on highway bridges, they provide a range of structural data and design procedures that are useful for designers and which have applicability to the design of blast-resistant structures.

2.1.2 Nature of Explosions

Explosive materials are designed to release large amounts of energy in a short time. The explosion arises through the reaction of solid or liquid chemicals or vapor to form more stable products, primarily in the form of gases. A high explosive is one in

which the speed of reaction (typically 5,000-8,000 m/s) is faster than the speed of sound in the explosive [Mays and Smith (1995)]. High explosives produce a shock wave along with gas, and the characteristic duration of a high-explosive detonation is measured in microseconds (10^{-6} s). Explosives come in various forms, commonly called by names such as TNT, PETN, RDX, and other trade names [USDOA (1998)]. The lethality of high explosives has been increasing since the nineteenth century [Baker et al. (1983); Fickett (1985); McGraw-Hill (1989)].

The effects of explosions on structures are directly related to stress-wave propagation as well as impact and missile penetration. In all close-in explosions, where shock waves must travel through the surrounding medium to cause damage to a facility, a realistic description of the wave-propagation phenomena is needed. The literature on these subjects can be divided into two groups: one group addresses the classical issue of wave propagation with emphasis on linear type problems, and the second group is more focused on nonlinear problems. Various theoretical aspects of the explosive effects in materials are discussed in Han and Yin, 1993; Batsanov, 1994; Smith and Hetherington 1994; and Mays and Smith 1995.

The effects of explosion are varied. For explosions close to the targeted object, the pressure-driven effects occur quickly, in the order of microseconds to a few milliseconds. The air-blast loads are commonly subdivided into (1) loading due to the impinging shock front, its reflections, and the greatly increased hydrostatic pressure behind the front, all commonly denoted as overpressure; and (2) the dynamic pressures due to the particle velocity, or mass transfer, of the air. It is customary to characterize the pressure loadings in terms of scaled range, given by $Z = R/W^{1/3}$, in which Z is the

scaled range, R is the radial distance between the explosion center and the target, and W is the explosive weight (normally expressed as an equivalent TNT weight). Units for charge weight and distance should be pounds and feet.

If an explosion is confined by a chamber or room, the gas pressure increases rapidly to a sustained level and then decays because of venting out. Under these conditions, shock reflections occur and the overall effect can be greater than that of the incident shock pressure. The effects of internal explosions can be devastating to buildings and their occupants. There is a considerable body of knowledge available concerning blast-effects mitigating techniques for buildings subject to accidental explosions, which may have applicability to the design of civilian office structures, bridge box girders, etc. [USDOA (1990)].

There are three additional explosion-related phenomena relevant to this study, namely impact of objects propelled by the explosive environment [Jones (1989)], penetration of such objects [Bangash (1993); Zukas (1990)], and ground-transmitted shock [DTRA (1997); USDOA (1990), (1992)].

2.1.3 Inducted Physical Behavior

If the explosion originates at a sufficiently great scaled range (i.e., a small charge or a large distance from a structure), then the structure will be loaded in a manner that leads to global deformation, meaning that all the elements provide some degree of resistance to the loading. Dynamic analysis and design in such cases depends on the expected loading and the provision of resisting elements to accommodate the loading, which are addressed in the previously cited design manuals and by the computational approaches discussed later in this chapter.

If the explosion is sufficiently close to a pier or deck (that is, with a small scaled range Z), there can be gross disintegration of structural components, with either spalled fragments coming off the front and back sides or wall fragments themselves being propelled as missiles. These fragments can injure people, damage property, and cause the structure to collapse if the structural support is sufficiently disrupted. At intermediate scaled ranges, both global and localized response, including severe cracking, with near-face disintegration and spalling on the rear face, can be expected.

When an explosion impinges on a structural element, a shock wave is transmitted internally at high speed. For example, dilatational waves (tension or compression) propagate at speeds in the range of 2,700-3,400 m/s in typical concrete and 4,900-5,800 m/s in steel. At these speeds, reflections and refractions occur quickly within the material (within milliseconds), and, depending on the material properties, high-rate straining and major disintegration effects can occur. For example, under extremely high shock pressures, concrete, a relatively brittle material, tends to undergo multiple fractures which can lead to fragmentation. In steel, under similar conditions, depending on the material properties and geometry, yielding and fracture can be expected, especially if fabrication flaws are present, with fragmentation occurring in some cases. Primary fragments are produced when a detonating explosive is in contact with materials such as concrete or steel. Initial velocity of the primary fragments depends in part on the detonation pressure. Secondary fragments are produced by the effect of the blast wave on materials not in contact with the explosive.

Other explosion-generated effects are also produced, such as fire (including smoldering fires), smoke, pressure damage to ears and other organs, and violent motion

of the structure and its contents. Such shock-related motion can result in personal injury, equipment damage and can cause the loss of lifelines such as utilities and communications cables. Specially, the consequences of attack expressed as damage to bridges and tunnels that are of concern are as follows:

- Threats to the integrity of the structure (e.g., resulting in replacement of the facility or major repairs)
- Damage that inhibits the structure's functionality for an extended period of time, such as closure of the facility for 30 days or more
- Contamination of a tunnel resulting in extended closure or loss of functionality
- Catastrophic failure resulting from an attack based on the threats described above

After considering the nature of the bridge and tunnel components of the highway system and lessons learned from natural disasters, the effects of transportation-related consequences of the September 11th attack, and the recent barge collision in Oklahoma, the BRP panel [BRP (2003)] has determined that the loss of a critical bridge or tunnel at one of the numerous "choke points" in the highway system could result in hundreds or thousands of casualties, billions of dollars worth of direct reconstruction costs, and even greater socioeconomic costs.

2.2 PROGRESSIVE COLLAPSE

As noted in ASCE 7-05 [ASCE (2005)], except for specially designed protective systems, it is usually impractical for a structure to be designed to resist general collapse caused by gross misuse of a large part of the system or severe abnormal loads acting directly on a large portion of it. However, precautions can be taken in the design of structures to limit the effects of local collapse, and to prevent or minimize progressive

collapse. **Progressive collapse** is defined as the spread of an initial local failure from element to element resulting, eventually, in the collapse of an entire structure or a disproportionately large part of it.

The Ronan Point collapse in England in 1968, initiated the interest of engineers in the subject of progressive collapse. Since then, many events that may not truly be examples of progressive collaps have influenced the development of guidelines on progressive collapse. Figure 2.1 illustrated the timeline of development of guidelines compared against various events since 1970.

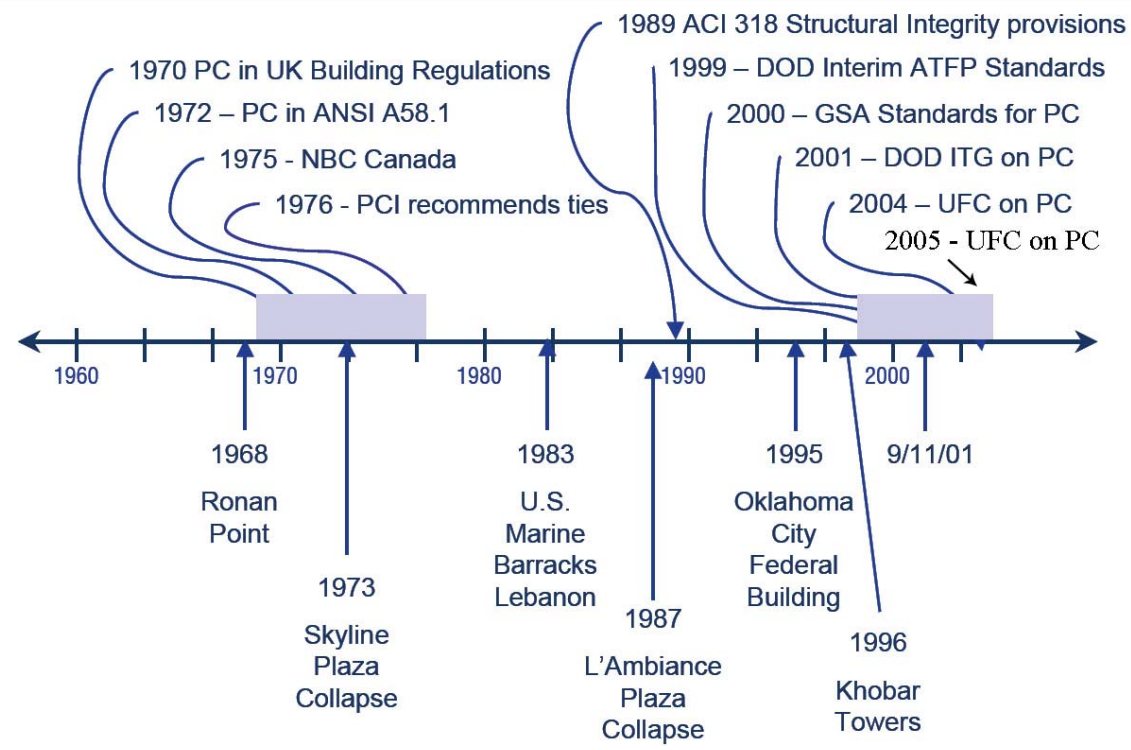

Figure 2.1 Timeline of development of Guidelines on Progressive Collapse.

McGuire [McGuire (1974)] have discussed the problem of progressive collapse and various measures for its prevention. Differences between traditional and newer structures (at that time) and the then-existing state of design codes are reviewed with

specific reference to the collapse of the Ronan Point apartment building. The changes in the United Kingdom code following the incident and the criteria adopted thereafter to design to progressive collapse resistant structures also are discussed.

Ellingwood and Leyendecker [Ellingwood and Leyendecker (1978)] have examined the development of design criteria to control progressive collapse and have proposed methods for their implementation in existing standards. They have revisited the three approaches that have been categorized previously to prevent progressive collapse: event control, indirect design and direct design. They observed that the main objective of designing for "damage tolerance" is to minimize the loss of life and to permit safe evacuation of occupants from a damaged structure. Accordingly, they have recommended the alternate load path/damage control approach over the specific local resistance approach, with judicious combination of both strategies, if required.

Ghali and Tadros [Ghali and Tadros (1997)] have investigated a multi-span bridge for its progressive collapse vulnerability. For the 12,910 m long bridge on Northumberland strait in Canada, they proposed a modified design where a drop-in span will just separate from rest of the bridge during local damage to the bridge deck.

Mlakar et al. [Mlakar et al. (1998)] have summarized the findings of the Building Performance Assessment Team (BPAT) on investigation of damage caused by the bombing of Alfred P. Murrah Federal Building in Oklahoma City, Oklahoma. Their have observed that special moment frame detailing would be more effective against blast loading than an ordinary moment frame and have also provided recommendations for the design and construction of new federal buildings.

The National Workshop on the Prevention of Progressive Collapse was held in

Chicago during July 10-12, 2002 [MMC (2002)]. The codes and standards breakout group during this workshop led discussions on the merits of direct and indirect design approaches and identified 14 areas of research. The structural systems and analytical tools breakout group identified the need to establish the accuracy of the various analytical assumption, determine performance criteria relating elastic response analyses to inelastic behavior and validate simplified methods through test and empirical data through instrumentation on controlled demolition projects.

Weidlinger Associates, Inc. has examined the software and modeling techniques available in-house for analyzing global behavior of multi-story buildings exposed to abnormal loadings that damage or destroy columns or other load-bearing elements at the ground level. They have developed a fast running analytical tool, named as FLEX, for progressive collapse analysis of frame buildings [Ettouney (2004); Ettouney et al. (2004); Ettouney et al. (2006); Hansen et al. (2005); Smilowitz (2006b)].

Starossek [Starossek (2006)] have studied progressive collapse of bridges. He has proposed an approach for designing against progressive collapse and has presented a set of corresponding design criteria, including requirements, design objectives, design strategies, and verification procedures. In addition to the better-known design methods providing specific local resistance or alternate load paths, an approach based on isolation by compartmentalization is presented and discussed. He has observed that that the terms continuity, redundancy, and robustness should be carefully distinguished when considering progressive collapse of bridges.

Bazant and Verdure [Bazant and Verdure (2007)] have investigated the mechanics of progressive collapse. Rather than using classical homogenization, they have found it

more effective to characterize the continuum by an energetically equivalent snap-through. The collapse, in which two phases—crush-down followed by crush-up—must be distinguished, is described in each phase by a nonlinear second-order differential equation for the propagation of the crushing front of a compacted block of accreting mass. Expressions for consistent energy potentials are formulated and an exact analytical solution of a special case is given. It is shown that progressive collapse will be triggered if the total (internal) energy loss during the crushing of one story (equal to the energy dissipated by the complete crushing and compaction of one story, minus the loss of gravity potential during the crushing of that story) exceeds the kinetic energy impacted to that story. Regardless of the load capacity of the columns, progressive collapse driven by gravity alone is inevitable if this criterion is satisfied (for the World Trade Center it is satisfied with an order-of-magnitude margin).

2.3 DESIGN CODES

There are several design codes that prescribe provisions related to design of structures (mostly buildings) to resist explosive loads or progressive collapse. A brief review of these codes is presented in this section.

American Society of Civil Engineers Minimum Design Loads for Buildings and Other Structures [ASCE (2005)]

ASCE 7-05 gives the concepts, causes and analysis methods of progressive collapse. It also lists some examples of design concepts and details, including good plan layout, providing an integrated system of ties, retaining walls, changing directions of span of floor slab, load-bearing interior partitions, catenary action of floor slabs, beam

action of walls, redundant structural systems, ductile detailing, providing additional reinforcement and use of compartmentalized construction in combination with special moment resisting frames.

ISC Security Criteria

The Interagency Security Committee (ISC) developed the ISC Security Criteria to ensure that security becomes an integral part of the planning, design, and construction of all new Federal Courthouses, new Federal Office Buildings, major modernization projects, and leased facilities. The criteria consider security in all building systems and elements.

The ISC was established by Executive Order in 1995 to develop long-term construction standards for locations requiring blast resistance or other specialized security measures and is chaired by the General Services Administration (GSA). It has three primary security responsibilities for nonmilitary activities: (a) establish policies for security in and protection of federal facilities; (b) develop and evaluate security standards for federal facilities, develop a strategy for ensuring compliance with such standards, and oversee the implementation of appropriate security measures in federal facilities; and (c) take such actions as may be necessary to enhance the quality and effectiveness of security and protection of federal facilities. The ISC criteria were updated in September 2004, and include three primary documents:

- ISC Security Design Criteria for New Federal Office Buildings and Major Modernization Projects: Part I, September 2004 (For Official Use Only).
- ISC Security Design Criteria for New Federal Office Buildings and Major

Modernization Projects: Part II: Tables, Design Tactics, and Additional Risk Guidelines, September 2004 (For Official Use Only).

- ISC Security Standards for Leased Space, September 2004 (For Official Use Only).

The DoD Minimum Antiterrorism Standards for Buildings [DOD (2003)]

The Unified Facilities Criteria (UFC) system is prescribed by MIL-STD 3007 and provides planning, design, construction, sustainment, restoration, and modernization criteria, and applies to the Military Departments, the Defense Agencies, and the DoD Field Activities. UFC is required to be used for all DoD projects and work for other customers where appropriate.

The DoD Minimum Antiterrorism Standards for Buildings (UFC 4-010-01) were developed by the Security Engineering Working Group with the intent to minimize the possibility of mass casualties in buildings or portions of buildings owned, leased, privatized, or otherwise occupied, managed, or controlled by or for DoD. The minimum standards provide appropriate, implementable, and enforceable measures to establish a level of protection against terrorist attacks for all inhabited DoD buildings where no known threat of terrorist activity currently exists. The minimum standards were originally released in December 1999 as interim standards and were released as Unified Facilities Criteria in July 2002. They were subsequently updated in December 2003 and in early 2005. The standards are published in two separate documents, UFC 4-010-01 and UFC 4-010-02, DoD Minimum Antiterrorism Standoff Distances for Buildings [DOD (2007)]. The first of the two documents lays out the actual standards while the second document is limited to establishing the specific explosive weights upon which the minimum standards are based. The second document is “For Official Use Only” due to the sensitivity of the

information related to minimum explosive weights required to be considered in design.

The minimum standards include 22 standards and 17 recommendations that apply to new and existing DoD buildings. A number of the standards have significant impacts on structural design of buildings. The most significant such standards are the ones that establish minimum standoff distances to buildings. Those standoff distances represent the standoff distances at which conventional construction can resist the minimum explosive weights and achieve the minimum levels of protection. The levels of protection reflect specific building responses.

Design of Buildings to Resist Progressive Collapse [DoD (2005)] incorporates a prudent, effective, and uniform level of resistance to progressive collapse without expensive or radical changes to typical design practice.

Structures to Resist the Effects of Accidental Explosions, Army TM 5-1300/Navy Publication NAVFAC P-397/Air Force Manual (AFM) 88-22 [USDOA (1990)]

When originally published in 1969, TM 5-1300 [USDOA (1969)] represented the state-of-the-art in blast resistant design. As such, it focused almost exclusively on reinforced concrete components. In 1990, the manual was updated by expanding its scope and the depth of coverage [USDOA (1990)]. Detailed, step-by-step examples were have been retained in the appendix of each chapter. TM 5-1300 does not establish regulatory requirements. An explosives safety standard, such as DoD Ammunition and Explosives Safety Standards [DDESB (2004)] or a commercial building code should be consulted for this purpose. Instead, TM 5-1300 provides comprehensive blast analysis and design procedure that may be used to satisfy any code's explosive safety requirements.

Recommendations for Stay Cable Design, Testing and Installation [PTI (2001)]

At present, design and analysis rules only exist for special types of structures. For the design of cable-stayed bridges, for instance, the PTI Recommendations (PTI 2001) require that the sudden rupture of one cable shall not lead to structural instability and specify a corresponding load case "loss of cable."

2.4 METHODS FOR ANALYSIS OF BLAST EFFECTS

Although explosion experiments are very important in the analysis of blast load effects of structures, computer models and programs have become indispensable in characterizing blast load effects. The complexity and dependability of the models varies dramatically.

2.4.1 Experimental Methods

Experimental data may be combined with certain aspects of explosion theory to properly characterize material behavior at high strain rates, which in turn can be used in developing computational approaches for estimating effects of blast loads. Nevertheless, it is important to validate these computational results using experiments involved scaled or full models of structures subject to blast loads. Several researchers have presented results based on blast testing of structures, e.g., blast tests on 1/4-scale concrete masonry unit (CMU) walls [[Dennis et al. (2002); Muszynski and Purcell (2003); O'Toole et al. (2006); Sun (1998); Turkmen and Mecitoglu (1999); Zhang et al. (2006)]. More recently, Nog et al [Ngo et al. (2007)] have presented experimental investigation of the blast-resistance of concrete panels made of ultrahigh-strength concrete (UHSC) material.

Most commonly, blast tests are carried out on scaled models of structures subjected to blast loads generated by explosive charge. In fact, These types ofv experiments have been used to develop the database for Design and Analysis of Hardened Structures to Conventional Weapons Effects [USDOA (1998)].

Bruneau et al (2006) has performed a series of experiments on 1/4 scale multi-hazard bridge piers. The concrete-filled circular steel columns exhibited a ductile behavior under blast load, and no significant damage was suffered by the fiber reinforced concrete cap-beam as a result of the blast pressures. FHWA has carried out blast experiments on scaled steel bridge piers [Wong (2007)]. Chen et al [Chen (2007)] has performed blast load tests on scaled wood bridge.

A majority of tests were conducted to determine the survivability of existing or proposed blast-hardened structures. In fact, there are very few tests that focus on a range of scaled sizes and charge weights to develop detailed knowledge base on blast load effects. Nevertheless, blast test data can be used to develop reliable material models and understand mechanics of different structural components. These material models can be used in numerical simulation models to improve reliability of simulation results in predicting blast load effects on a particular bridge component.

2.4.2 Computational Methods

Most of the computational models are based on finite-element or finite-difference methods. Finite-element methods have the versatility to deal with complicated geometries. In finite-difference methods, the discretization is accomplished by superimposing a network of nodes or grid points on the geometry. The arrangement of these grid points is usually structured, which diminishes the versatility in dealing with

complex geometries, but these methods generally offer higher computational speed.

Blast load simulations are generally carried out by first-principle and semi-empirical methods. In first-principle programs, mathematical equations describing basic laws of physics, e.g., laws of conservation of matter, momentum, and energy, are solved. In addition to these equations, constitutive equations describing physical behavior of materials are also needed. Semi-empirical computational methods are based on simplified models of physical phenomena, which are developed through analysis of test results and application of engineering judgment. **S**imulation of blast load effects on structures is highly nonlinear because of behaviors such as fracture, fragmentation, and flow due to high-pressure sources. Besides this, there are many mathematical and physical complications and phenomena whose underlying physics is not well understood, e.g., behavior of different types of joints and connections during blast loads.

In most cases, as structure can be replaced by an idealized (or dynamically equivalent) system which behaves time-wise in nearly the same manner as the actual structure. The distributed masses of the given structure are lumped together into a number of concentrated masses. The strain energy is assumed to be stored in several weightless springs which do not have to behave elastically; similarly, the distributed load is replaced by a number of concentrated loads acting on the concentrated masses. Therefore, the equivalent system consists merely of a number of concentrated masses joined together by weightless springs and subjected to concentrated loads which vary with time [USDOA (1990)]. This concentrated mass-spring-load system is defined as an equivalent dynamic system. Many blast prediction programs, such as ConWep and

SpanW, are using SDOF models for calculation.

It is possible to obtain close-form solution using SDOF method. But close-form wave propagation solutions usually assume a simple load distribution, neglect the elastic response and cannot be used for 3D cases [Jones (1989); Symonds and Mentel (1958)]. Naito and Wheaton's research showed that the simplified method have to assume proper failure type before obtaining the correct prediction [Naito and Wheaton (2006)].

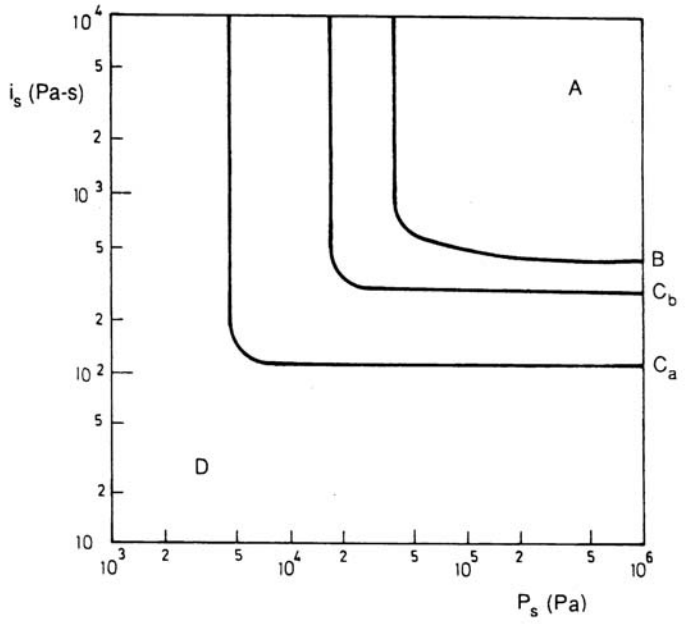

Figure 2.2: Pressure-impulse diagrams for damage to houses and small buildings.

It is possible, with relatively little extra work, to convert representation of SDOF system response to a pressure-impulse (P-I) or iso-damage curve which allows the load-impulse combination that will cause a specified level of damage to be assessed very readily. The bounds on behavior of a target structure are characterized by a pressure and an impulse (which can be a total impulse I (as here) or a specific impulse i_s or i_r). A typical P-I diagram is shown in Figure 2.2.

Li and Meng 2002 has studied the loading shape effect using pressure-impulse diagram and have found that that load shape factor affects a lot in elastic range for PI diagram method analysis.

Some programs, such as BlastX [SAIC (2006)] and Extreme Loading for Structures [ASI (2005)] utilize testing data, applied element method or smoothed particle hydrodynamics (SPH) method and can predict blast loading or structural response with medium resolution and fast calculation time.

Mair (1999) had reviewed hydrocodes for structural response to explosions. "Hydrocodes" are computational continuum mechanics tools that simulate the response of both solid and fluid material under such highly dynamic conditions (e.g., detonation and impact) where shock wave propagation is a dominant feature. It has been observed through literature review that, of the four hydrocode methodologies (Lagrangian, Eulerian, Coupled Eulerian-Lagrangian, and Arbitrary Lagrangian-Eulerian), only the Eulerian method is not practical for the simulation of structure-medium interaction during blast loads. All other methods are applicable to various extents. The most versatile methods are the Coupled Eulerian-Lagrangian and Multi-Material Arbitrary Lagrangian-Eulerian.

2.5 LS-DYNA

LS-DYNA is a general purpose finite element code for analyzing the large deformation dynamic response of structures including structure-fluid coupling. The main solution methodology is based on explicit time integration. LS-DYNA has been used extensively in blast load simulations. Mcdonald (2005) has developed the capability to model linear shaped charge jet formation and target penetration using the

commercially available nonlinear dynamics version of LS-DYNA. Yen (2006) has evaluated the capacity of the progressive failure model integrated within LS-DYNA by performing simulations of blast and ballistic impact on composite panels. Martinea and Romero (1996) has investigated the response of a stainless steel cylindrical vessel with asymmetric internal blast loading by experiments, computations, and analysis. These results (experimental and computational DYNA-3D results) are then compared with analytical predictions and have been proven to correlate well at distances away from the ends. Experimental and computational results compare well at all other locations. Mahmadi et al (2003) have conducted an air-blast simulation using LS-DYNA to demonstrate the capabilities Eulerian Multi-Material and ALE formulations to treat air-blast problem using an explicit finite element method. Dang and Chan (2006) have demonstrated the feasibility of using a composite blast shield for hardening an overhead bin compartment of a commercial aircraft. Three designs, the basic, thick, and thin shields, were field-tested using a frontal fuselage section of the Boeing 737-100 aircraft. The design was carried out using LS-DYNA finite element model simulations. The basic and thick shields protected the integrity of the fuselage skin with no skin crack. This work provides very encouraging results and useful data for optimization and implementation of the blast shield design for hardening overhead compartments against the threat of small explosives. Luccioni (2006) has investigated pressures and impulse of blast load to carry out computational dynamic analysis over a congested urban environment that corresponds to the opposite rows of buildings of a block on in the same street. The analysis of the structural failure of a reinforced concrete building caused by a blast load is presented in Luccioni et al. (2004)

2.6 LITERATURE REVIEW ON BLAST RESISTANT DESIGN OF BRIDGES

Ray et. al. [Ray et al. (2003)] compared prediction of blast load beneath a bridge overpass with low resolution, medium resolution and high resolution and discussed factors such as charge shape and clearing distance. Baylot et. al. [Baylot et al. (2003)] presented prediction method for response of steel bridge beams and girders to blast and fragment loads. These papers aimed at predicting the load and response quickly for design purpose and did not discuss failure scenario of bridge pier.

Marchand et al (2004) summarizes the results of ongoing research to develop performance-based blast design standards tailored specifically for bridges. The potential effects of blast loads on bridge substructures are presented, and structural design and retrofit solutions to counter these effects are discussed.

Since there is only limited resources for blast research on bridges, one of the main funded research is NCHRP project 12-72 [NCHRP (2005)]. The project group presented a series of paper in 2005 [Williamson and Winget (2005); Winget et al. (2005a); Winget et al. (2005b)]. The project summarizes the results of ongoing research to investigate economical, unobtrusive, and effective methods to mitigate the risk of terrorist attacks against critical bridges. It outlines a recommended plan to reduce these threats through proven risk management techniques, lists possible cost-effective security measures, discusses blast effects on bridges, and provides structural design and retrofit guidelines. It also discusses ongoing research oriented towards the development of a performance based design methodology. In using proper risk management techniques, transportation managers and bridge engineers can mitigate the risk of terrorist attacks against critical bridges to an acceptable level, while ensuring

efficient use of limited resources. Until then, their bridge pier was modeled as an SDOF flexural member, fixed at the foundation and the bent.

The latest AASHTO specifications [AASHTO (2008)] adds section 3.15 for blast loading. It listed some aspects to be considered in blast design. No blast analysis tool or methodology was introduced in this code.

CHAPTER 3. BLAST LOAD

3.1 INTRODUCTION TO EXPLOSIVE

Blast is an energy distribution process in which a large amount of energy disperses in a very, very short time. The time duration for blast/shock environments of interest are typically in the range of .5 to 1.0 ms with loadings in the range of several thousands of pounds per square inch.

Although there are different forms of explosive threats [see Smith and Hetherington 1994], major explosive threat to highway bridges may be caused by high explosive bombs (e.g., general purpose bombs which cause damage by blast and fragmentation and light case bombs which primarily produce blast damage), vehicle bombs and incendiary bombs (in which blast effects are augmented by a fireball from a burning fuel such as fuel). When a building is designed to resist blast loads, lethal fragmentation of glass or concrete is a very important factor because of its potential to cause injury and death to occupants. This is less important for blast-resistant design of bridges. Hence, In this research, we assume that the structure is damaged by high explosive blast wave load without piercing or fragmenting effects.

When a bridge deck is subjected to explosive loads or missile attacks, it is possible that the explosive may cause local damage in the deck. The bridge may not collapse in such situations and can still sustain the traffic. Figure 3.1 shows a bridge in Palestine after a missile attack.

Figure 3.1. Damages to a Bridge in Palestine After a Missile Attack.

3.1.2 Effects of explosives

If a detonating explosive is in contact with a solid material, the arrival of the detonation wave at the surface of the explosive will generate intense stress waves in the material, producing crushing and shattering disintegration of the material. This hammer-blow effect is called 'brisance'. The dynamic pressure at the detonation wavefront is the detonation pressure p_1 given in kilobars by the empirical equation [Smith and Hetherington 1994].

$$p_1 = 2.5 \times 10^{-9} \rho D^2 \qquad (3.1)$$

where ρ (kg/m^3) is explosive density and D (m/s) is detonation wave speed. Thus if D is 7400 m/s and ρ (kg/m^3) = 1500 kg/m^3 for RDX, then the detonation pressure p_1 is, by Equation 3.1, 205.4 kilobars, which is far in excess of the compressive strength of most

materials.

3.2 BLAST WAVE FORM

3.2.1 Simplified Model of Unconfined Blast Load

A structure is likely to be subjected to various types of hazards during its life time. These hazards can be subdivided into two general categories: man-made (blast) and natural (earthquakes, wind, etc). For a successful approach to any system design, it is essential to understand the nature of the hazard. Dynamic hazards can be described by their relative amplitudes and relative time (frequency) attributes. Figure 3.2 shows a schematic representation of the amplitude-frequency relationships of several dynamic hazards [PCI 2004].

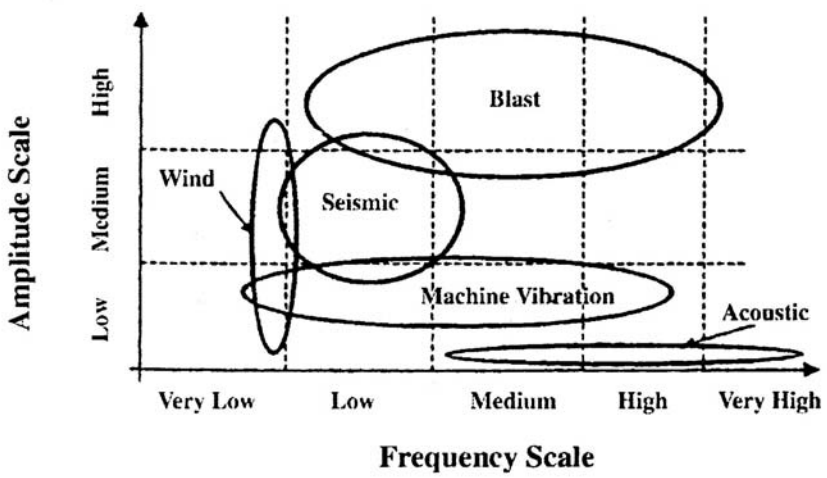

Figure 3.2: Qualitative amplitude-frequency distribution for different hazards.

It is important to emphasize the principal differences between static, dynamic and short-duration dynamic loads. Typically, static loads do not produce inertia effects in the structural response, are not time dependent, and are assumed to act on the structure for long periods of time (e.g. gravity loads). Dynamic loads, such as induced by earthquake or

wind gusts, have strong time dependencies and their typical durations are measured in tenths of seconds. Short-duration dynamic loads, such as those induced by explosions or debris impact, are non-oscillatory pulse loads, and their duration is about 1,000 times shorter than the duration of typical earthquakes. Structural responses under short-duration dynamic effects could be significantly different than those during much slower loading cases. A multi-hazard design of bridges must explicitly address the effects conventional loads as well as severe loading environments imposed by different hazards [PCI 2004].

Interactions of various hazards and their effects on structural response are not well understood. For example, after the collapsing of WTC towers, investigations have been carried out to simulate the entire collapse process. To simulate the observed free-fall collapse correctly, gravity load is the most important factor and a relatively simple model can simulate this well. However, very detailed model consisting of millions of degree of freedoms, even including the plane engine propeller, is required to include impact load effects [Smilowitz 2006a]. A similar situation exists in case of blast loads, where understanding of interactions between gravity, shock wave and impact loads is vital in identifying potential collapse mechanisms of a highway bridge subject to blast loads.

An explosion is a very rapid release of stored energy characterized by an audible blast. Part of the energy is released as thermal radiation, and part is coupled into the air (air-blast) and soil (ground-shock) as radially expanding shock waves. Air-blast is the principal damage mechanism. Air-blast phenomena occurs within milliseconds and the local effects of the blast are often over before the structure (building or bridge) can globally react to the effects of the blast. Initial peak pressure intensity (referred to as overpressure) may be several orders of magnitude higher than ambient atmospheric pressure in case of

air-blast. Fig. 3.3 illustrates some of the terminologies used in defining blast loads acting on structures. [PCI 2004].

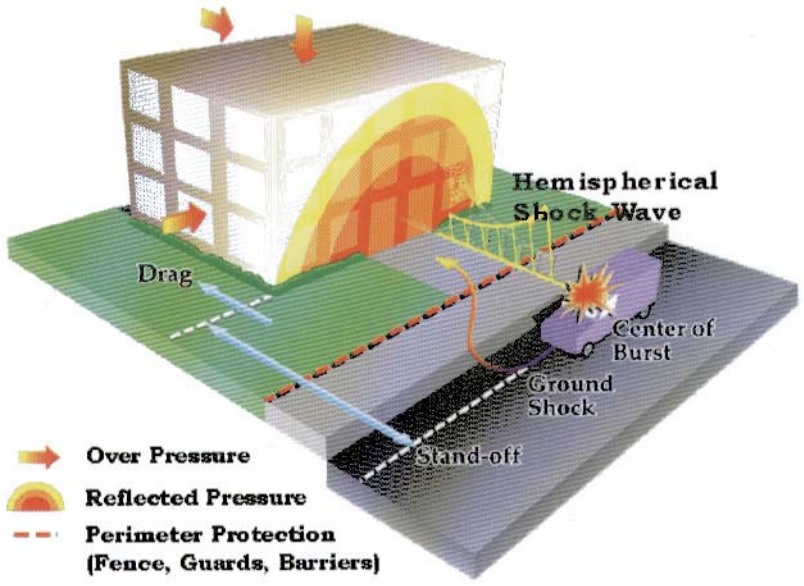

Figure 3.3: Illustration of Terminologies Used in Defining Blast Loads on Structures.

As illustrated in Figure 3.3, blast overpressure radiates from the point of detonation but decays exponentially with distance from the source and time, and eventually becomes negative (outward-rushing force) subjecting the building surfaces to suction forces as a vacuum is created by the shock wave. Fig. 3.4 shows this pressure time-history during a typical blast event. In many cases, the effect of the negative pressure phase is ignored because it usually has little effect on the maximum response. The impulse delivered to the structure is the area under the positive phase of the pressure-time curve. Both the pressure and impulse (or duration time) are required to define the blast loading.

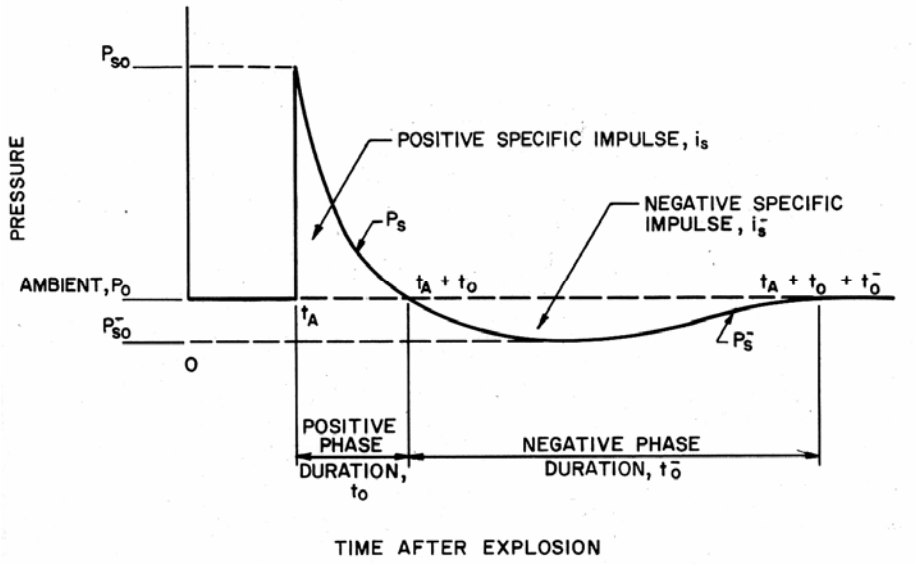

Figure 3.4: Simplified Model of Unconfined Blast Load on Structures [Army 1990]

For any blast loading, the total dynamic pressure (in psi) and the positive phase duration (in milliseconds) are found in terms of equivalent weight, W, of the explosive in TNT and the distance from the blast center, R. Generally, blast loads are defined in terms of the scaled distance parameter Z (ft per lb TNT equivalent) as

$$Z = R/W^{1/3} \qquad (3.2)$$

With the scaled distance in the correct units, published curves can be used to find the total dynamic pressure and the positive phase duration. Similar blast waves are produced at identical scaled distances when two explosive charges of similar geometry and of the same explosive, but of different sizes, are detonated in the same atmosphere.

3.2.2 Blast Wavefront Parameters

Equations for wavefront parameters such as blast wavefront velocity U_s, air density behind the wavefront ρ_s, and the maximum dynamic pressure q_s were first presented by Rankine and Hugoniot in 1870 to describe normal shocks in ideal gases and are available in

a number of references such as Liepmann and Roshko [Rankine (1870), Liepmann and Roshko (1957)]. These equations for blast wavefront velocity U_s, air density behind the wavefront ρ_s, and the maximum dynamic pressure q_s are given as

$$U_s = \sqrt{\frac{6p_s + 7p_0}{7p_0}} \cdot a_0 \qquad (3.3)$$

$$\rho_s = \frac{6p_s + 7p_0}{p_s + 7p_0} \cdot \rho_0 \qquad (3.4)$$

$$q_s = \frac{5p_s^2}{2(p_s + 7p_0)} \qquad (3.5)$$

where p_s is peak static overpressure, p_0 is ambient air pressure ahead of the blast wave, ρ_0 is the density of air at ambient pressure ahead of the blast wave and a_0 is the speed of sound in air at ambient pressure. Figures 3.5 and 3.6 show plots of equations 3.5 and 3.3, respectively. Assuming p_0 as 101 kPa, dynamic pressures in a blast wave in free air for different values of static overpressure, p_s, obtained from Eqs. (3.5) are shown in Table 3.1. It is seen from Table 3.1 that the dynamic pressure q_s is less than the static pressure for $p_s <$ 500 kPa. For $p_s >$ 500 kPa, dynamic pressure is larger in magnitude than that of static pressure p_s.

Table 3.1 Air-blast pressures

Ps (kPa)	Qs (kPa)
200	110
350	290
500	518
650	778

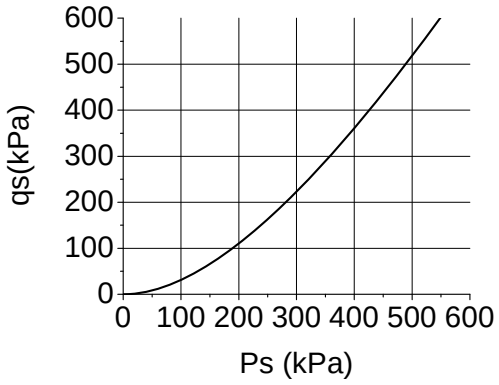

Figure 3.5: Dynamic pressure versus side-on overpressure

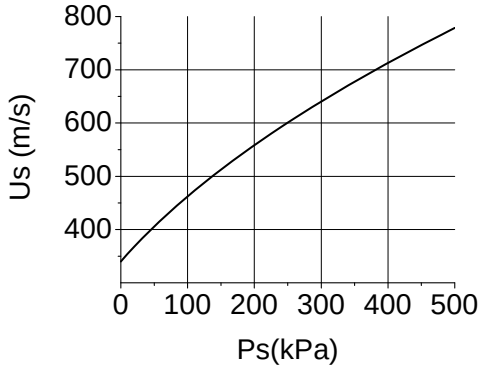

Figure 3.6: Wavefront velocity versus side-on overpressure.

Brode's analysis [Brode 1955] leads to the following results for peak static overpressure p_s in the near field (when p_s is greater than 10 bar) and in the medium to far field (p_s between 0.1 and 10 bar) regions,

$$p_s = \frac{6.7}{Z^3} + 1 \text{ bar} \quad (p_s > 10 \text{ bar}) \tag{3.6}$$

$$p_s = \frac{0.975}{Z} + \frac{1.445}{Z^2} + \frac{5.85}{Z^3} - 0.019 \text{ bar} \quad (0.1 < p_s < 10 \text{ bar}) \tag{3.7}$$

where the scaled distance Z is given by Eq.(3.2).

It is a universal practice to express explosive weights in equivalent of "TNT" by multiplying the mass of the explosive by a conversion factor based on specific energies of the explosive and TNT. For example, 100 kg charge of RDX converts to 118.5 kg of equivalent TNT, since the conversion factor for RDX is 1.185. Table 3.2 shows conversion factors for a range of explosives based on Baker et al. 1983.

Table 3.2: TNT Equivalent Conversion Factors for Explosives

Explosive	TNT Equivalent Factor
Amatol 80/20 (80% ammonium nitrate 20% TNT)	0.586
Compound B (60% RDX, 40% TNT)	1.148
RDX (Cyclonite)	1.185
HMX	1.256
Lead azide	0.340
Mercury fulminate	0.395
Nitroglycerin (liquid)	1.481
PETN	1.282
Pentolite 50/50 (50% PETN 50% TNT)	1.129
Tetry1	1.000
TNT	1.000
Torpex (42% RDX, 40% TNT, 18% Aluminium)	1.667
Blasting gelatin (91% nitroglycerin, 7.9% nitrocellulose, 0.9% antacid, 0.2% water)	1.000
60% Nitroglycerin dynamite	0.600

An alternative approach makes use of two conversion factors where the choice of which to use depends on whether the peak overpressure or the impulse delivered is to be matched for the actual explosive and the TNT equivalent. Table 3.3, adapted from the document TM5-855-1 [Army 1998], gives examples of these alternative conversion factors.

Table 3.3: Equivalent Factors Based on Pressure and Impulse.

Explosive	Equivalent pressure factor	Equivalent impulse factor
Composition B (60% RDX, 40% TNT)	1.11	0.98
ANFO	0.82	0.82
PETN	1.27	Not available
Pentolite	1.40	1.07
Tetry1	1.07	Not available
TNT	1.00	1.00

Existing numerical simulation methods or experimental data are all based on TNT equivalent of explosives. If there is an explosion involving explosive other than TNT, such as ANFO bomb attack in Club EL Nogal in 2003, it should be converted into equivalent TNT using factors in Table 3.2 & 3.3 before the analysis.

3.2.3 Air burst blast

The air burst environment is produced by detonations which occur above the ground surface and at a distance away from the protective structure so that the initial shock wave, propagating away from the center of explosion, impinges on the ground surface prior to arrival at the structure. As the shock wave continues to propagate outward along the ground surface, a front known as the Mach front (see Fig. 3.7) is formed by the interaction of the initial (incident wave) and the reflected waves. This reflected wave is the result of the reinforcement of the incident wave by the ground surface [Army 1990]. Hence, uniform pressure can be assumed for a structure below triple point in Figue 3.7. A detailed knowledge of wave propagation is necessary to calculate blast load profile above the triple point. Prediction of airblast loads can be done by various semi-empirical analytical tools, most notably AT-Blast, ConWep and BlastX.

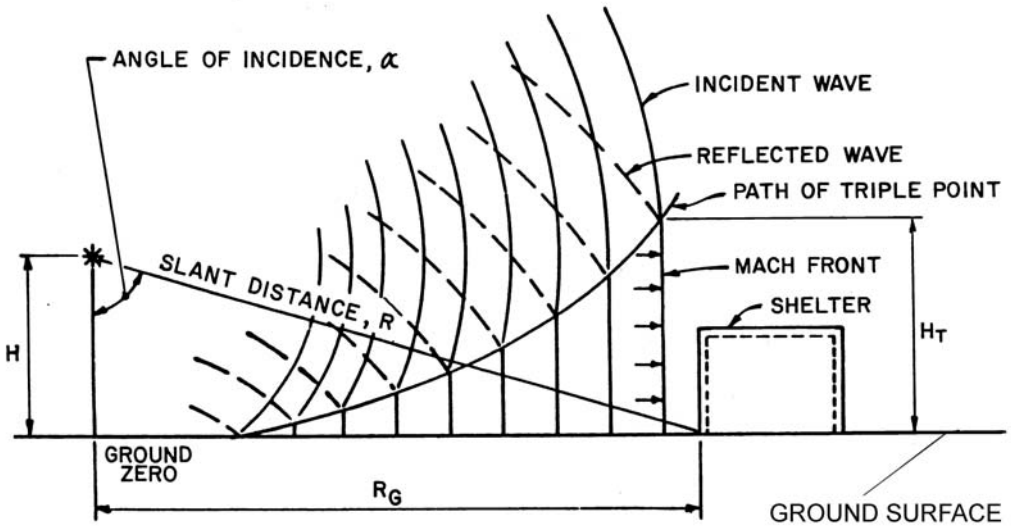

Figure 3.7 Air burst blast environment [Army 1990]

AT-Blast 2.2 [GSA 2006] is a software program that estimates the blast loads that develop during an open-air explosion. The program allows the user to input minimum and maximum range, explosive charge weight, and angle of incidence. From this information, AT-Blast 2.2 calculates the following values: Shock Front Velocity (V), Time of Arrival (TOA), Pressure (P), Impulse (I), and duration (td). The results are displayed on screen in a tabular format and may be printed. In addition, the resulting pressure and impulse curves may be displayed graphically. AT-Blast may be available for free from the U.S. General Services Administration (www.oca.gsa.gov). At-Blast cannot estimate explosion pressure because of interactions in a confined area, such as inside a building.

Using data from AT BLAST [GSA 2006], Figure 3.8 gives the pressure vs. angle of incidence (Range=20 ft, Weight=100 lb). It shows another feather of air blast wave.

The peak pressure and impulse patterns on the structure vary with distance from a maximum at the normal distance R_A to a minimum (incident pressure) where the plane of

the structure's surface is perpendicular to the shock front. When the angle of incidence is 0, pressure on the structure is the highest. When the angle reaches 90 degrees, the pressure gets minimum value. However, the curve has a peak when the angle is approximately 45 degrees.

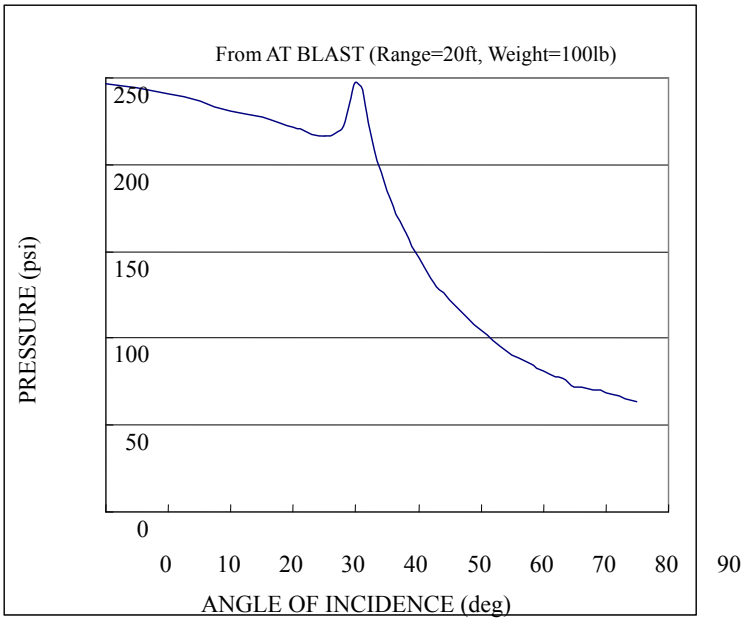

Figure 3.8 Pressure vs. angle of incidence

Designers of government projects may request ConWep [USAE Engineer Research & Development Center 2005], another software product, through the agency that they have a contract with. ConWep is a collection of conventional weapons effects calculations from the equations and curves of TM 5-855-1 [Army 1998]. Users should be thoroughly familiar with TM 5-855-1 before using this program as a design tool. ConWep code can consider only open-air blast. Since 1980s', engineers have found the blast load prediction

from ConWep can meet engineering requirements. Randers-Pehrson and Bannister have incorporated ConWep into LS-DYNA [LSTC 2003] to simulate blast load.

BlastX [SAIC 2006] computer code provides the internal airblast environment in structures with multiple chambers for both internal and external explosions using fast-running analytical/empirical models. The code treats shockwave propagation through strings of "rooms" (i.e., defined volumes and areas) to model blast transmission through multi-room structures. Interpretation of the results requires familiarization with the basic blast principles outlined in the Design and Analysis of Hardened Structures to Conventional Weapons Effects manual from the Defense Threat Reduction Agency [DTRA 1997]. However, in the bridge blast simulation, the blast wave's time duration can extend 2-3 times longer because of the reflection from the large bulks of bridge members. BlastX code cannot consider the "clearing time" [Winget et al. 2005a].

All these blast load prediction programs has their advantages and disadvantages and cannot be applied for the simulation of blast loads on bridge components directly. A new blast load generation method for applications to highway bridge components is investigated and presented in the following section.

3.3 BLAST LOADING SIMULATION IN LS-DYNA

3.3.1 Blast loads on Bridge Components

Blast wave pressure decreases rapidly with the standoff distance. Because of large size and complex geometries of a bridge structure, applying blast wave load accurately on different bridge members is a changeling work. For example, assume that a 1500-lb TNT charge is detonated under a 60-ft span hypothetic highway bridge at point C, as shown in

Figure 3.9. The TNT charge is 10 ft away from column A and 50 ft away from column B. Pier section size is 3 ft ×3 ft.

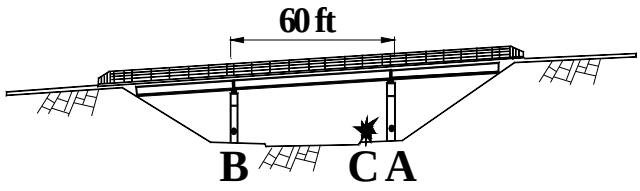

Figure 3.9 A hypothetical highway bridge subject to blast load.

The simulated blast load on bridge components should at least satisfy the following:

1. Near points A and B, the pressure and impulse of blast wave should be similar to that generated by experimental data or standard semi-experimental data using ConWep program [USAE Engineer Research & Development Center 2005];
2. The time of arrival of blast waves reaching point A and B should be similar to those by ConWep program so that the time sequences of blast wave load and structural response have correct dynamic effects;
3. The load should be able to assign to bridge members.

Many methods exist for evaluating structural behavior under impact loads. Closed-form wave propagation solutions usually assume a simple load distribution, neglect the elastic response and cannot be used for 3-dimensional analysis [Jones 1989; Symonds and Mentel 1958]. Commonly used simplified methods include single or multi-degree-of-freedom, pressure-impulse (P-I) diagrams, and response surfaces developed from finite element analysis [Sunshine et al. 2004]. These methods have relatively low accuracy in the prediction of either load or structural performance. Li [Li and Meng 2002] have studied the loading shape effect using pressure-impulse diagram and

have observed that load shape factor affects structural behavior significantly in elastic range using PI diagram method analysis. Naito and Wheaton [Naito and Wheaton 2006] have shown that the simplified methods have to assume a proper failure type before obtaining the correct prediction. Methods with median accuracy levels include semi-empirical codes such as BlastX [SAIC 2006].

A blast load can be applied as a point load on a SDOF structure. However, failure mechanisms of structure members have to be assumed to simplify a structure as a SDOF model. In this research, since our goal is to investigate failure mechanisms of bridge under blast load, simplified modeling of the structure as SDOF system is not an accurate and acceptable approach.

A more accurate structure behavior can be obtained by simulating blast loads using Hydro codes such as LS-DYNA [LSTC 2003] and FLEX developed by Weidlinger Associates, Inc. These hydro codes use explicit solver designed for general purpose analysis. However, specific requirements must be met to obtain correct simulation results for blast effects on reinforced concrete structures. Examples of blast simulation using LS-DYNA can be found in Wang [Wang 2001], Krauthammer and Otani [Krauthammer and Otani 1997]. Traditionally, there are two approaches of blast load simulation in LS-DYNA: applying ConWep blast load directly on a structure or simulating the detonation process by ALE method. Both methods have their own advantages and disadvantages. In this research, a new approach is proposed by combining two traditional approaches on blast load simulations on structures.

3.3.2 Blast Load Generation by ConWep

As described previously, ConWep is a collection of conventional weapon effects

calculations from the equations and curves of TM 5-855-1 [Army 1998; Hyde 2005; USAE Engineer Research & Development Center 2005]. The ConWep equation has been merged into LS-DYNA to apply a pressure load on structures [Randers-Pehrson and Bannister 1997]. This method controls load magnitude accurately and does not consume extra calculation time. However, it is only suitable for analysis before failure of structure surface. When elements fail in the FEM simulation, eroding technique is used to avoid element distortion, i.e., "damaged" elements or nodes are removed from the structure. Since blast load generated by ConWep acts directly on exposed structural surface, it will be lost once the load contact surface (i.e., exposed structural surface) is eroded. Figures 3.8(a) and (b) illustrate ConWep pressure directly acting on the surface of a column. When FEM elements in concrete cover are eroded, blast pressure is lost with the erosion of these elements. On the other hand, blast load continues to act on uneroded elements. Therefore, the simulation in Figure 3.10(b) underestimates the damage to the structure since the load is not transmitted to concrete core after the spalling of the concrete surface.

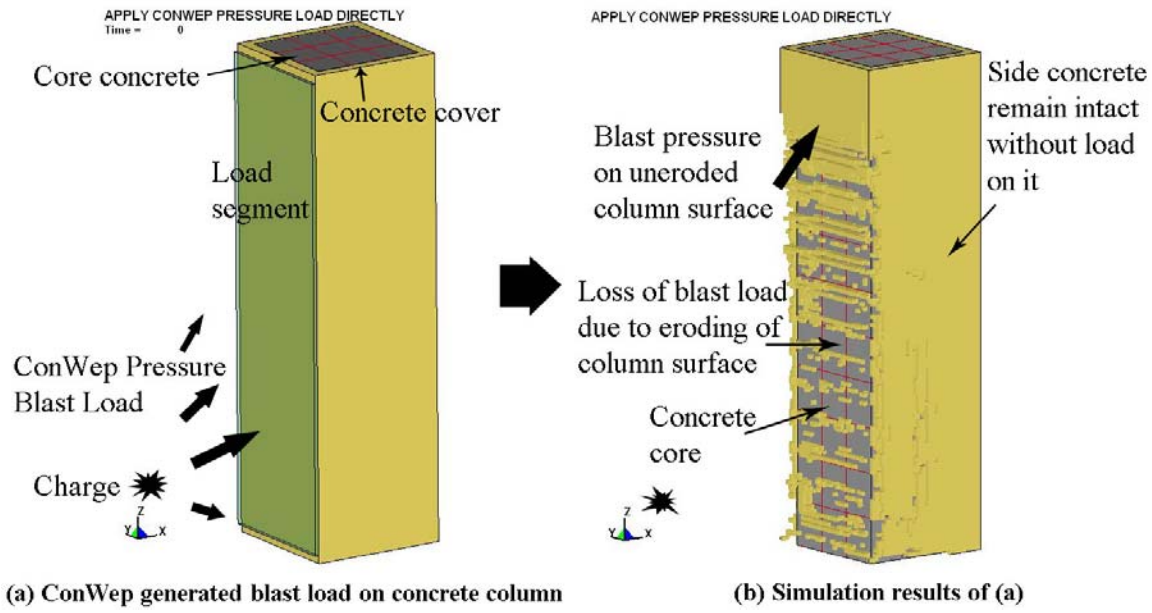

Figure 3.10. Application of ConWep blast load directly on concrete structure.

3.3.3 Detonation simulation

Detonation Simulation approach generates blast loads through detonation of high explosives using Arbitrary-Lagrangian-Eulerian mesh and *MAT_HIGH_EXPLOSIVE_BURN control card in LS-DYNA. The reason using Arbitrary-Lagrangian-Eulerian (ALE) mesh lies in two facts. First the simulation of explosion events requires large deformation of element mesh, which usually exceeds the ability of Lagrangian mesh (nodes moving along with material transferring). Eulerian mesh (nodes fix while the material transfer among different elements) is used to solve the large deformation problem. However, when we calculate the action between the structure with Lagrangian mesh and the Eulerian mesh, there arouses another problem called dynamic boundary problem which is difficult to handle [Gong 2006]. Therefore, we choose ALE mesh to simulate the explosion environment in this bridge blast research. An ALE formulation consists of a Lagrangian time step followed by a "remap" or "advection" step. The advection step

performs an incremental rezone, where “incremental” refers to the fact that the positions of the nodes are moved only a small fraction of the characteristic lengths of the surrounding elements. Unlike a manual rezone, the topology of the mesh is fixed in an ALE calculation. An ALE calculation can be interrupted like an ordinary Lagrangian calculation and a manual rezone can be performed if an entirely new mesh is necessary to continue the calculation [Hallquist 1998].

This method simulates the process of detonation and gives accurate evaluation of incident blast wave pressure through the explosive material. It is perfect for the simulation of interaction action between structure and close blast such as landmine explosion [Wang 2001]. But in simulation of civil structures, standoff distance has to be considered. Explosion generates blast wave in the air and the air blast wave blows the structure. As shown in Figure 3.11, blast pressure waves are carried to column surface using air as a medium because of standoff distance between charge and structure. This approach has several advantages over direct application ConWep pressure: (i) the blast wave load continues to act on the structure after the eroding of structural surface elements; (ii) it can predict the reflection and diffraction of the blast wave; and (iii) this method can account for the mutual interaction between structures and blast wave. This interaction cannot be ignored when the structural material yields under blast wave load with the elastic modulus approaching zero.

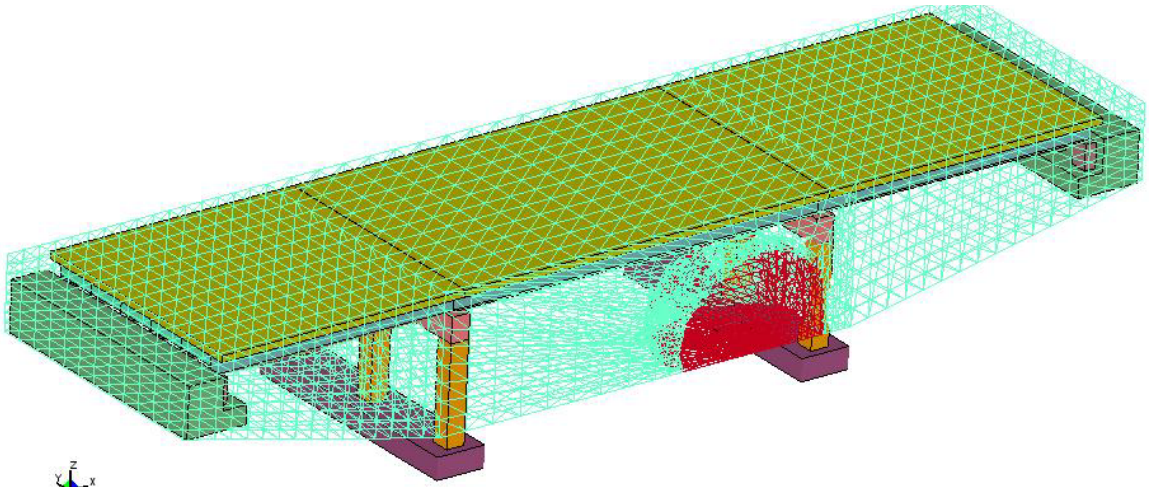

Figure 3.11 Blast Load Simulation on Highway Bridges Using Detonation Process in LS-DYNA.

Theoretically, we can simulate the reflection process by setting air mesh and reflecting boundaries using "Detonation Simulation". Problems arise when we assume air as an ideal gas, since it is difficult to simulate air under different pressure loads using simple constitutive equations. For example, blast load of 1500 lb TNT at standoff distance R=10 ft is simulated using ConWep and "Detonation Simulation" (method 2), as shown in Figure 3.12 (a). It is observed from Figure 3.12 (a) that although peak pressure generated both by ConWep and Detonation Simulation are identical, blast wave impulse (i.e., area under pressure curve) by Detonation Simulation (method 2) approach is much smaller than that by ConWep. Figure 3.12 (b) shows blast load time history of 1500 lb TNT at standoff distance R=50 ft in the same simulation. The pressure by "Detonation Simulation" (method 2) drops to zero very quickly as the standoff distance increases.

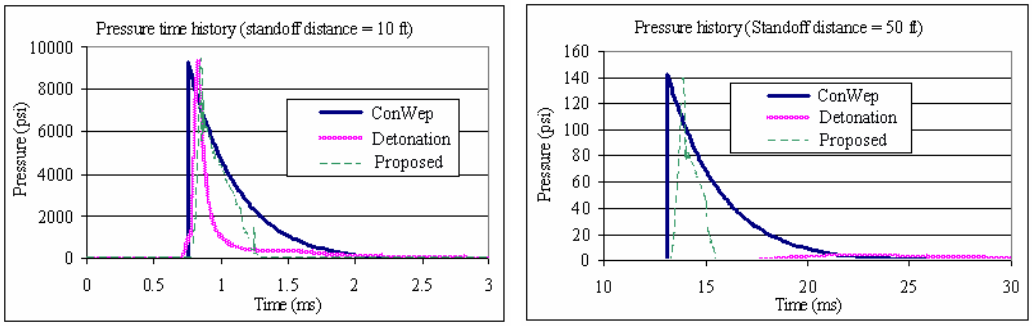

(a) Pressure at near point (b) Pressure at far point

Figure 3.12 Blast Wave Pressure History.

3.3.4 Proposed Approach for Blast Load Simulation

In order to overcome limitations of existing approaches, a new approach that can simulate loads on structural elements similar to ConWep is presented. In this approach, ConWep pressure generated for a specific charge weight is transferred to an air layer near structural element. The blast wave front propagates through the surrounding air layer. The air mesh interacts with Lagrangian structure element to apply the load on structural elements. This approach of applying blast loads on structural members is shown in Figures 3.11(a) and (b).

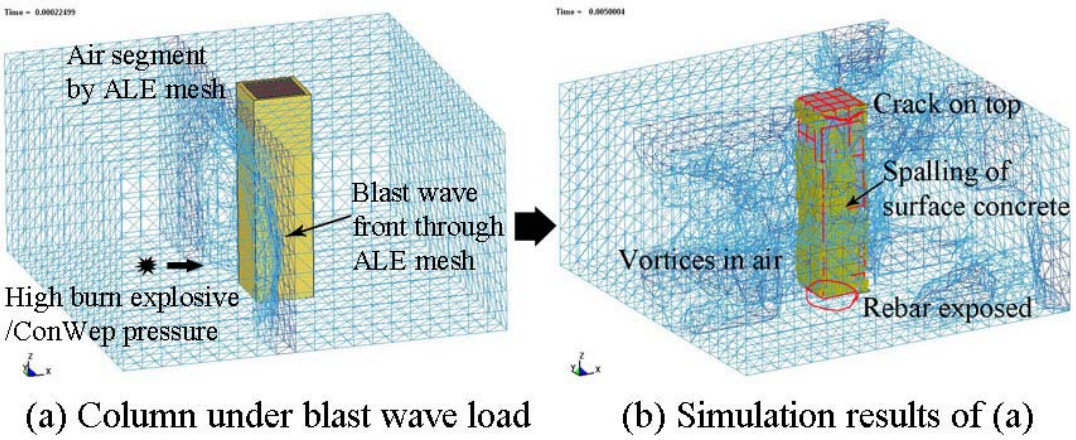

Figure 3.13 Simulation of Column Under Blast Wave Using Proposed Approach.

The proposed approach of blast load generating has advantages of both ConWep and "Detonation Simulation". It produces correct pressure field with the same arriving time of blast wave as ConWep, as seen from the method 3 curve in Fig. 3.12, and can simulate wave reflection and diffraction. When simulation involves complex geometry or non-airblast waves such as inter-explosion in box girder and air pressure near deck, other experiment data or program such as BlastX [SAIC 2006] are necessary to calibrate the load effect parameters.

In the proposed approach, we assume that when pressure load is applied on a air layer segment, the pressure of nearest air element should have the same peak as the applied load. Then, we can calibrate the applied loads by BlastX codes.

There are two key factors in the proposed approach. The first one the arrangement of load segments. Since ConWep reflected air blast pressure with a scale factor is used to simulate the load on structures including internal reflected blast pressure and incident blast pressure, the smaller for each load segment, the more accurate the simulation results. In our research, one load segment is set for each structure member.

The second factor is the air density of the air layer sustaining the segment load. As shown in Figure 3.13(a), after the load is applied to air layer before the structure, the air layer will be compressed first and form a blast wave front. Then the blast wave front moves on and transfers the blast load further. Usually, the wave front air density is 2-6 times of the air density of approximately 1.29 kg/m^3. It is found that the smaller the air density (1/10 to 1/100 of the normal air density), the bigger the pressure transferred to structural elements. If the air density of the load air layer is set to smaller than 1.29×10^{-2} kg/m^3, the transferred load drops down. It has been observed from simulation results that

the blast pressure is transmitted accurately to structural elements when air density of surrounding air layers is 1/10 of normal air density. In this case, the density of compressed air layer is approximately twice of the normal air density value of 1.29 kg/m^3. This value is close to shock density parameter obtained from ConWep.

CHAPTER 4. BRIDGE MODELING

4.1 HYPOTHETIC TARGET BRIDGE

A detailed review of the National Bridge Inventory (NBI) database has been carried out to investigate blast load effects on a typical highway bridge in the United States. The National Bridge Inventory (NBI) is a database of the structural configuration, condition assessment, and appraisal data of bridges the United States [NBI (2003)]. Although individual states maintain their own inventory of bridges in the country, Federal Highway Administration (FHWA) complies bridge inventory data provided by all states. Currently, the NBI database includes 687,346 bridges located in 52 states.

In order to select a typical bridge for blast load effects, bridges in NBI database have been investigated by classifying bridges according to various structural and design parameters, e.g., length of maximum span, number of spans in main unit, design load, deck width (out-to-out), lanes on structure, minimum vertical underclearance, material types, design types, bridge median, navigation vertical clearance, average daily traffic, designated level of service. For example, Figure 4.1 shows the frequency distribution of length of maximum span length. It is observed that 5.7% bridges have a maximum span length of 3.0 m. However, 95% of these bridges are culverts. The second highest peak in Figure 4.1 is at 9.1m with a frequency (number of bridges) of 20124 (2.9% of bridges in NBI). It has been observer that 44% of bridges in this category are stringer / multi beam or girder construction type.

Based on similar type of study for other geometrical features of a bridge and through a detailed search of NBI database, a three-span bridge has been selected as a hypothetical

bridge for the development of finite element model of the bridge.

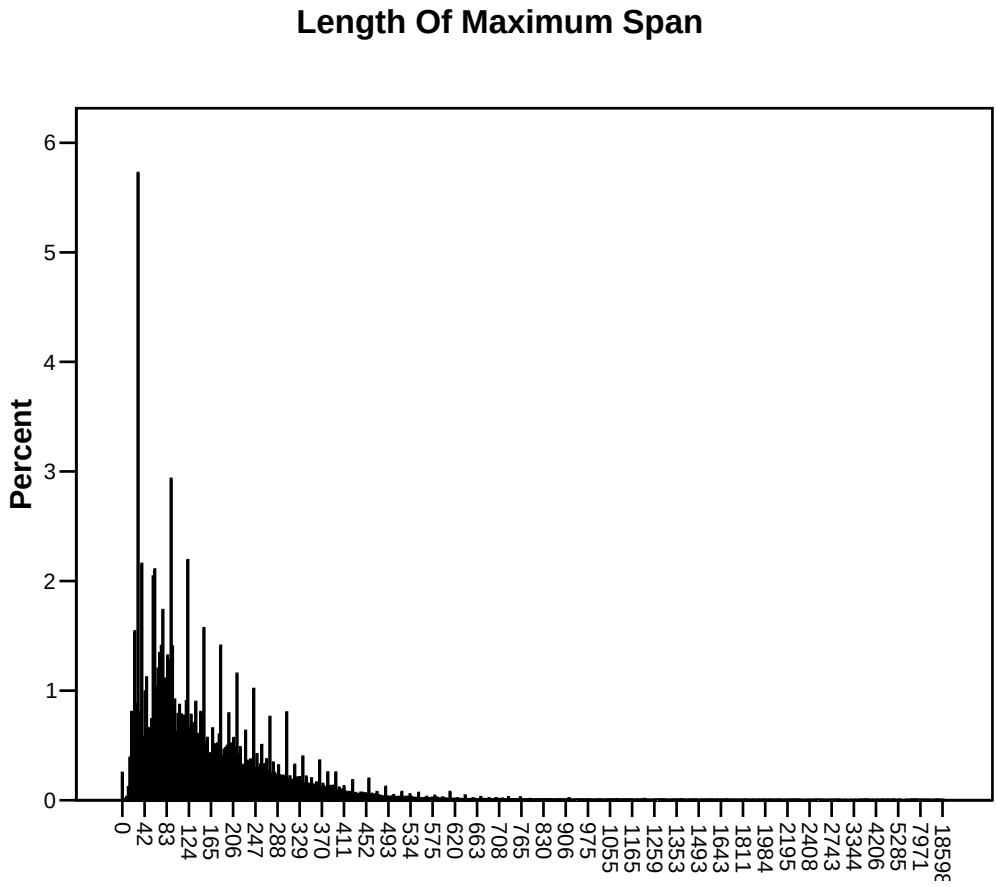

Figure 4.1: Distribution of Bridges in USA Based on the Length of Maximum Span (abscissa Length unit: 10cm.)

For the hypothetical bridge selected through the search of NBI database, as built drawings of the bridge with similar feature were obtained. Figure 4.2 shows the plan of the bridge on the drawing.

Figure 4.3 shows plan and elevation of the bridge. The hypothetical bridge is 3-span non-continuous bridge. Table 4.1 shows key parameters of the bridge geometry and design load. A non-continuous bridge has been selected as a hypothetical bridge so that effects of blast loads on bridge components, e.g., bearings on interior pier bents, could

also be investigated, in additional to damages to major components such as piers, deck, girders, etc.

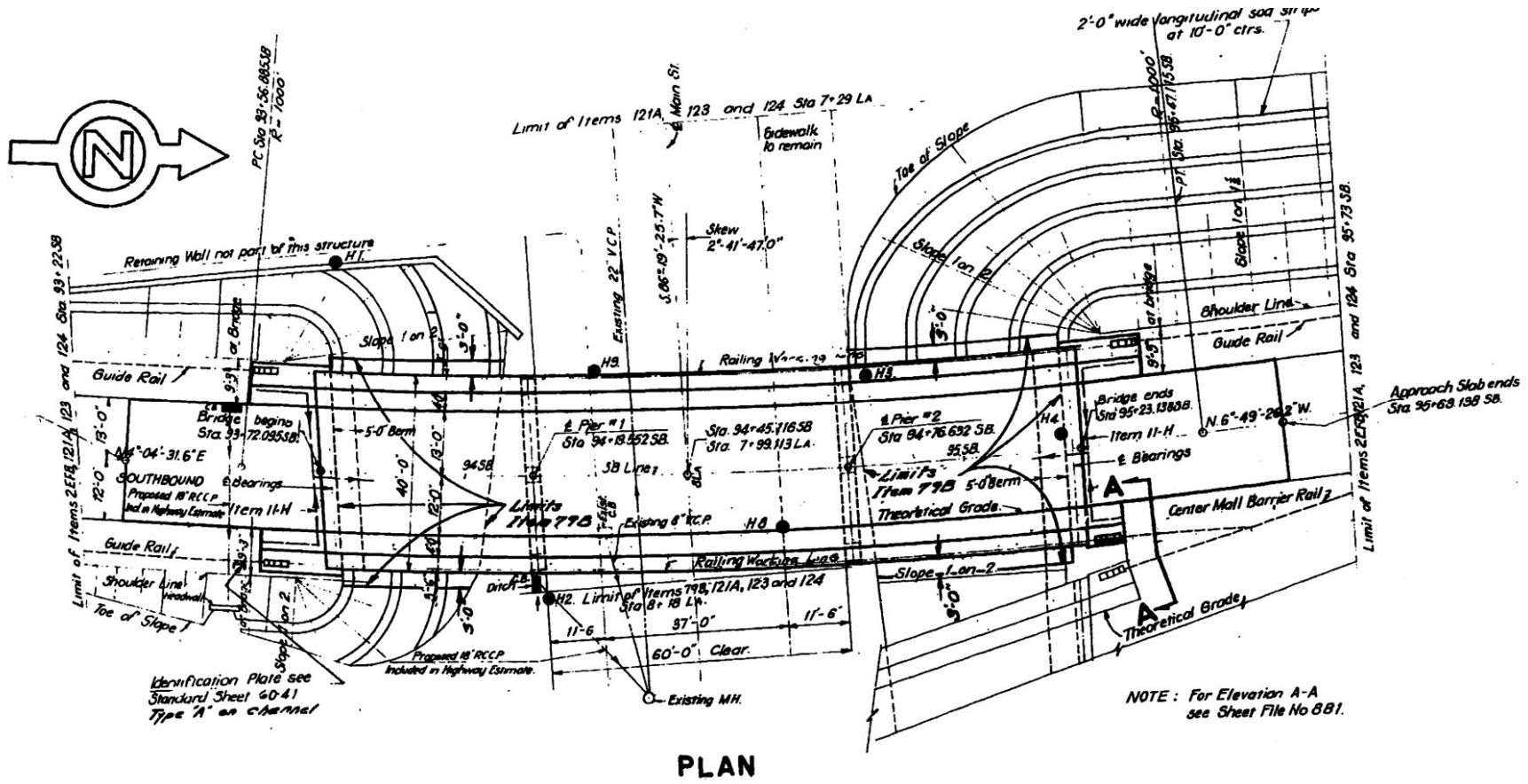

Figure 4.2 Plan of typical bridge

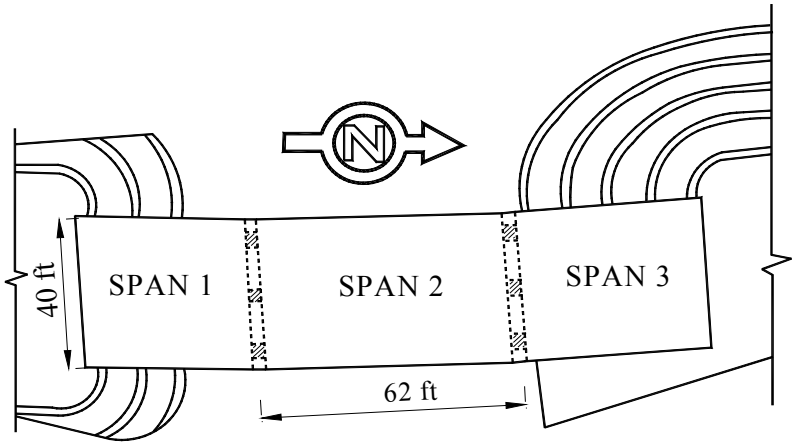

PLAN

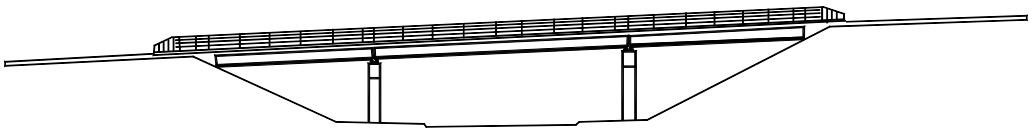

ELEVATION

Figure 4.3 Plan and Elevation of the typical bridge

Table 4.1 Parameters of the typical hypothetical bridge.

ITEM	VALUE
Redundancy	Non-continuous
Length of Maximum Span	62 ft
Number of Spans in Main Unit	3
Design Load	MS 18 or HS 20
Deck Width	40 ft
Deck Thickness	13 in.
Lanes on Structure	2
Height of Pier	16 ft
Number of Piers	3×(2 group) = 6
Pier section	Rectangular 3.0 ft × 3.0 ft
Material / Design Type	RC concrete pier, bent & deck, steel stringer

Figure 4.4 shows rebar detailing in piers and bent. It has been observed that

longitudinal rebars from piers go into bents as well as footings. Table 4.2 shows sections used for stringers. Another key member of the bridge is a bearing which defines the boundary condition of piers and stringers. Although the actual bridge has different types of bearings, elastomeric bearings are used in this research, since they are used extensively to replace old bearings.

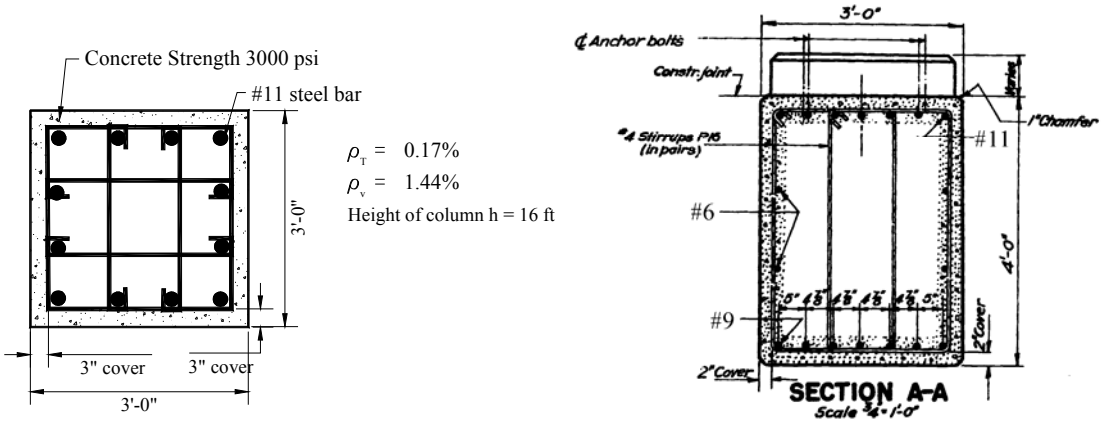

(a) Pier Section (b) Bent Section

Figure 4.4. Details of (a) pier (b) bent

Table 4.2: Sections Used for Stringers of the bridge

Stringer	Span	Stringer No. 1,6	Stringer No. 2, 3,4,5
	1	36WF150	30WF116
	2	36WF150	36WF150
	3	36WF150	30WF108
Diaphragm	Intermediate	16WF36	
	End	18C42.7	

4.2 MODELING OF BRIDGE MEMBERS

A detailed model of the bridge described previously has been built in LS-DYNA. Figure 4.5 shows the step-by-step procedure of modeling the bridge for simulation. For finite element simulation of the bridge, explicit solver in LS-DYNA has been chosen since it can handle a large number of elements. In LS-DYNA, elements can be meshed either by the Lagrangian mesh or the Eulerian mesh. Mesh nodes moves with material in Lagrangian mesh while material transfers among elements with fixed nodes in Eulerian mesh. Hence, the Lagrangian mesh is used for simulations with relatively small deformation. Constitutive equations can easily be applied to the Lagrangian element, which makes it suitable for simulation of structures. Although large deformations occur in bridge member elements subject to blast loads, element eroding technique is used to avoid severe element distortion during the simulation (calculation) of blast load effects.

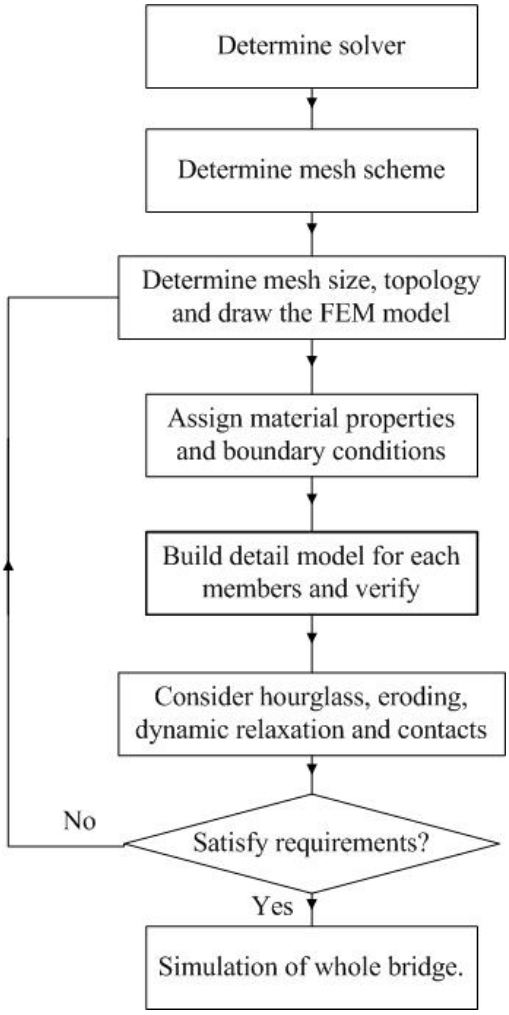

Figure 4.5: Step-by-Step Procedure of FEM modeling of the Hypothetical Bridge.

Traditionally, finite element analysis of bridges using commonly used software packages such as SAP2000, STAAD Pro, etc., is carried out by modeling typical members as frames. However, for blast simulation, since the geometry details may change the load characteristics significantly, a detailed bridge member shape using FEM modeling is desired. In addition, since the failure mechanism for bridge components under blast load is not well understood, a detailed finite element model should include as much details on bridge geometry and behavior as possible so that all failure modes could be identified. In this research, solid elements are used for most bridge members including footing, abutment,

pier, bent, bearing and deck. For stringers and diaphragms, shell elements are used since thin solid elements increase calculation time drastically and cause element distortion problem.

In the step-by-step procedure in Figure 4.5, behavior of each component should be investigated separately using available blast test data on bridge components, since blast test experiment of the full-bridge model is unlikely to be available. A detailed description on modeling of different components is described in the following.

Concrete Piers, Pier Bents and Footing

Pier consists of concrete core, cover and steel rebar, as shown in Figure 4.6.

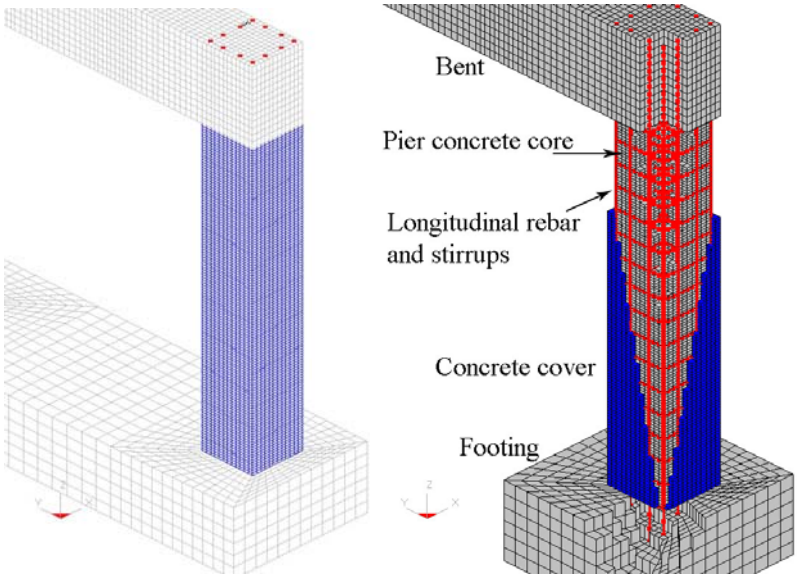

Figure 4.6 Modeling of pier

According to Krauthammer and Otani (1997), a detailed modeling of rebars is important for the simulation of blast load effects on concrete structures. Generally, reinforced concrete members are modeled by an equivalent monolithic element that can represent combined behavior of both concrete and steel during hazards such as

earthquakes, wind, etc. However, this type of monolithic element is not appropriate for reinforced concrete members subject to blast loads. This can be demonstrated by modeling a concrete column subject to blast loads (i) as consisting of pure concrete, (ii) by equivalent monolithic element and (iii) by modeling pure concrete and rebars separately. Figure 4.7 shows damages to the three types of columns because of blast loads. It is observed from Figure 4.7 that the column made of pure concrete shear completely in the area where blast load is the most significant. For the column modeled by an equivalent monolithic model, the column does not undergo significant damage except for spalling at the concrete surface. For the column with concrete and rebars modeled separately, a plastic hinge forms at the bottom of the column. It has been observed from recent experimental data on reinforced concrete columns that the results obtained for the third case, i.e., column with concrete and rebars modeled separately, are more reasonable [Magnusson and Hallgren (2004)].

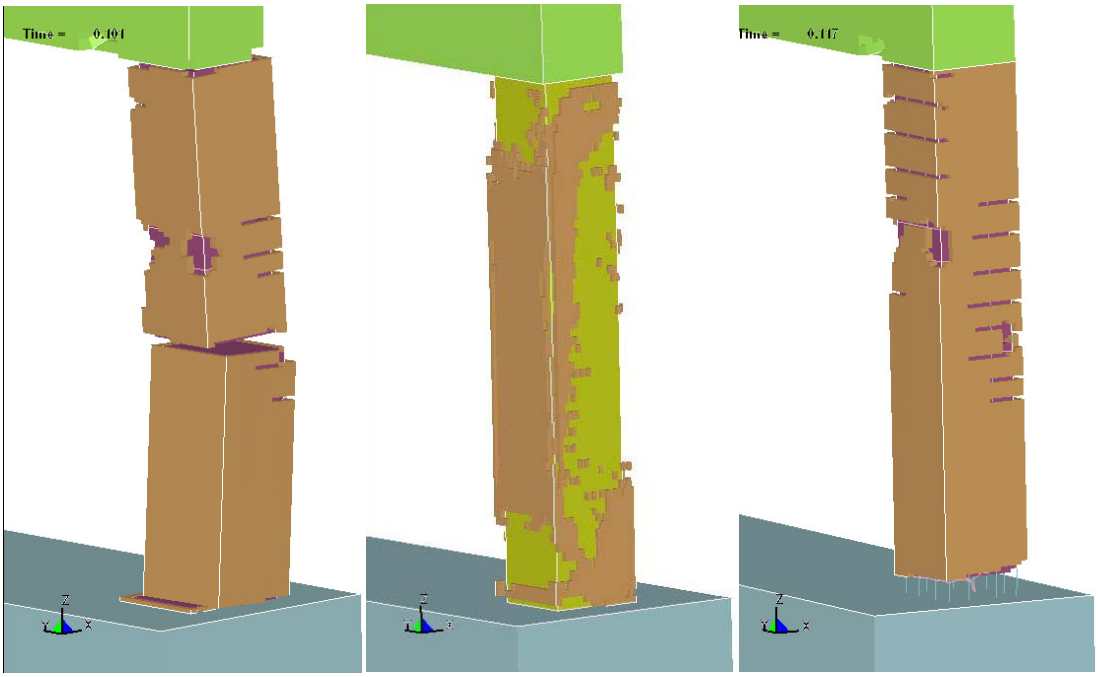

(a) Pure concrete column (b) RC col., monolithic model (c) RC col., separate model

Figure 4.7 Modeling of Reinforced Concrete Columns.

In modeling bridge piers, core concrete and cover concrete are modeled as separate layers to include confinement effects of rebars on core concrete. Longitudinal rebar have been extended into the footing and the bent as per as-built drawings of the bridge. Pier footings have been modeled as per construction drawings to assign correct boundary conditions under the bottom of the footing. A detailed modeling of the bridge pier, pier bent and footing has been done so that the failure mechanism of the pier system can be identified during a blast load event.

Stringer System

The stringer system in the bridge consists of wide flange girders with heights of 36 and 30 inches, 16 inches high wide flange middle diaphragms and 18 inches high channel end diaphragms, as shown in Figure 4.8. All stringers are modeled by shell elements.

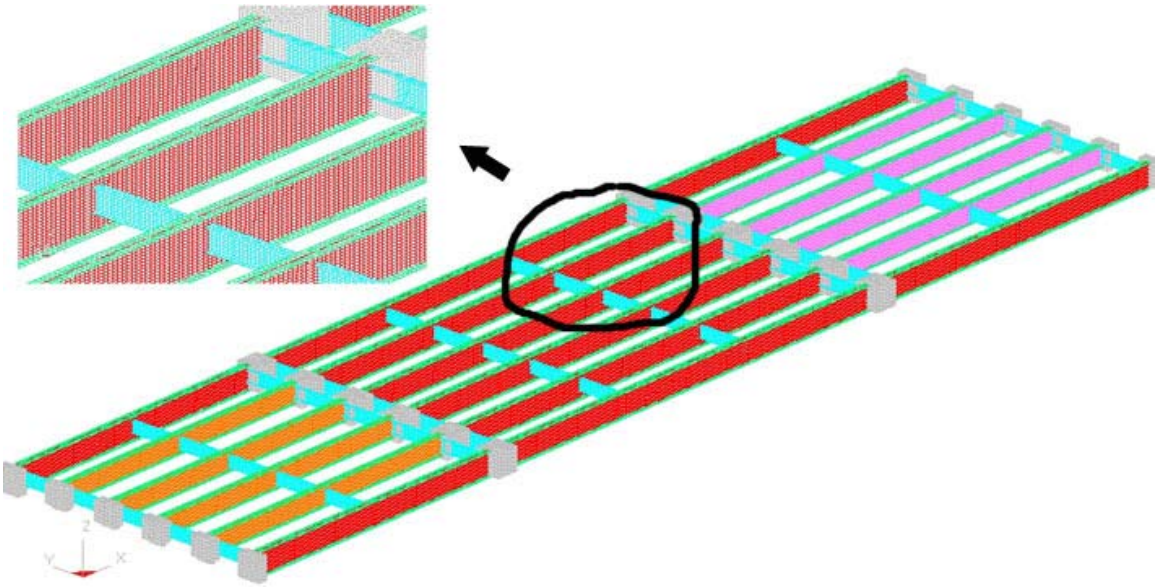

Figure 4.8 FEM modeling of stringer system

By modeling stringers by shell elements, shape of stringers, their height and stand-off distance can be modeled correctly. Accurate modeling of these features is very important for the identification of failure mechanism during the simulation of blast load effects on bridges. There are some stiffeners at the end of each stringer. However, in this research, we replace the support detail with a block which has equivalent weight and stiffness.

Deck, Abutment and Bearing

There are gaps between different decks, abutment and deck, as shown in Figure 4.9. The deck is discontinuous with the 3-inch gap. Contact functions are defined to evaluate the possible impact force aroused by touch between decks. Elastomeric bearing is studied in this research. Elastomeric bearing consists of elastomer and steel shims. It is less stiff in horizontal than in vertical direction so that it can accommodate the displacement of bridge superstructure. Literature review and detail FEM study have been carried for

bearing performance under blast load. The verification of the bearing model will be discussed in this chapter later.

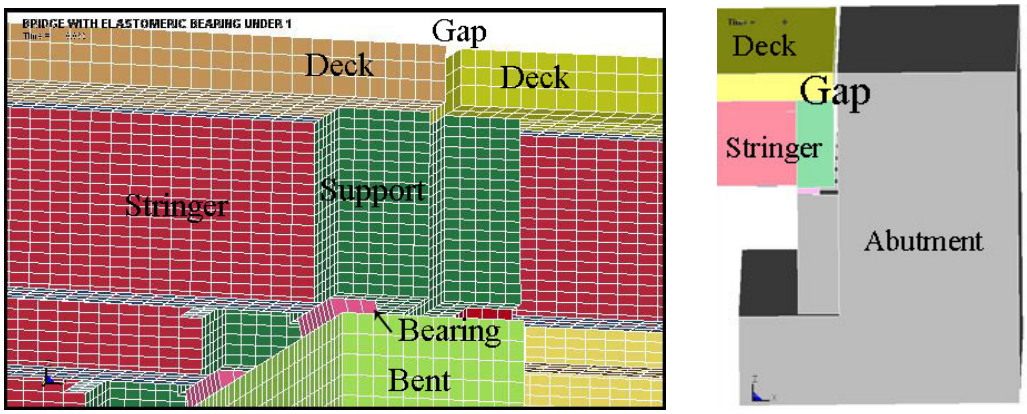

(a) Gap between decks (b) Gap near the abutment

Figure 4.9: Modelling of deck, Abutments and Bearings.

4.3 MATERIAL PROPERTIES AND CONSTITUTIVE MODEL

There are many existing concrete constitutive models to simulate blast load effects in LS-DYNA. Table 4.3 presents main characteristics of four of these models. Among these models, JHC concrete material model has been found to be the most appropriate to simulate blast load effects. JHC model is a computational constitutive model for concrete subjected to large strains, high strain rates, and high pressures; and is well-suited for both Lagrangian and Eulerian codes. The model is similar to smeared crack model, but is expanded to include material damage, strain rate effects, and permanent crushing as a function of the pressure and air void ratio [Holmquist et al. (1993)]. There are 26 parameters for JHC model, among which the failure type is the most important one to predict structure's failure mechanism.

Table 4.3 Constitutive model for concrete in LS-DYNA

No.	Name	Description	Concrete	High Strain Rate	Reinforced Concrete	Special for Large Strain
1	Plastic kinematic model	Von Misses Criteria, for metal in essential	No	Yes	No	No
2	Winfrith concrete model	Smeared crack model, 1995	Yes	Yes	Yes	No
3	JHC concrete model	By Holmquist et al. 1993	Yes	Yes	No	Yes
4	Microplane model M4	Smeared crack model, by Bazant et al. 2000	Yes	No	No	Yes

An example on the behavior of the JHC concrete model is illustrated in Figure 4.10 by simulating a quasi-static, uniaxial strain compression test. In Figure 4.10, concrete behaves essentially elastic from point 1 to point 2, although there is a small amount of plastic volumetric strain that occurs. At point 2, the yield surface is reached and equivalent plastic strain begins to accumulate. From point 2 to point 3, increase in equivalent plastic strain causes the material to damage, which in turn causes a gradual loss of cohesive strength. At point 3, the maximum strength is reached and the material continues to flow plastically and accumulate damage until the loading is reversed at point 4. From point 4 to point 5, the unloading is elastic. The yield surface is again encountered at point 5 and the material continues to flow plastically until the load is removed at point 6. Of special interest is the elastic unloading response between points 4 and 5. The unloading path is different than the elastic loading that occurs between points 1 and 2 due to the crushing of the material.

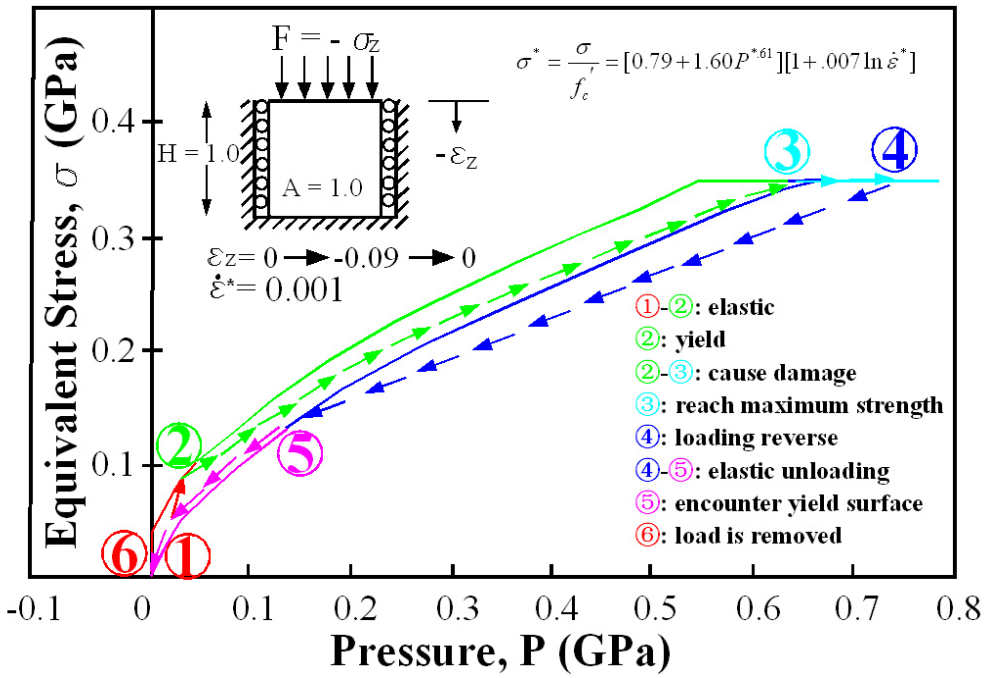

Figure 4.10 Example using JHC concrete model

The illustration in Figure 4.10 demonstrates elastic behavior, nonlinear behavior and damage of the material. Under extreme load, we also need the ability to "fail" the material. LSDYNA has 6 failure criteria besides failure time. These criterion are: maximum pressure criterion, maximum principal stress criterion, deviatioric stress criterion, maximum principal strain criterion, shear strain criterion and Tuler-Butcher criterion (impulse criterion) [Hallquist (1998)]. From the experience in seismic analysis, we know that structure does not fail because of load but because of displacement, since structural materials usually have ductility and can sustain more loads after yielding. In microscopic view of civil structures, material fails always by tension, not compression. Hence, we can choose the maximum principal strain criterion as a failure criteria for materials. Another competitive criteria is the Tuler-Butcher criterion [Tuler and Butcher (1968)]. This criterion is based on impulse implied on structures. It works well for high

pressure loads and can predict the spalling phenomenon very good. But if the simulation time is long and the structure sustains a relatively low pressure, it will overestimate the damage. Hence, this criteria is inappropriate for structures subject to blast loads.

Under the action of rapidly applied loads, the rate of strain increases, which can affect mechanical properties of structural materials significantly. Figure 4.11(a) and 4.11(b) show typical stress-strain curves for concrete and steel, respectively, including effects of high strain rates. A more clear explanation of properties of steel rebars can be found in [Malvar (1998)]), as shown in Figure 4.12. Main characteristics of strain-strain relationship observed in Figures 4.11 and 4.12 are as following:

First, all these material experiments are under monotonic loading. Repeated loading is usually not considered for blast loads. Second, the yielding stress of steel and the compressive strength of concrete are increased by more than 25% which is called high-strain rate effects. Third, percentage elongation at failure remain roughly unchanged for both concrete and steel [Fu et al. (1991)]. Fourth, ultimate strain is slightly reduced [Malvar (1998)], or the strain at maximum stress and rupture remain nearly constant according to TM-1300 [Army (1990)]. At last, elastic modulus remain the same for steel, or increase slightly for concrete.

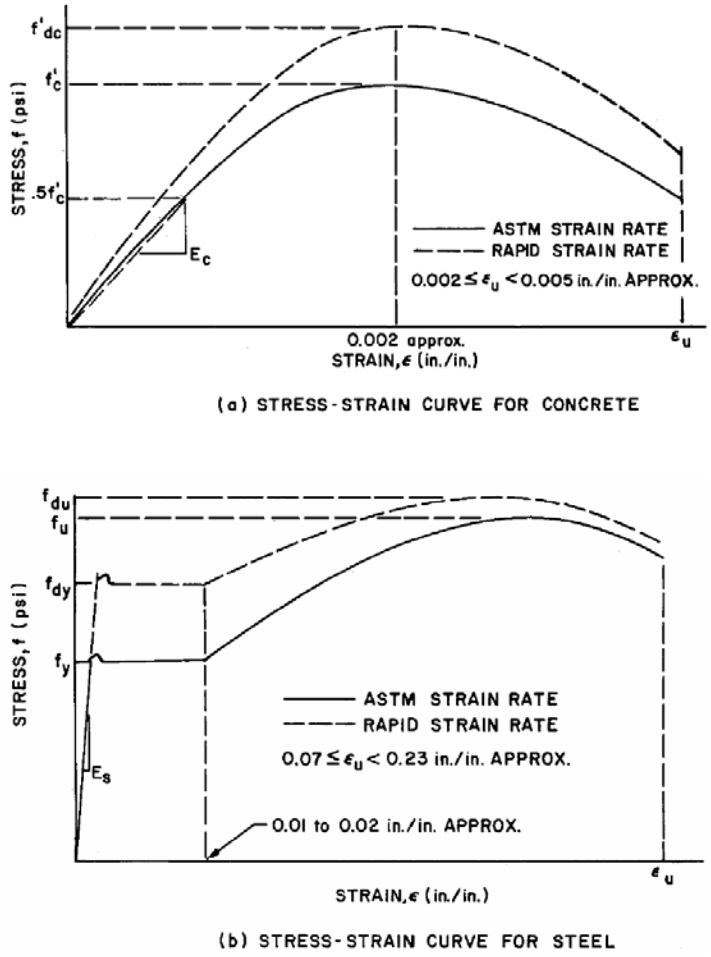

Figure 4.11 Typical stress-strain curves for concrete and reinforcing steel [Army (1990)]

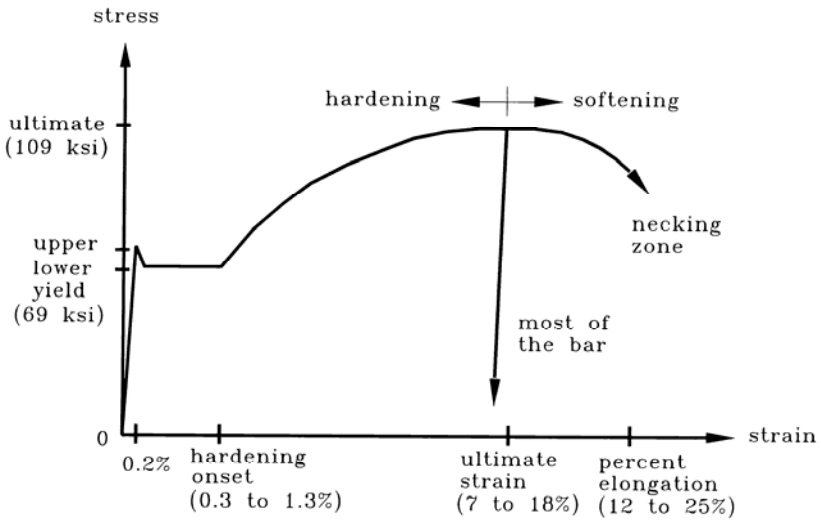

Figure 4.12 Stress-strain curves for steel reinforcing rebar [Malvar (1998)]

Current research shows that strain effects primarily increase structural material strength and have very little influence on the failure strain. Hence, strain rate effect is usually considered a factor of static yield stress [Drysdale and Zak (1985); LSTC (2003)]. This strain effect factor is only a function of strain rate and material intrinsic properties. Hence, tensile failure strain can be assumed as 0.002 for concrete cover, 0.005 for concrete core, 0.23 for reinforcing rebar and 0.20 for steel stringers on the basis of static experiments.

It should be noted that the values mentioned above are ultimate strains. If we use design values recommended by AASHTO [AASHTO (2002)], i.e., ductility factor 3 for concrete and 5 for steel, the failure strains will be much smaller. In this case, steel stringers close to the explosion will break, as shown in Figure 4.13. This is less likely to happen in reality when steel stringers are subjected to relatively low magnitude of explosion.

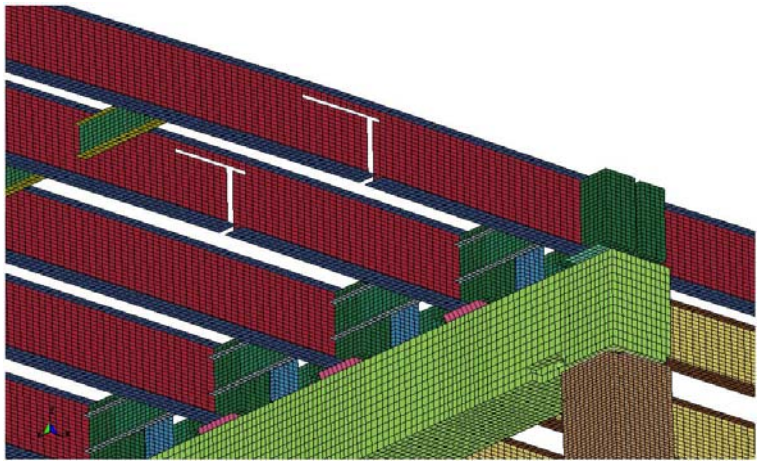

Figure 4.13: Failure of stringers at failure strain of 0.0059 during blast loads acting on a bridge.

4.4 ELASTOMERIC BEARING

Bearings in bridges are used primarily to allow movements of the superstructure caused by different loading conditions, such as temperature change, earthquakes, impact loads, etc. Bearing types are classified according to the bearing functions as shown in Table 4.4.

For expansion movements of 2 to 3 in. (50 to 75 mm), elastomeric bearings can be used in all types of bridges. For expansion movements up to 6 in. (150 mm), single rollers 6 to 10 in. (150 to 250 mm) in diameter and small rockers may be used. When movement exceeds 6 in. and may be as much as several feet (or approximately a meter), large rockers, connecting links, long compression arms, or rollers with gear racks are used.

Bearings with small rollesr, roller nests, and pin connections tend to get jammed or corroded frequently. Elastomeric bearings don't have these limitations and mostly move because of temperature changes [English et al. (1994)].

Table 4.4 Classification of Bridge Bearings by Function [TRB (1977)]

1.	Sliding plates
	a. Steel on steel
	b. Steel on bronze
	c. Lead sheets between steel plates
	d. Bronze plates with graphite inserts
	e. TFE sliding on stainless steel
	(1) Steel plates faced with TFE
	(2) Fabric pads faced with TFE
	(3) Elastomeric pads faced with TFE
	f. Felt, oil and graphite, tar paper
2.	Rolling devices
	a. Roller nests
	b. Single rollers
	c. Segmental rockers
	d. Pinned rockers
	e. Rack and pinions
	f. Steel balls
3.	Linkage or eyebar devices
	a. Simple link hangers
	b. Compression-tension struts
	c. Pin connections permitting rotation but no horizontal movement
4.	Elastomeric devices
	a. Simple elastomeric pads (or combined with TFE)
	b. Stacked pads with intermediate restraining layers
	c. Circular restrained or “pot” bearings
5.	Other devices
	a. Hydraulic cylinders or dash-pots
	b. Floating arrangements
	c. Spherical bearings
6.	Structural flexibility
	a. Timber structures
	b. Tall flexible piers
	c. Curved bridge designs

Although different types of bearings in Table 4.4 are generally used in bridges across

the country, the bridge model considered in this research only has elastomeric bearings. Elastomeric bridge bearings have been widely used throughout the United States and Europe since 1950's. These bearings are designed to carry vertical loads, and accommodate longitudinal movements of the bridge superstructure. They maintain compressive stiffness, shear stiffness and rotational stiffness while in service. The condition of these elastomer pads and the interface between pads and bridge consists of the support boundary conditions of the bridge superstructure. In the design of bridge girders, simple support conditions are normally assumed with no horizontal bearing restraint forces applied on the girders. Yazdani and Green (2000) have analyzed the influence of bridge elastomeric bearing stiffness on the performance of bridge girders. They found that a change of bearing stiffness for bridge with zero degree skewness angle causes 2% percent difference in maximum deflection and 23% in maximum tensile stress. Sen and Spillett (1994) studied this influence experimentally and obtained similar results. The focus of above studies has been on normal and long term service load, such as temperature change. Hoo Fatt and Ouyang (2006) have studied the behavior of elastomers at high strain rates lower than 400 s^{-1} and found that the elastomer stiffness increased when the strain rates was higher than 180 s^{-1} and decreased when the strain rates was between 180 s^{-1} and 280 s^{-1}. Typically, strain rate during blast load is generally between the order of 10^3 and 10^5 s^{-1}. These is very little or virtually no information available on behavior of elastomers during high strain rates encountered during blast loads. In this report, the performance of elastomeric bearing under high strain rate loads and its influence to the performance of bridge girders is investigated based on available information in the literature.

4.4.1 Literature Review on Mechanical Performance of Bearings

Elastomeric bridge bearings require significantly lesser maintenance as compared to other types of bearings and typically consist of a steel reinforced elastomeric pads bonded to a steel mounting plate, as shown in Figure 4.14.

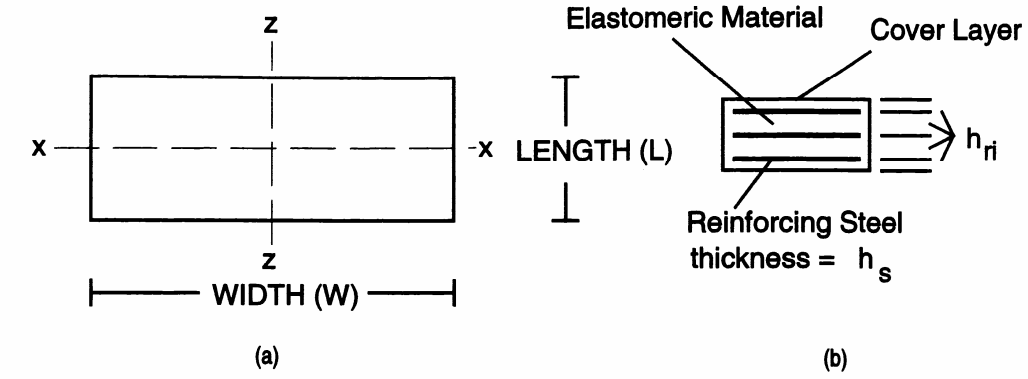

Longitudinal Axis (z-axis) = Axis parallel to the longitudinal axis of the bridge girder

Transverse Axis (x-axis) = Axis perpendicular to the longitudinal axis

h_{ri} = Thickness of elastomer layer number i

h_{rt} = Total elastomer thickness of the bearing = Σh_{ri}

h_s = Thickness of reinforcing steel shim

W = Width, Gross dimension of the bearing parallel to the transverse axis

L = Length, Gross dimension of the bearing parallel to the longitudinal axis

Figure 4.14: Detailed Layout of Elastomeric Bearings

Based on review of representative literature[e.g., Ash et al. 2002; Muscarella and Yura 1995; TRB 1977], mechanical properties of elastomers and elastomeric bearings are summarized in the following.

4.4.1.1 ELASTOMER

Compressive performance

The stress-strain curve of plain rubber pads based on laboratory tests for

compressive stiffness is shown in Figure 4.15. The slope of the load displacement curve in Figure 4.15 is found to be 27.6 kN/mm (157.7 kips/in) which, gives a compressive modulus of E_c = 15.8 MPa (2,291 psi) using h_{rt} (total elastomer thickness of the bearing) = 46.5 mm (1.83") and A (cross-sectional area) = 0.0813 m^2 (126 in^2).

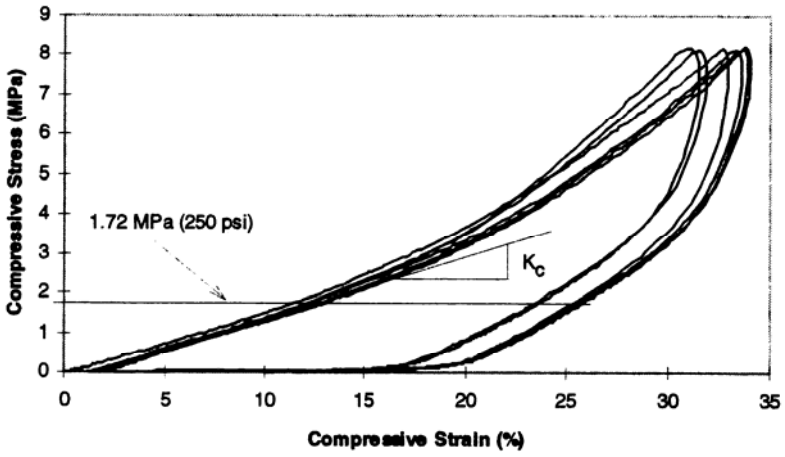

Figure 4.15: Compressive Stress-Strain Relationship For Plain Rubber Pads

The maximum compressive stress of elastomer is affected by the following two factors:

i). Bulging of the elastomer under compressive load results in the compressive deformation of the bearing. Elastomeric materials with lower hardness ratings have very little volumetric change. Volumetric change of the material becomes more significant with an increase in the hardness of the elastomer. In most cases, the elastomer material is damaged in tension due to bulging.

ii). Ability to resist shear stress also affects the maximum compressive stress because the bulging due to compressive load creates shear stress in the material.

Shear performance

Shearing behavior of bearings is necessary to accommodate longitudinal movements of the bridge superstructure caused by external loads, such as thermal, earthquakes. Shear strain of a bearing is defined as the shear deformation divided by the original elastomer thickness before compressive loading. Shear strain is directly proportional to the applied shear force and an increase in shear strain increases the possibility of slip failure of the bearing. Current AASHTO design specification [AASHTO (2002)] requires the shear strain to be less than 50 percent of the pre-loading elastomer thickness to keep stresses in the elastomer low. However, failure in elastomers has been observed in experimental tests only when the shear strains was excess of 100%. In simulation of shear failure of elastomeric bearings in this report, we are using 150% shear strain as the shear failure criterion.

Tensile performance

When a tensile force is applied on the elastomer sample, stiffness of the elastomer remains the same as in case of compressive loading until 3 ksi stress. With increase in tensile load beyond this threshold, tensile stiffness dropped to 5% of the original stiffness and the tensile strain develops quickly. In general, tensile strain has been found to be in the range of 200% - 600% at the time of failure of the elastomer [Constantinou (2006)].

4.4.1.2 ELASTOMERIC BEARINGS

Compressive performance

Reinforcing steel shims offer a good confinement to the bulging of elastomers and increase the compressive stiffness of elastomeric bearing significantly. A nominal 0.7 MPa

(100 psi) shear modulus reinforced (2 steel shims) bearing has been found to yield a load-displacement curve with a slope of 181 kN/mm (1033 k/in) between loads of 3.45 and 10.35 MPa (500 and 1500 psi) and a compressive modulus of 101.2 MPa (14,675 psi). This is a significant increase over the unreinforced speciment of elastomer [Muscarella and Yura (1995)].

Muscarella and Yura (1995) has presented the reinforced bearing compression test stress-strain relationship shown in Figure 4.15. AASHTO requires that the average unit pressure due to combination of dead loads and live loads on unconfined elastomeric bearings should not exceed 5.5 MPa (800 psi). Minimum pressure on the pad should be not less than 1.4 MPa (200 psi) to prevent the tensile failure. A linear stress-strain relationship is reasonably assumed for elastomeric bearing in this loading range according to Figure 4.15. At approximately 59.6 MPa (8640 psi) the steel shims yielded and the compressive stiffness of bearing decreased. Debonding along the elastomer/steel interface occurred at 86.2 MPa (12,500 psi) and 105 MPa (15,250 psi). The stress level is so high that the reinforcement approaches fracture even the bond is still intact in some regions. At 124 MPa (18,000 psi), the bearing lost its compressive capacity because of the fracture of steel.

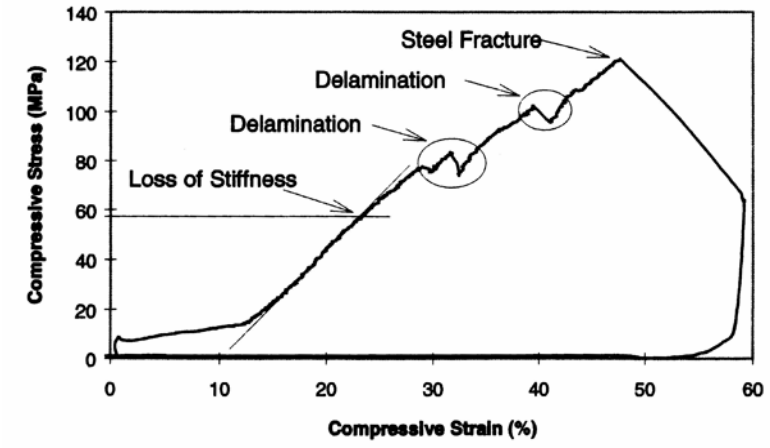

Figure 4.16 Reinforced bearing compression test stress-strain relationship

Shear performance

Shear capacity of elastomers is mostly unaffected by steel shims. It is much more likely that delamination of bond between steel/elastomer interface will occur before shear failure of an elastomeric bearing.

Tensile performance

Ash et al. (2002) have tested bond between elastomers and steel following ASTM D 429 B procedures. The peel test showed that in 100% adhesion case, the peel strength was in the range of 20 MPa to 25 MPa in case of 100% adhesion. This is comparablre to the tensile strength of elastomer in the range of 22.31 MPa to 26.06 MPa. The elongation in elastomer at failure was 420% - 470%.

4.4.2 FEM Modeling of Elastomeric Bearings

4.3.2.1 MECHANICAL PROPERTIES

A 3-steel-shim elastomeric bearing with durometer hardness of 56 was selected for the FEM analysis. The dimension is 22 inches in width and 9 inches in length. There are 4

layers of 0.5 inch thick elastomer. The thickness of steel shim is 0.1 inch. Mechanical properties of the elastomer, steel and the bearing based on the literature review are presented in Table 4.5.

Table 4.5: Mechanical Properties of the Elastomer, Steel and the Elastomeric Bearing

Elastomer	Density	1150 kg/m3	1.076E-04 lbs2/in4
	Poisson's ratio	0.4997	
	Bulk modulus	2000-2200 MPa	290 - 319 ksi
	Compressive strength	Approx. 1000 MPa	145 Ksi
	Short time shear modulus	0.5 - 4.0 MPa	72.5 - 580 psi
	Long term shear modulus	0.5 -1.6 MPa	72.5 - 232 psi
	Shear failure strain	1.5	
	Tensile stiffness	At low strains, equal to the compressive modulus	
	Tensile Strength	15 - 30 MPa	2175 - 4350 psi
	Tensile failure strain	200 - 600%	
Steel	Density	7800 kg/m3	7.295E-04 lbs2/in4
	Yield stress	276 MPa	40 ksi
	Elastic modulus	210000 MPa	3.05E+7 psi
	Failure strain	0.23	
Bearing	Compressive modulus	113 MPa	16462 psi
	Stress at loss of stiffness (compressive)	84.8 MPa	12300 psi
	Fracture stress (compressive)	140 MPa	20300 psi
	Short time shear modulus	0.596 MPa	86.4 psi
	Long term shear modulus	0.539 MPa	78.2 psi
	Shear failure strain	1.5	
	Tensile strength	25 MPa	3626 psi

4.4.2.2 FEM MODELING

Since the failure modes of elastomeric bearings are mainly caused by the yielding of steel shims or delamination of steel/elastomer interface, it is necessary to model these two

materials separately in the finite element model to identify these failure modes. In our FEM model of Elastomeric bearings, elastomeric layers are modeled by solid elements and steel shims by shell elements. Elastomer and steel shim elements are connected together at shared nodes. The steel/elastomer interface is not modeled separately in the FEM model since the peel strength of steel/elastomer interface is almost the same as tensile strength of elastomer [Ash et al. (2002)]. Hence, eroding of elastomer elements in this FEM simulation means tensile failure of elastomer and it can also imply delamination of steel/elastomer interface.

Material behavior of elastomers is simulated using linear viscoelastic material model in LS-DYNA (Mat 6). This model is for rubber material and can consider the rate effects by a convolution integral of stress tensor. However, strain effects of elastomer have been ignored in this study because of the lack of data on the performance of elastomers during blast events. Tensile stiffness was assumed to be the same as the compressive stiffness. Hence, tensile strength instead of tensile strain controls the failure of bearings. Plastic kinematic material model (material Mat 3 in LS-DYNA) has been used to characterize behavior of steel shims. This material model is suited to model isotropic and kinematic hardening plasticity with the option of including rate effects.

Generally in finite element modeling of structures, a finer element mesh gives more accurate results. However, this may not be true in case of modeling of elastomer and steel plates separately. For example, Figure 4.17(a) shows the finite element model of Elastomeric bearings where every layer of elastomer has been modeled by several layers of solid elements. Figure 4.17(b) shows the deformed shape of the bearing under the application of uniform pressure on top of the bearing. It is observed from Figure 4.17(b)

that the elastomer elements in the edge which are not connected to steel shims deform significantly, resulting in the failure of the bearing well before the experimental failure strength.

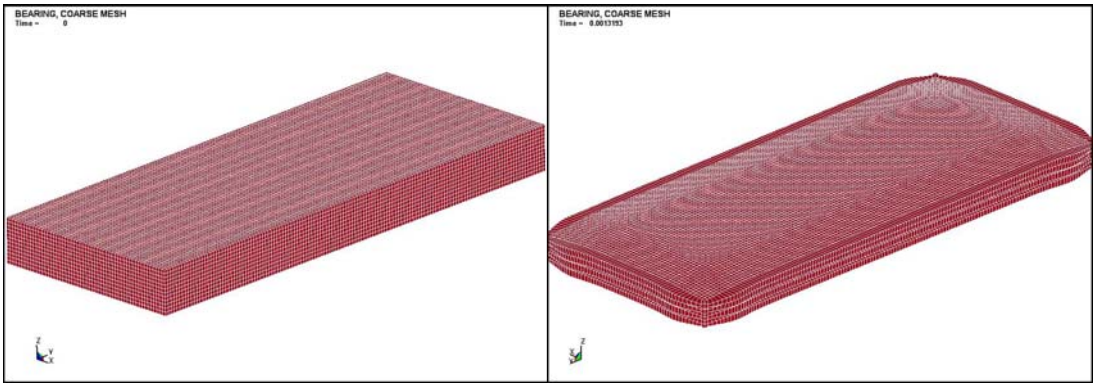

(a) Bearing model (b) Deformed shape

Figure 4.17 FEM bearing model with fine mesh

The fine mesh model of bearings in Figure 4.17(a) also cannot account for confinement of elastomers between steel shims/plates and friction between elastomer and steel shims/plates. In order to simulate these effects correctly, a coarser mesh, where every elastomer layer is modeled only by one layer of solid elements, is developed, as shown in Figure 4.18. Table 4.6 shows parameters of the elastomer that have been used in the bearing model in Figure 4.18. Table 4.8 shows a comparison between properties of elastomeric bearings observed through numerical simulation to those from experimental results [Muscarella and Yura (1995)].

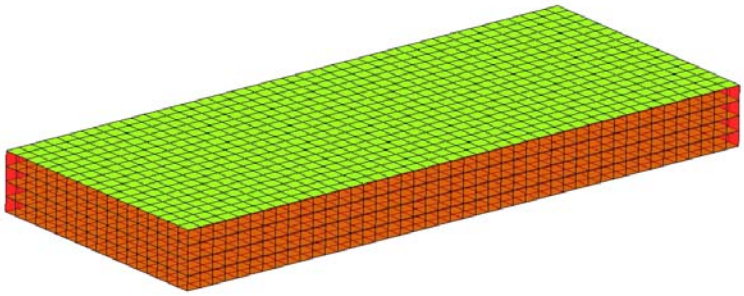

Figure 4.18 Elastomeric model with coarse mesh

Table 4.6 Selected parameters for elastomer material in FEM model

Bulk modulus	12050 psi
Shear modulus	86 psi
Tensile failure strain	0.305
Compressive failure stress	20300 psi

Table 4.7 shows that the compressive modulus and tensile strength predicted by the FEM model. It is observed that compressive modulus and tensile strength of the bearing in Figure 4.18 matches with values observed during experiments. The compressive strength of the bearing in Figure 4.18 falls on the lower side of the range of variation observed during experiments. Compressive strength of bearings during experiments varies from 12,300 to 20,300 psi because of yielding of steel shims and hardening of steel material. Since elasto-plastic stress-strain relationship is assumed for steel material , the bearing will fail quickly in tension because of bulging of elastomer after initial yielding of steel shims. Hence, matching of compressive strength of bearings in the lower range is reasonable during numerical simulation. On the other hand, bearings during numerical simulations fail at 35.6% tensile strain where as tensile failure during experiments has been observed in the range of 200-600%, even though tensile failure strength is the same. A more detailed material model of elastomers based on experimental results is required to capture this

tensile stra behavior in numerical simulation. In this report, this issue has been addressed by considering tensile strength, instead of tensile strain, as the failure criterion because of lack of detailed information on tensile behavior of Elastomeric bearings. Hence, comparison in Table 4.7 show that the finite element model of bearings in Figure 4.18 captures mechanical characteristics of bearings observed during experiments fairly well. Failure of bearings based on tensile strength criteria indicates delamination between elastomers and steel shims before complete tesile failure occurs at much higher tensile strains.

Table 4.7. Validation of FEM bearing model

	Calculation	Experiment
Compressive modulus	16463.4 psi	16462 psi
Compressive strength	14564 psi	12300 – 20300 psi
Tensile strength	3679.5 psi	3625 psi
Tensile failure strain	35.6%	200% - 600%
Shear failure strain	61.9%	-

4.5 FINITE ELEMENT MODEL OF THE WHOLE BRIDGE

A detailed finite element model of the whole bridge has been developed in LS-DYNA. First of all, bridge footings are constructed using solid elements and fixed boundaries at the bottom of footings, as shown in Figure 4.19(a).

Rebar cage for concrete piers has been developed by modeling rebars by beam elements, as shown in Figure 4.19(b). Rebars extend into the footings and bent beams as per rebar detailing on as-built bridge drawings. Figure 4.19(c) shows the details of rebar detailing in footings, pier and bent beam.

Core concrete is added to the rebar cage and cover concrete is added as a separate layer with different material properties on top of core concrete. Bent beam is added on top

of concrete piers.

Elastomeric bearings are modeled as a block consisting of layers of elastomers and steel shims connected by shared nodes. Elastomeric bearing blocks are added on top of pier bents at locations specified in bridge drawings. Steel stringers and diaphragms, modeled by shell elements, are added next, as shown in Figure 4.19(e). Steel Stringers are connected to elastomeric bearing blocks through shared nodes. Deck, constructed by using solid elements, is added next, as shown in Figure 4.19(f).

The bridge structure model is put into air mesh so that the blast air wave load can be transferred to the structure. Hence, an air ALE mesh, as shown in Figure 4.19(g), is created by setting reflecting boundary condition at the bottom of the air block to simulate the reflected blast waves from the ground. Other air block surfaces have non-reflecting boundary conditions.

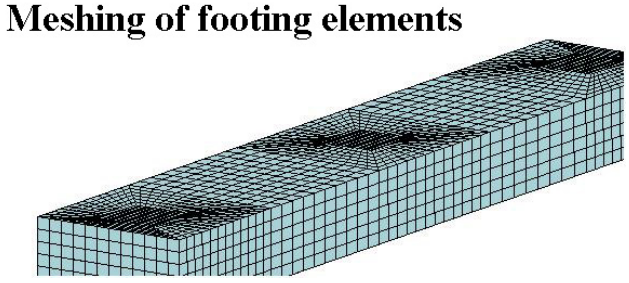

(a) Add footing

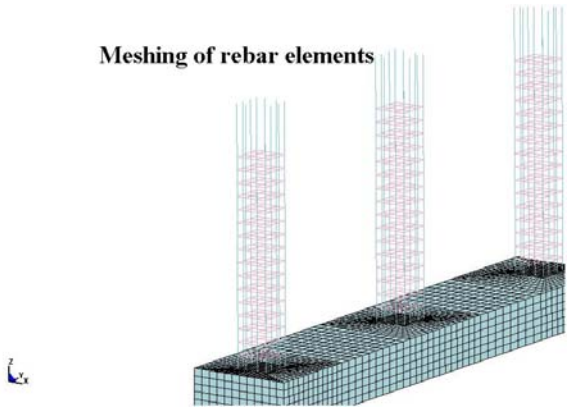

(b) Add rebar cage for concrete pier

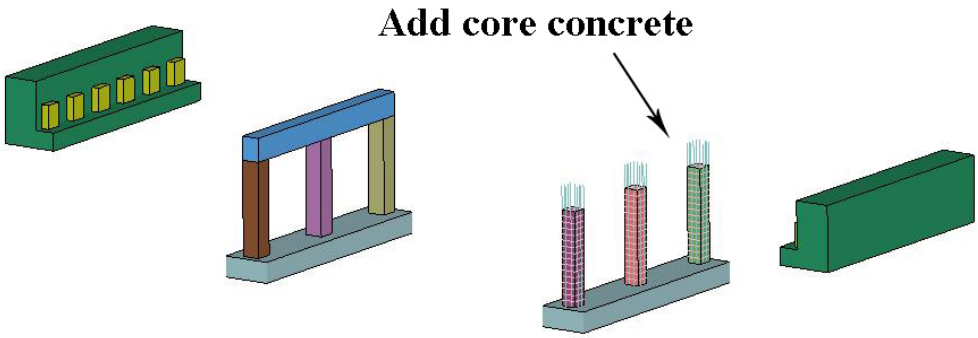

(c) Add core concrete, surface concrete of concrete pier and pier bent

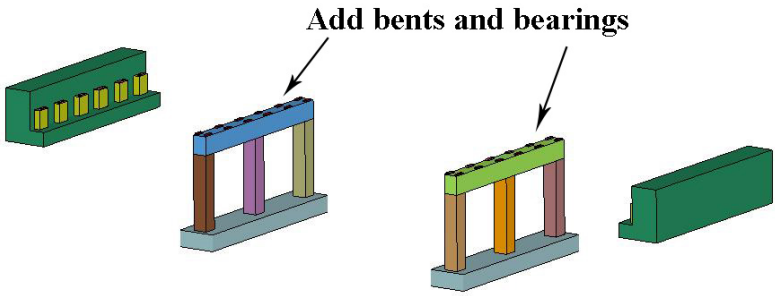

(d) Add bearing

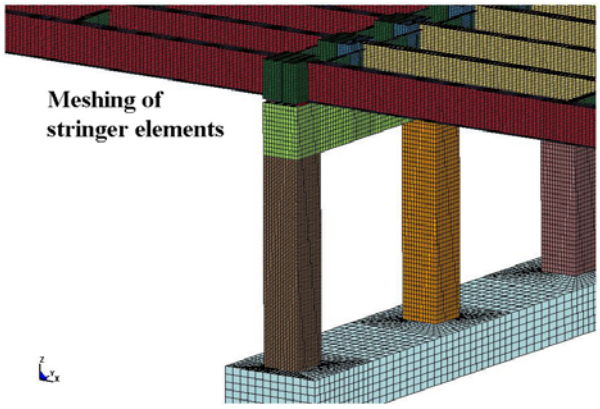

(e) Add stringer

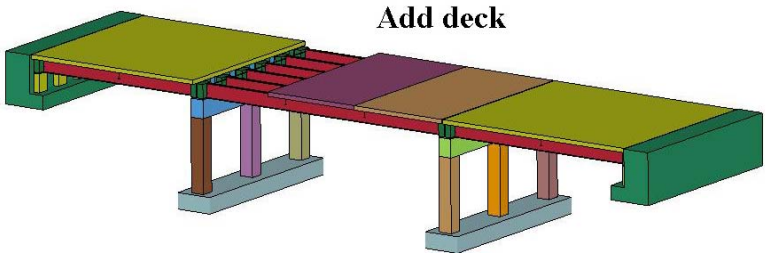

(f) Add deck

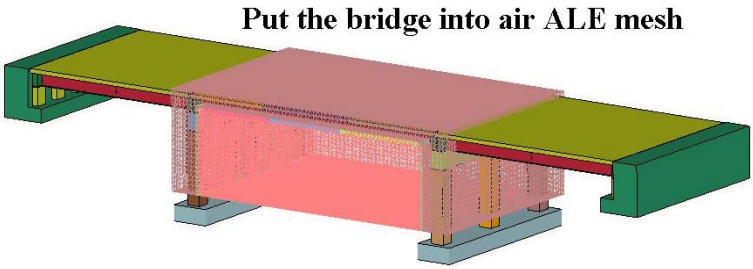

(g) Put the bridge model into air ALE mesh

Figure 4.19 FEM modeling of bridge under blast load in LS-DYNA

4.6 HOURGLASS, GRAVITY LOAD, DYNAMIC RELAXATION AND CONTACTS

HOURGLASS EFFECTS

In the simulation of high strain rate problem by the explicit method, small damping is usually added into the system to avoid a numerical problem called "Hourglss" because of one-point integration [Hallquist (1998)]. Undesirable hourglass modes tend to have periods that are typically much shorter than the periods of the structural response, and they are often observed to be oscillatory. Hourglassing technique helps in avoiding all numerical stability problems caused by zero energy modes, which means the explicit method with small damping is not suitable to study buckling problem for structure under high strain rate loads.

GRAVITY LOAD AND DYNAMIC RELAXATION

Gravity loads are applied as body force and are important in simulation of blast load effects on structures [Krauthammer et al. (1997)]. In the simulation using explicit solver, all the loads, including gravity loads, are applied as dynamic loads. As a results, effects of gravity loads also undergo dynamic magnification. This undesirable dynamic effect is removed by dynamic relaxation, which essentially creates a critically damped dynamic system to attenuate the dynamic effects quickly. As a result, using dynamic relaxation, undesirable dynamic effects are eliminated after a simulation time equal to structural natural period. During the application of blast loads on the bridge, dynamic relaxation is applied to the case of gravity load case only in the beginning. Once dynamic effects of gravity loads are neutralized after simulation for first 30-40 milliseconds, and blast loads are applied after removing the dynamic relaxation condition. Hence, stresses in the bridge components because of dynamic relaxation act as initial condition for the blast load analysis. The duration of simulation during dynamic relaxation is not included in the simulation time of blast loads, i.e., t = 0 at the instant of application of blast loads. Effect

of dynamic relaxation is illustrated using stress time history in Figure 4.20 at mid-span of the stringer system in the three-span bridge. Considering the weights of non-structural elements and live loads, gravity load would cause approximately 9.4 ksi initial stress in the girder flange. This value has been verified using simpler FEM model in SAP2000. Without dynamic relaxation, it is observed from Figure 4.20(a) that although initial stress is zero, it varies between 0 to 0.5 ksi during 100 milliseconds of simulation time. On the other hand, the stress is constant around 9.4 ksi using dynamic relaxation. Simulation of blast load effects is also different with and without dynamic relaxation, as shown in Figure 4.19(b). It is observed that stresses in flange of the stringers at the mid-span without dynamic relation are almost 40% higher that those using dynamic relaxation.

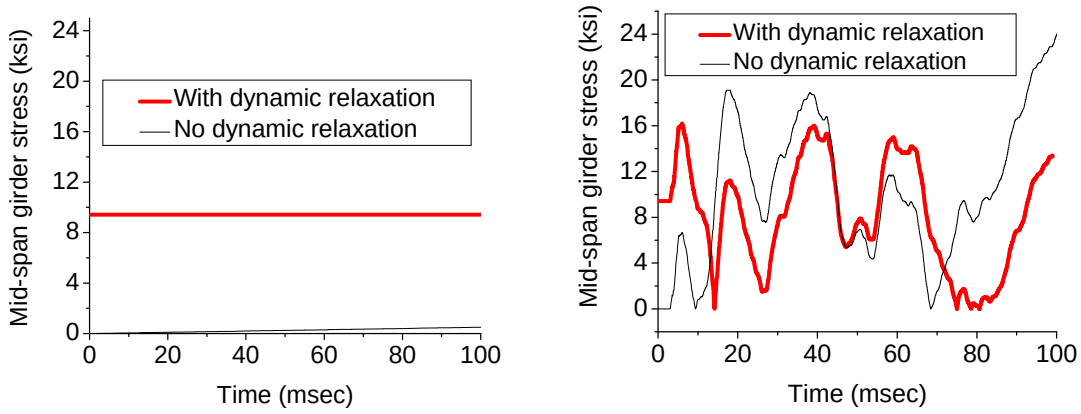

(a) Dead load only (b) Blast Load

Figure 4.20 Effects of dynamic relaxation

CONTACTS

In the bridge blast simulation, after the shared nodes get eroded, we need to consider extra contacts between different bridge members and fragments. For example, after the pier is sheared away from the footing under lateral blast wave load, we should define the

contact between pier and footings. Otherwise, the pier will pierce into the footing without any counterforce from the footing, as shown in Figure 4.21.

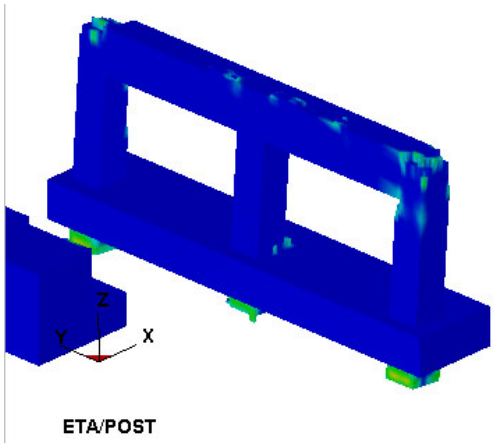

Figure 4.21 Pier piercing into footing because of lack of contact definition in simulation

Similarly, we also need to define contact between deck/stringer, stringer/bent, bearing/bent, and bent/pier.

4.7 NONLINEARITY

Simulation of blast loads on bridges is a highly nonlinear problem because of both geometric and material nonlinearities. Structural components undergi large displacement during a blast loading event. For example, shear displacement of pier is several inches before failure. Middle span deflection of stringer system goes may be 1-2 ft, or 1/30 of the span length. Contact and eroding techniques are helpful in dealing with large displacement problem during blast loads on highway bridges.

Besides large displacement, structural member may also undergo large strains, Structure steel or steel rebars can exhibit plastic strain as high as 20%. The large strain in an element results in extra forces applied on the element because of the P-Δ effects. P-Δ

effects must be considered in finite element model of blast loads on bridges.

Material nonlinearity governs structure behavior because of significant damages to structural member. This behavior is illustrated using hysteretic behavior of pier concrete subject to blast loads. First, we consider an element in the concrete core at the bottom of the pier, as shown in Figure 4.22. Plots of vertical stress versus stain because of blast loads acting on the pier are shown in Figure 4.23 for low, medium and large levels of blast loads.

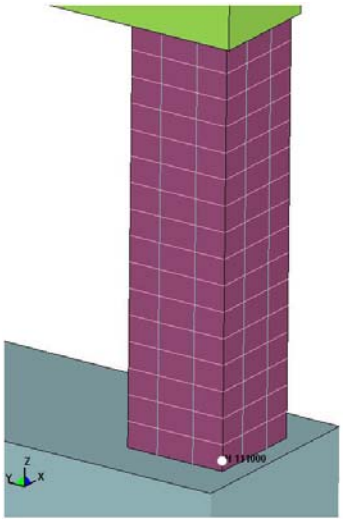

Figure 4.22 Bottom Element of core concrete in Pier

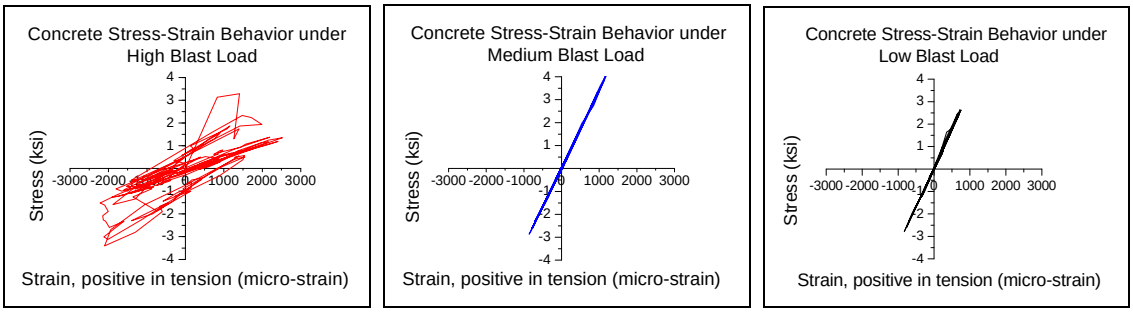

(a) high load (b) medium load (c) low load

Figure 4.23: Stress-Strain Plots of Core Concrete Element Near Bottom of the Pier.

It is observed from Figure 4.23 that the core concrete material near the pier bottom is elastic under low and medium levels of blast loads. However, , the core concrete bursts into large nonlinear strain and then rebounds back when the pier is subject to high level of blast loads. High strain rate effects are also shown in this figure. The highest concrete stress reaches approximately 4 ksi while the comrete compressive strength is 8 ksi. Consequently, core concrete undergoes nonlinearity both in tension and compression under the interaction forces from bridge superstructures. Similar to seismic hysteretic behavior, the material is damaged and plastic strain accumulates.

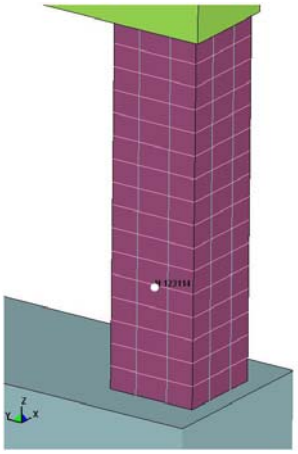

Figure 4.24 Core concrete elements at the pier directly facing the blast wave center

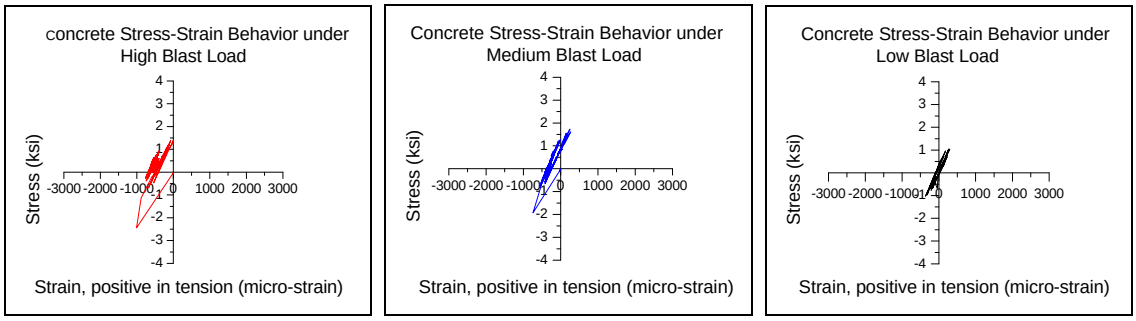

(a) high load (b) medium load (c) low load

Figure 4.25 hysteretic graph of pier concrete element facing the blast wave

Figure 4.25 shows vertical stress-strain plot of pier concrete facing the blast wave at a point shown in Figure 4.24. It is observed that the concrete facing air blast waves undergoes compression. It is observed that concrete demonstrates predominantly nonlinear behavior during all three levels of blast loads, although strain magnitude is smaller than that in Figure 4.23.

Figure 4.26 shows vertical stress-strain curves for core concrete at the back of the pier, i.e., on the surface that is behind the surface directly exposed to blast loads. It is observed from Figure 4.26 that the core concrete shows highly nonlinear behavior for all levels of loading. After the compressive blast load hits pier surface, the compressive stress wave propagates in concrete material. When the compressive wave meets the back surface of pier, it changes into tensile stress wave and reflects back, causing tension strain on the back surface. The core concrete material is in tension first because when the compression blast wave load is reflected from the back surface of pier, it becomes a tension wave.

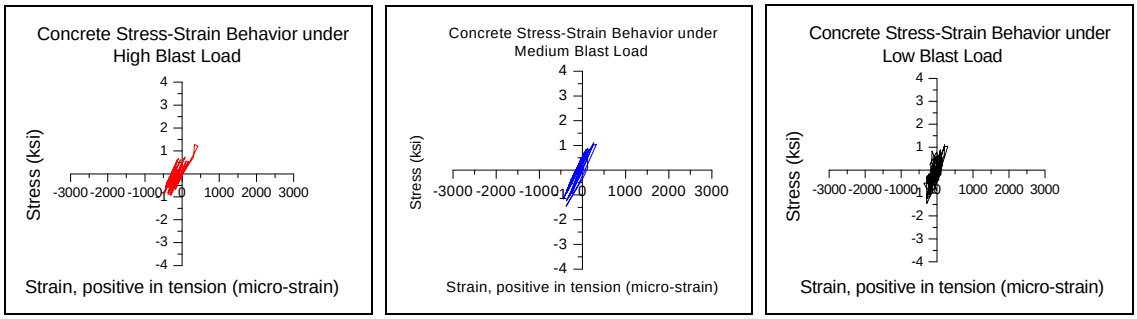

(a) high load (b) medium load (c) low load

Figure 4.26 hysteretic graphs of core concrete elements of the pier back surface

Following observations on behavior of bridge components subject to blast loads can be made from the above example:

1. Both local and global damage modes exist in bridges subject to blast loads.
2. Global damage mode for bridge under blast loads is similar to that for seismic loads. It is in elastic range during low and medium levels of load and goes into inelastic range during high level of blast load. .
3. Local damage can lead the core material into nonlinear region, even under low level of blast load.
4. Global damage mode (such as plastic hinge formed in the middle of column) has bigger energy absorption ability than the local damage mode (such as compressive failure of concrete which directly facing the blast wave load). Hence, designing bridges that fail in global mode before failing in local mode can lead to better blast load resistance in bridge components.

CHAPTER 5 BEAM AND COLUMN ANALYSIS

Detailed description on the finite element model of a highway bridge subject to blast loads has been presented in Chapter 4. Because of the highly nonlinear damage processes involved in the simulation of blast loads on bridge components, calibration or correlation of finite element model parameters, such as simulation time step, and mesh size, with observed or experimental data is required. Unlike elastic finite element problems where finer mesh size and smaller time steps give better results, mesh size in case of highly nonlinear problem encountered during blast loads may depend on material characteristics. Likewise, too small a mesh size may create stability problems. Hence, calibration of time step and mesh size for the highway bridge model is carried out using selected blast experimental results on a beam and a column, since data on blast tests on bridge components are not available in literature.

5.1 EXPERIMENT MODELS FOR CALIBRATION OF MESH SIZES

Since blast test data on bridge components are not available, one can carry out the calibration of mesh size by using blast test data on components made of similar material types, e.g., reinforced concrete, steel, etc. Although this process doesn't ensure that the results using calibrated model will be accurate, results are expected to be better than the case when FEM parameters are selected using parametric analysis of the FEM model itself. During the literature search, it has been observed that very few tests on blast loads on structural components are available in the literature. In this report, we use blast tests data on two reinforced concrete beams by Magnusson and Hallgren (2004) for the calibration of concrete member mesh sizes and time step control. Figure 5.1 shows elevation and

cross-sectional area of the beam. Table 5.1 shows strength properties and tensile reinforcement of the two beams. The concrete beams were assembled in a test rig, which was positioned in the test area of the shock tube (1.6m×1.2m) as shown in Figure 5.2. Table 5.2 presents the results from the air blast tests.

Table 5.1 Strength Properties of the Two Beams.

Beam type	f_{cc} [1] (MPa)	Tensile reinforcement	Reinforcement ratio	f_{sy} (MPa)
B40	43	5Φ16 mm	0.34	604
B100(12)	81	4Φ12 mm	0.087	555

1 Refers to the concrete compressive strength of $\Phi 150 \times 300$ mm cylinders.

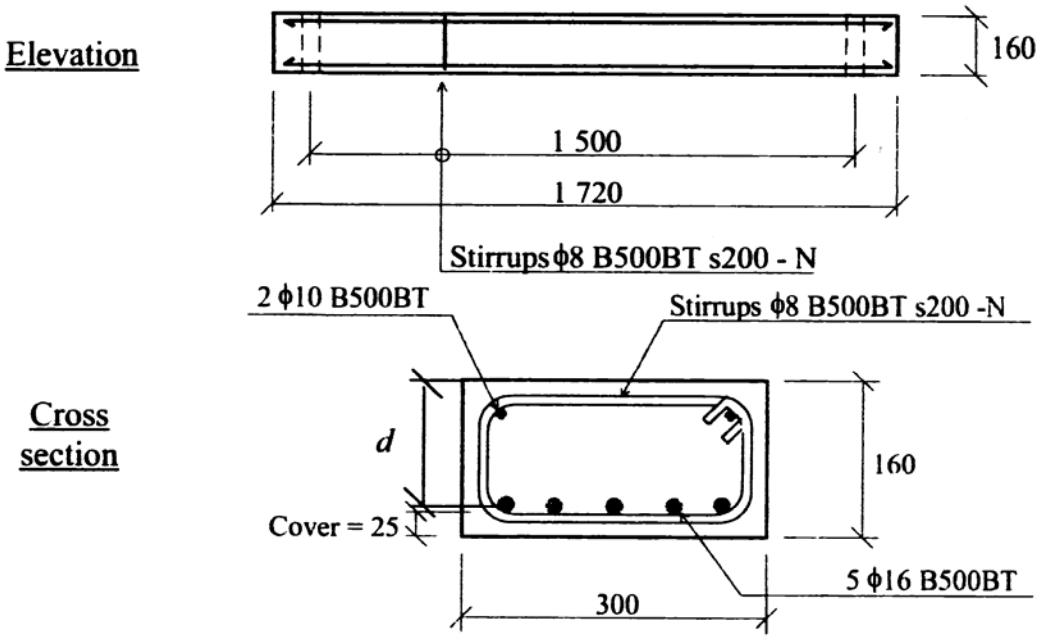

Figure 5.1: Elevation and Cross-Sectional of the Beam with Dimensions in mm.

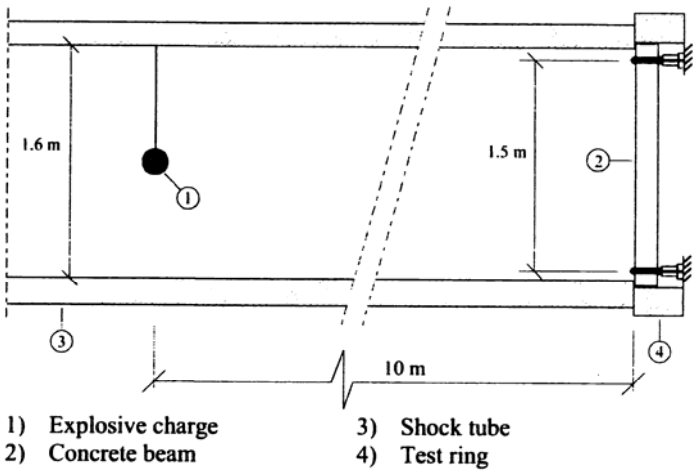

Figure 5.2 Experimental set-up of the air blast tests.

Table 5.2 Results from the air blast tests.

Beam	p_r kPa (psi)	i kPas	$F_{tot,u}$ (kN)	δ_u mm (in.)	Failure type
B40-D4	1249 ± 80 (181.2±11.6)	6.38 ± 0	348	17.5 (0.689)	Brittle
B100(12)-D3	1946 ± 15 (282.2±2.2)	9.58	324	44.6 (1.756)	flexural

p_r = maximum reflecting pressure (mean value ±scattering)

i = impulse density (mean value ± scattering)

$F_{tot,u}$ = maximum total support reaction

δ_u = ultimate deflection at mid-span

For the beam in Figure 5.1, an analytical model of simply-supported beam subject to step pressure, as shown in Figure 5.3, is considered. Properties of the beam in Figure 5.3 are presented in Table 5.3.

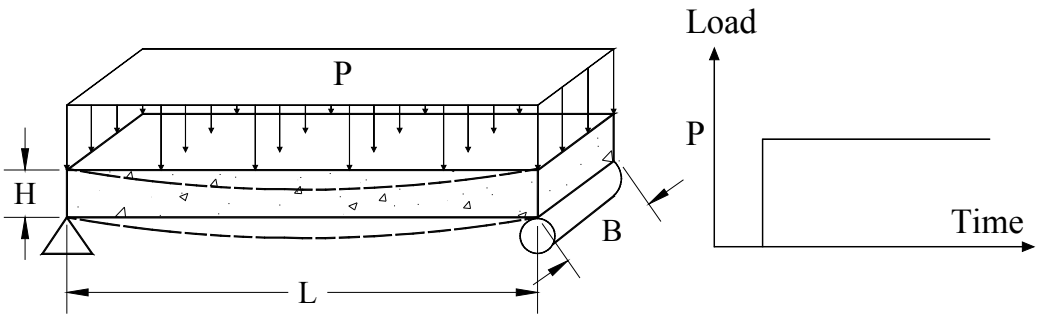

Figure 5.3 Simply supported beam under impact load

Table 5.3: Elastic Properties of the Beam in Figure 5.3.

Items	Value
Length L	1500 mm (59.055 in)
Width B	300 mm (11.811 in)
Height H	160 mm (6.2992 in)
Elastic modulus	2.6E+04 MPa (3.771E+06 psi)
Density	2400 kg/m3 (2.2447E-04 lb s2/in4)
Pressure	1946 kPa (282.2 psi)

For the beam in Figure 5.3, the midpoint deflection can be obtained as $\Delta_A = \frac{5PBL^4}{384EI}$ =14.45mm=0.57in. The natural frequency of first mode of the beam with distributed mass is $\omega_1 = \frac{\pi^2}{L^2}\sqrt{\frac{EI}{m}}$ =667 and the corresponding natural period is $T_n = \frac{2\pi}{\omega}$ =9.42E-03 sec. Since the loading period is longer than $0.5T_n$, the maximum dynamic magnification factor is 2. Therefore, the maximum dynamic midpoint deflection is 28.90 mm (1.1379 in.) using the Euler-Bernoulli equation [Chopra 2001]. If the shear deformation and rotational inertia are considered using Timoshenko equation, the natural frequency of first mode becomes T_n=9.584E-03 sec [Warburton 1976] which is 1.7% longer than that using the Euler-Bernoulli equation. Then, the deflection considering shear strain is $\Delta = \frac{5PBL^4}{384EI}(1+3\frac{h^2}{l^2})$= 14.94 mm = 0.588 inch [Timoshenko 1962].

5.2 INFLUENCE OF TIME STEP SIZE

5.2.1 Numeric stability

Belytschko et al. (2000) have defined the numerical stability during finite element simulations . Consider a process that is governed by an evolution equation such as the equations of motion or heat conduction. Let the solution for the initial conditions $\mathrm{d}_A(0) = \mathrm{d}_A^0$ be denoted by $\mathrm{d}_A(t)$. Now consider solutions for initial conditions $\mathrm{d}_B(0) = \mathrm{d}_B^0$, where d_B^0 are small perturbations of d_A^0. This means that d_B^0 is close to d_A^0 in some norm (to be specific we use the ℓ_2 vector norm):

$$\left\|\mathrm{d}_A^0 - \mathrm{d}_B^0\right\|_{\ell_2} \le \varepsilon \qquad (5.1)$$

A solution is stable if for all initial conditions that satisfy (5.1), the solutions satisfy

$$\left\|\mathrm{d}_A(t) - \mathrm{d}_\mathrm{B}(t)\right\|_{\ell_2} \le C\varepsilon \qquad \forall t > 0 \qquad (5.2)$$

According the above definition, numerical stability can be determined by applying a small perturbation to a process and then obtaining an expression for its response. If the perturbation grows, the process is considered unstable; otherwise it is stable.

To guarantee the numeric stability in the simulation, Hallquist (1998) has proposed to etermine a time step size by taking the minimum value over all elements, i.e.,

$$\Delta t^{n+1} = \alpha.\min\left\{\Delta t_1, \Delta t_2, \Delta t_3, \ldots, \Delta t_N\right\} \qquad (5.3)$$

where N is the number of elements. For stability reasons, the scale factor α in Eq.(5..3) is typically set to a value of .60 for impact simulation.

Generally, a critical time step size should satisfy the following equation,

$$\Delta t_{crit} \leq \min_{e} \frac{\ell_e}{c_e} \tag{5.4}$$

where ℓ_e is the smallest distance between any two nodes of the element and c is the instantaneous wave speed. Physically, Eq. (5.4) implies that the stress wave should not propagate further than the shortest length of one element in each time step to guarantee the numerical stability.

Two aspects of above definition of numerical stability should be understood. Firstly, the critical time step is deduced from linear or linearized physically stable systems. Very little is known about the stability behavior of numerical procedures during physically unstable processes. We assume that numerical methods which are stable for linear systems is stable for nonlinear systems and this turns out to be true for most cases from our experience. Secondly, the above deduction considers only the numerical stability and doesn't take material stability into account.

5.2.2 Influence of time step size on blast wave load generation

The time step size controlled by eq. (5.4) is not a constant. Its variance can be of the order of 10^2, even though the simulation has proper parameters and a smooth mesh is assigned to the structure. The mesh always became distorted after a short time of simulation for structures under extreme load, which will decrease the time step drastically.

Time step influences the maximum pressure in air elements. Relatively low accuracy of prediction of blast wave is mainly a consequence of the inability of coarse meshes to resolve sharp gradients. For example, one can simulate the blast wave propagation without structure using the method proposed in in chapter 3. Figure 5.4 shows the internal energy

of blast wave simulation. Since the energy is input to the ALE mesh by applying pressure load on a segment and the mesh in ALE method will get remapped (which is a nonlinear change), the system energy becomes C_1 discontinuous (the function is continuous and its first derivative is discontinuous). However, when the structure gets involved, the internal energy will be smoothed as shown in Figure 5.5. From chapter 3, we have already known that the predicted blast wave load matches with that by ConWep program.

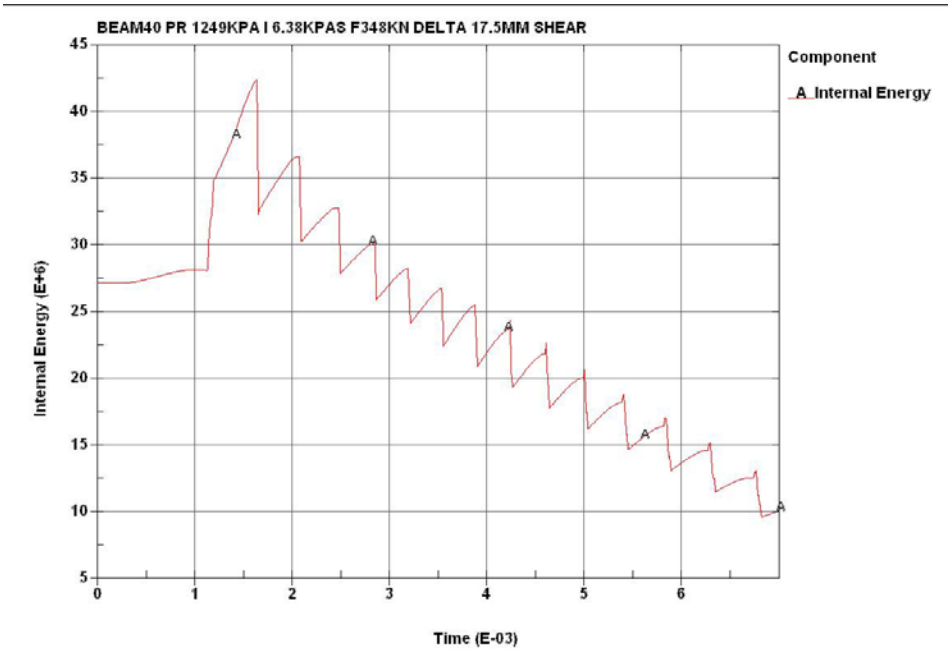

Figure 5.4 Internal energy of blast wave simulation

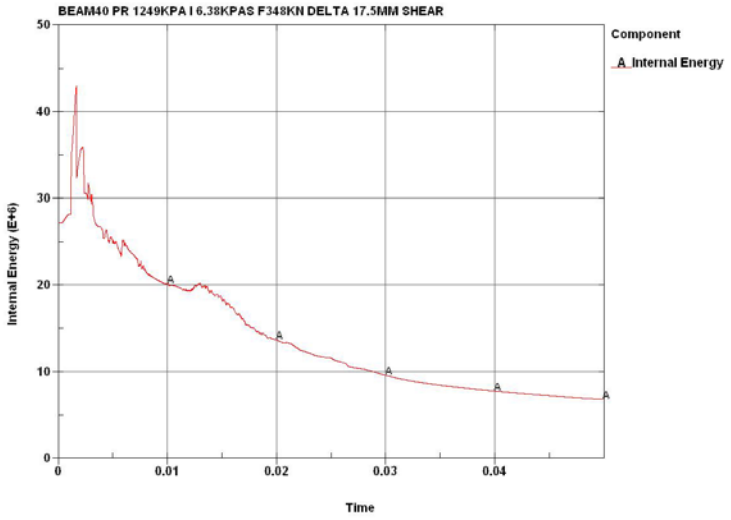

Figure 5.5 Internal Energy of the Beam and Blast Wave Simulation.

ConWep assumes an exponential decay of pressure with time of the form:

$$P_s(t) = P_{s0} \times [1 - \frac{t - t_a}{t_0}] \times \exp[\frac{-(t - t_a)}{\alpha}] \qquad (5.5)$$

where $P_s(t)$ = pressure at time t, P_{s0} = peak incident pressure, t_0 = positive phase duration, t_a = arrival time and α = decay coefficient.

Eq. (5.5) shows that the blast wave pressure attenuates with time exponentially. Experiments also show that the pressure of air blast wave attenuates with distance exponentially [Army 1990]. Exponential attenuation has startling sharp gradients. It is desirable to capture the exponential gradients perfectly in cases such as simulation of penetration problem using very fine mesh, since the order of time integration error is $O(t^2)$, where t is the time step interval. However, a fine mesh with very high accuracy is not necessary in the simulation of structures subject to blast loads provided that the available verification data is not of much accuracy. In fact, a coarse mesh (about 1 ft in element length) for air will satisfy the necessary accuracy for engineering analysis and will have

advantages of controlling the calculation stability and saving computation time greatly. In order to investigate effects of time step on air blast load predictions, Table 5.4 presents results using several time steps. It is observed from Table 5.4 that, compared to a time step of 5.0×10^{-9}, maximum error introduced in the prediction of air blast because of a time step of 2.0×10^{-6} is only 2.59%.

Table 5.4 : Influence of Time Step on Air Blast Load Prediction

Time Step Size (s)	Max. Pressure (psi)	Percent Difference (%)
2.00E-06	196.4	0.00
1.00E-07	195.94	-0.23
5.00E-08	195.95	-0.23
4.00E-08	196.1	-0.15
2.00E-08	199.06	1.35
1.00E-08	200.32	2.00
5.00E-09	201.48	2.59

In order to study the influence of parameters such as geometry, shape, material strength and ductility, a stable simulation without the influence of time step is desirable. This can be achieved by following the following procedure:

(1) Carry out trial nonlinear simulation;

(2) Utilize a time step control to cover the minimum time step size in the simulation. For example, Figure 5.6 shows the time history for time step size in three cases. The time step in case A is determined by the codes default according to Eq. (5.4). Cases B and C correspond to controlled time steps. It is observed that the time-step control in Case C is preferred since the time step in case C doesn't fluctuate and it requires less computation time than the case B.

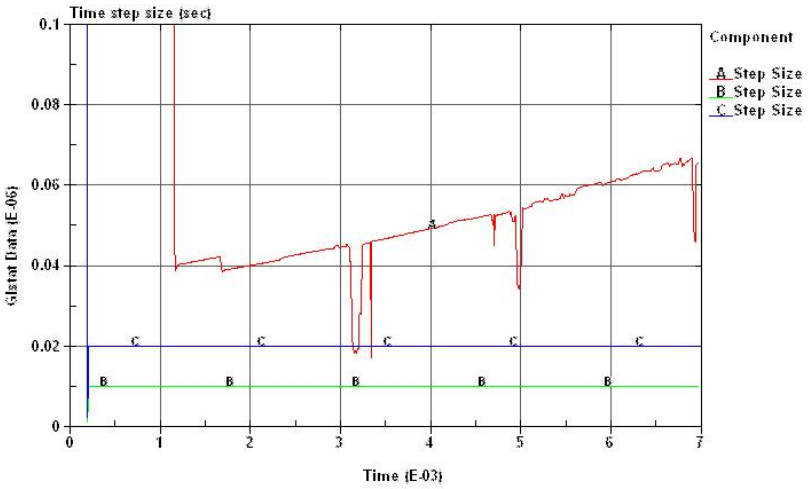

Figure 5.6. Time history for time step size in simulation using explicit method

(3) Verify results with ConWep & BlastX data.

(4) Repeat steps 1 through 3 until the selected time step satisfies eq. (5.4).

5.2.3 Influence of time step size on elastic structure

In order to investigate effects of time-step on elastic structures, we consider a model of elastic beam in Figure 5.1 subject to blast loads. Figure 5.7 shows finite element model of the beam. Table 5.5 shows maximum contact pressure (pressure load transferred from ALE air mesh to Lagrangian structure mesh) in simulations with different time step control using a penalty factor in contact PFAC = 2.06E-3. It is observed from Table 5.5 that maximum contact pressure increases with a decrease in time step size and contact pressure is nearly reciprocal to time step size. In the simulation, PFAC factor can be adjusted to obtain the same maximum contact pressure for a value of time step size. Table 5.6 shows PFAC factor and time step factors such that the maximum contact pressure remains around 284 psi.

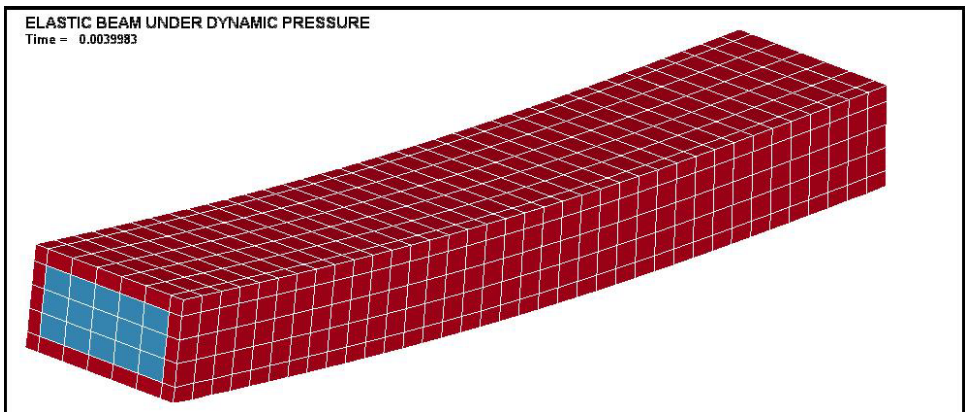

Figure 5.7 FEM model of elastic beam

Table 5.5 Change in Contact Pressure With Time Step

For an Elastic Beam Subject to Blast Loads.

Case	Time Step Size (sec)	PFAC factor	Max. contact pressure (psi)
1	1.00E-06	2.06E-03	328.2
2	5.00E-07	2.06E-03	792.6
3	5.00E-08	2.06E-03	7691
4	5.00E-09	2.06E-03	25780

Table 5.6 PFAC factor change with the time step size in elastic simulation

Case	Time Step Size (sec)	PFAC factor	Max. contact pressure (psi)
1	1.00E-06	1.69E-03	283.2
2	5.00E-07	1.06E-04	284.4
3	5.00E-08	1.06E-06	284.4
4	5.00E-09	1.16E-08	283.3

5.2.4 Influence of time step size on nonlinear structures

When the blast load is large enough to push concrete material into nonlinear range, the mechanism of contact is different since the elastic modulus of structure material is equal to or only a little bit bigger than zero, which makes the interaction between air and structure more like interaction between two fluid materials. In this case, the contact

pressure is relatively insensitive to both time step and penalty factor. This can be illustrated by the simulation of B100 beam in Table 5.2. We consider cases A and B, each with the same PFAC factor of 2.06E-6 and time steps of 4E-8 sec and 5E-8 sec, respectively. Figure 5.8 shows the contant pressures predicted in two cases are almost the same as those in Table 5.6 for elastic beam model.

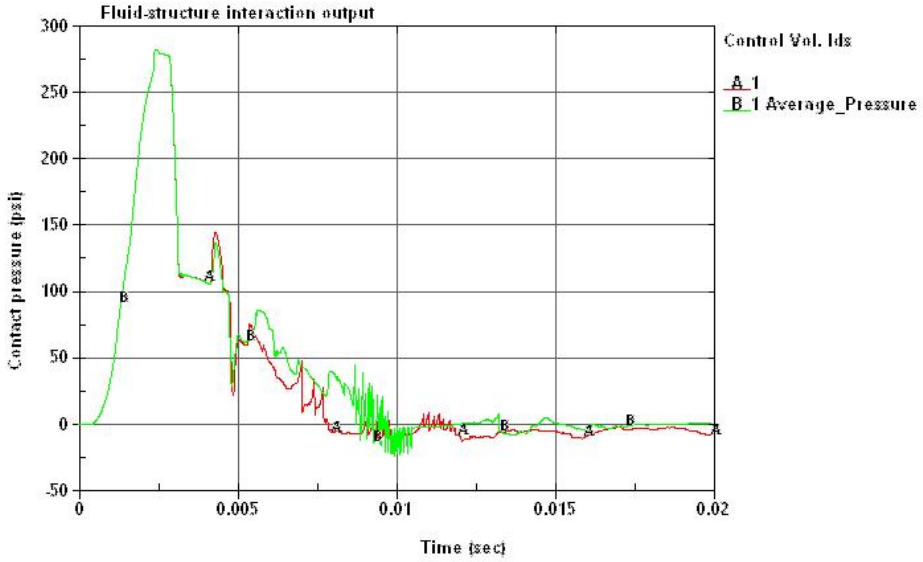

Figure 5.8 Contact pressure between structure and blast wave for for inelastic beam model.

It is also observed from Figure 5.8 that the contact pressure attenuates faster in case A where smaller time step is used. In fact, numerical dissipation will rise significantly in the fluid solver with a decrease in the time step, [Gong 2006]. Hence, largest time-step that satisfies critical time step requirement in Eq. (5.4) should be used. However, this observation should be used as a rule of thumb. To assure that the contact pressure will not vary in each time step, we need to control the time step size. A control card with very small time step size would be needed to satisfy Eq. (5.4) at each time step. A very small time step may cause faster attenuation of blast wave pressure because of the influence of

small time step on the fluid solver. This is an issue intrinsic to the computational approach used in hydro-codes such as LS-DYNA. Ideally, a contact algorithm and a fluid solver independent of time step are desired. However, since the goal of our research is on the response of structures, our approach on the selection of time steps is not expected to affect the response of bridge components significantly since blast wave pressures are also verified with those generated by LS-DYNA and BalstX.

5.2.5 Calculation time

The total calculation time of blast load simulations on a whole bridge model is a significantly important issue. In our simulation, a 0.2 second blast simulation of one-million-nodes model takes approximately one week on a quad-core 2.67 MHz computer with 4GB RAM. If we need to adjust the parameters several times because of highly nonlinear process, the calculation time will be one month for one case.

The total calculation time is traditionally reduced by three measures, namely, (i) taking advantage of symmetricity in structure and loading, (ii) using finer mesh near blast load and coarser mesh away from blast load and (iii) using largest step size possible. Since blast load isn't symmetric about the structure, the first approach doesn't apply in he blast load simulations on highway bridge components. An example of using more elements (or finer mesh) at important locations (e.g., near blast center) and coarser mesh at other locations is illustrated in Figure 5.9. In Figure 5.9, the length of the largest element is 10 times of that of the smallest element. This can lead to a reduction in the total number of elements by a factor of 1000. However, since the time step size is determined by the smallest element length, time step size will be reduced by a factor of 10^3-10^5 because of shrinkage in the element length by a factor of 10. Hence, a time step size of 10^{-6} seconds

will be reduced to 10^{-11} seconds because of element meshing in Figure 5.9. This will increase the total calculation time by a factor of 10 to 100. Additionly, the results may not be accourate because of high distortion of elements. The limitations of the third approach of using largest possible time step are related to prediction of blast wave pressure, as described in the previous section.

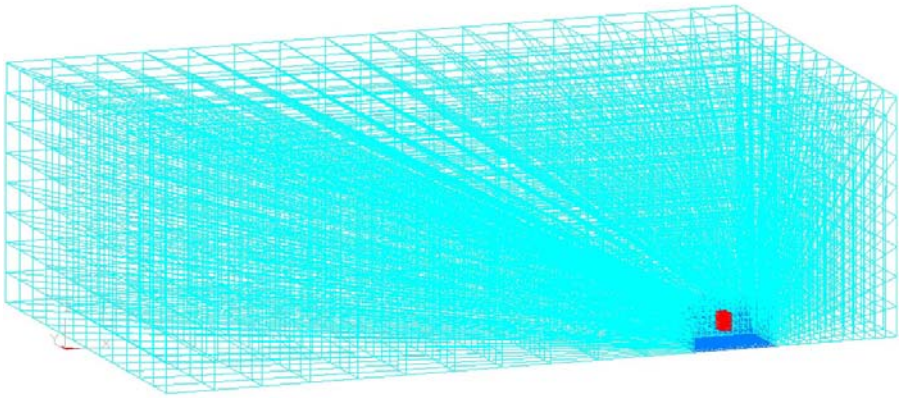

Figure 5.9 Air mesh for the explosion field

Some researchers propose using higher material density to reduce the calculation time. Blast wave velocity is slower in higher density materials. Since time step size depends on the blast wave velocity, one can reduce calculation time by increase time step size for denser material. However, increasing density will misrepresent inertia forces of bridge component, which is not desirable for blast load simulation on bridge components.

Based on extensive experience on simulating blast load effects on bridge components, one can use following guidelines to reduce total computation time.

(1) Using parallel computation architecture of LS-DYNA.

(2) Building homogenous mesh for air environment;

(3) Using fine mesh for structural components closer to blast source or for important structural members and coarser mesh for other components.

(4) Erosion of highly distorted element as early as possible.

5.3 INFLUENCE OF MESH SIZE

5.3.1 Influence of mesh size on the simulation of elastic rsponse

In order to investigate effects of mesh size of elastic response of the beam in Figure 5.1, four finite element models of the beam with different mesh sizes, as shown in Figure 5.10, have been developed.

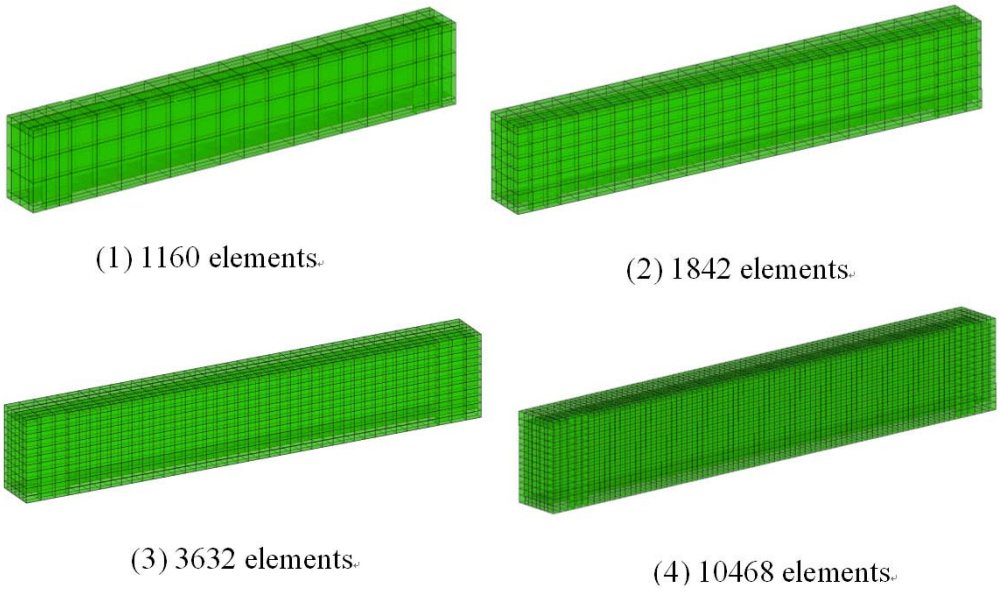

Figure 5.10 FEM beam models with different mesh sizes

Properties of the beam model are shown in Tables 5.1 and 5.3, and figure 5.1. In order to simulate different aspects of 4 beam models in Figure 5.10, 8 analysis cases, presented in Table 5.7, have been designed.

Table 5.7 Analysis Cases for Effects of Mesh Size on Elastic Response of Beam.

Case #	Description	Analysis Type
1	Mesh size is 2.953 inch	Influence of mesh size
2	Mesh size is 1.596 inch	Influence of mesh size
3	Mesh size is 1.0748 inch	Influence of mesh size
4	Mesh size is 0.6541 inch	Influence of mesh size
5	A wider, lower beam with the same EI as cases 1-4	Assumption of plan section
6	Supported nodes are fixed instead of simply supported in FEM model	Boundary condition
7	Pressure load is 0.1 lb/ft2	Influence of large deflection
8	Mesh size is 0.6541; simply supported BC; use Timoshenko solution to verify	Difference between Euler and Timoshenko theory

For beam models in Figure 5.10, theoretical displacement at midpoint can be calculated by using the Euler-Bernoulli equation, $\Delta_A = \frac{5PBL^4}{384EI}$ (see Section 5.1). Likewise, the theoretical natural period, using the Euler-Bernoulli equation, can be calculated by $\omega_1 = \frac{\pi^2}{L^2}\sqrt{\frac{EI}{m}}$, $T_n = \frac{2\pi}{\omega}$. Column 3 of Table 5.8 shows the difference between natural periods calculated by the Euler-Bernoulli equation and that by the FEM model. Similarly, last column of Table 5.8 presents the difference between midpoint displacements by the Euler-Bernoulli equation and that by the FEM model.

It is observed from Rows 1-4 of Table 5.8 that the difference in midpoint displacement decreases as the mesh size is decreased from Case 1 to Case 4. In fact, the difference is reduced by approximately 3.21% as the mesh size is reduced from 2.953 to 1.596 inches.

The Euler-Bernoulli equation is based on the assumption that "the plane section remains plane". In case 5 of the Table 5.8, solid elements are used to build the finite element model of the beam and the plane section assumption is not necessary in the FEM

analysis. As the beam depth is reduced, the FEM model is more likely to follow the plane section assumption. It is observed from Table 5.8 that the difference between natural periods calculated by the Euler-Bernoulli Equation and that by the FEM model decreases from 9.36% in Case 2 to 4.48% in Case 5 because of reduced depth of the beam in Case 5. Likewise, the difference between midpoint displacements is reduced from 10.75% in Case 2 to 6.28% in Case 5.

Table 5.8 Parameter analysis for elastic beam simulation

Case #	Analysis Type	Element size (in.)	Natural period (ms)	Difference in periods (%)	Midpoint deflection (in.)	*Difference in deflection (%)
1	Influence of mesh size	2.953	10.46	11.08%	1.2968	13.96%
2	Influence of mesh size	1.596	10.30	9.36%	1.2603	10.75%
3	Influence of mesh size	1.0748	10.24	8.71%	1.2438	9.30%
4	Influence of mesh size	0.6541	10.15	7.75%	1.2342	8.46%
5	Plane section assumption	1.596	15.50	4.48%	4.7235	6.28%
6	Boundary condition	1.596	10.09	7.13%	1.2399	8.96%
7	Influence of large deflection	1.596	10.28	9.11%		
8	Difference between Euler and Timoshenko theories	0.6541	10.00	4.34%	1.211	2.98%

Under a large load, large deflection occurs. When a small load is applied, case 7 shows that the geometry nonlinearity causes about 0.5% error in the beam simulation.

If we use Timoshenko equation for the theoretic solution, as what has been done in case 8, the FEM results differs from theoretic ones by only 2.98% error. We can conclude that structure analysis by LS-DYNA is trustable.

According to the foregoing analysis, the factors to influence the simulation results and their contribution can be summarized as Table 5.9. It suggests that the error can be

controlled in 3% using appropriate parameters in the structure simulation.

Table 5.9 Possible percentage difference aroused by different factors

Item	Difference contribution
Euler-Bernoulli assumption	4%
Boundary condition	4%
Element size	3%
Large deformation	0.5%

5.3.2 Influence of mesh size on the simulation of inelastic response

In the simulation of structures with nonlinear material properties, the calculation usually becomes unstable and results do not converge with mesh size. These types of difficulties have been encountered in computational analysis for unstable material models since 1970s. A closed-form solution for a rate-independent material model with strain softening in one dimension was constructed by Bazant and Belytschko (1985) to explain these difficulties. They explained that the strain of rate-independent materials grows to infinity at a single point when the material reaches a state of instability. Thus the strain localizes, as expected for a material instability. They also showed that the energy dissipation vanishes in some cases, although material fracture always involves significant dissipation. Therefore, models with strain-softening and without strain-rate dependency cannot represent fracture.

Hillerborg et al. (1976) offered one solution to these difficulties by matching the energy dissipation in fracture to the energy dissipated in the element which shows instability. In this way, the constitutive equation depends on the element size. Bazant (2002) has shown that there exists a characteristic length for concrete material fracture. Belytschko et al. (2000) pointed out that it is a strange but intriguing idea because the PDE now depends on a discretization parameter, the element size. It is a step in the direction of

constitutive formulations directly in terms of finite elements rather than the PDE.

In the constitutive model for a monolithic material, material models for concrete and steel have been verified separately and have not been shown to demonstrate the instability problem. However, if concrete and steel are modeled together in a component such as reinforced concrete member, the bond slip problem shows instability. This problem is caused because of eroding of elements modeled by strain-softening type strain-independent numerical material model..

Numerical modeling of bond-slip problem in reinforced concrete has been addressed by many researchers. Chen and Baker (2003) have investigated the influence of bond slip and have shown that, the damage near the reinforcement is distributed when the bond slip isn't considered in the modeling and it is localized when bond slip is considered. De Nardin et al. (2005) has tried to resolve the bond slip problem from contact surface approach while Mendola (1997) has investigated this problem by an analysis model alternative to that based on the usual discretization of concrete and steel into tri-dimensional axis-symmetric finite elements. Salem and Maekawa (2004) predicted successfully the degradation in bond due to yielding and the mechanics of bond in conventional concrete as well as self-compacting concrete through nonlinear three-dimensional asymmetric finite element analysis. Limkatanyu and Spacone (2002a, b) have presented the governing differential equations of reinforced concrete frame elements with bond slip in the reinforcing bars.

However, all existing approaches described above encountered difficulty in simulating blast loads on reinforced concrete member correctly because of eroding, which involves removal of distorted elements, and highly nonlinear interaction between concrete

and steel rebars resulting from eroding.

In order to investigate the effects on mesh size on response of reinforced concrete members subject to blast loads, we consider a reinforced concrete column with fixed bottom boundary condition, as shown in Figure 5.11. The section of column is 3ft×3ft and the height is 16 ft. Finite element models of the column with mesh sizes 1.0, 1.5, 3.0 and 10.0 inches have been developed to investigate effects of blast loads on these models. Figure 5.12 presents the time histories of column top displacement for the four models. In Figure 5.12, all models behave predominantly elastic till time < 0.5 msec. and behave inelastically when time > 0.5 msec. It is observed that the response of columns with mesh sizes ≤ 3 inch is significantly smaller than that with mesh size of 10 inch in elastic region (i.e., time < 0.5 msec). However, there is significant difference between response of columns with mesh sizes 3.0 and 1.5 inches in the inelastic region, particularly after time > 1.0 msec. In general, mesh size of 3 inches is appropriate for elastic structures and a mesh size of less than 1.5 inch for inelastic structures.

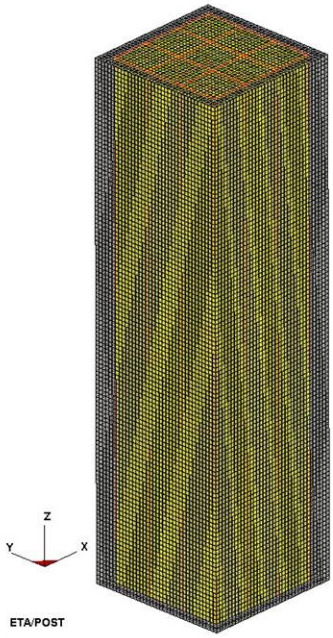

Figure 5.11 RC column model to study the influence of mesh sizes.

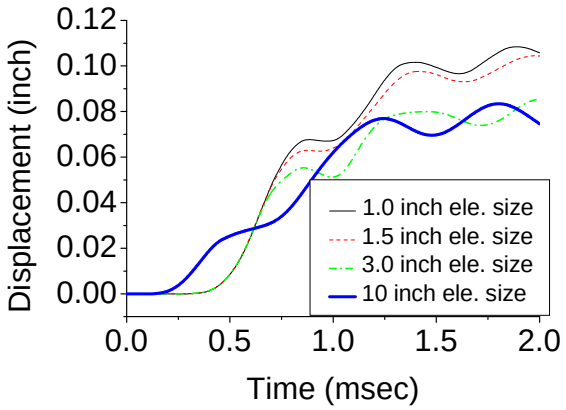

Figure 5.12 Column top displacement time histories

Ideally, proper mesh size for reinforced concrete members in the bridge model should be based on blast tests done on members of similar detailing. However, because of unavailability of data on blast tests of reinforced concrete members, blast test data on models of beam, as explained in Section 5.1, have been used to calibrate mesh sizes of

bridge components subjected to blast loads.

Four FEM models of the beam B100 in Section 5.1 with different element sizes have been developed to investigate the effects of mesh size. Table 5.10 presents results of numerical simulations of these four models.

Table 5.10 Influence of mesh sizes

Case	Mesh size length (in.)	Deflection at failure (in.)	Reaction (lb)	Penalty factor PFAC	Segment Pressure (psi)
A	2.46	4.8465	-251041	0.0294	282.0
B	1.64	2.064	-230241	0.0052	282.9
C	1.08	1.756	-246334	2.06E-03	282.9
D	0.7874	1.11	-211869	4.10E-04	282.3

It is observed from Table 5.10 that the midpoint deflection of the beam at failure decreases with decrease in mesh size. Comparing the experimental value of deflection at failure in Table 5.2 with those in Table 5.10, it is observed that the experimental value of 44.6 mm (1.76 in) matches with that of Case C in Table 5.10. Hence, mesh size of 1.08 inch can be used to model reinforced concrete components subject to blast loads.

It is also observed from Table 5.10 that the reaction force in Column 4 of Table 5.10 varies very little with mesh size, while the deflection at failure varies over 400%. This implies that the calculation of loads transferred from the beam to supports is stable. Hence, if we analyze a simply supported bridge with accidental explosion on the deck, response of columns can be predicted accurately, even if the simulation of load effects of girders is not reliable. Table 5.10 shows that mesh size affects the interaction between ALE air mesh and Lagrangian structure mesh a lot. Contact parameter PFAC needs to be verified with experimental data to apply the correct blast pressure load on structures

instead of using default values in LS-DYNA.

Similar to B100 beam, three FEM models of B40 beam with different element sizes have been built. Compared to B100 beam, which is under-reinforced, B40 beam is over-reinforced and may tend to show brittle behavior. Results of numerical simulations are shown in Table 5.11. It is observed from Table 5.11 that the midpoint deflections of beams at failure are almost in close range for various mesh sizes, although the deflection for Case 3 with mesh size of 1.12 inch is closest to the experimental value of 17.5 mm (0.689 inch). However, if we define the deflection at which the beam loses its whole section as the final deflection, the beam model with a larger mesh size of 1.97 inch has the largest deflection because of highly nonlinear bond-slip between concrete /rebar interface and fracture in concrete.

Table 5.11 Influence of mesh size for beam B40

	Element size (in.)	Element number	Deflection (in.) at failure	Final deflection (in.)
Case 1	1.97	2578	0.676	2.1846
Case 2	1.57	4471	0.63	0.935
Case 3	1.12	5745	0.687	0.819

5.4 SIMULATION OF BLAST LOAD EFFECTS ON BEAMS

Using mesh sizes identified for inelastic behavior of the beam, detailed blast load simulations have been carried out on reinforce concrete beams described in Section 5.1 using the explicit solver in LS-DYNA. The beam model consists of 3632 solid elements, each with a length (mesh size) of approximately 1 inch. Hourglass control is applied to avoid zero energy modes. Given the simulation duration is less than 10 milliseconds and blast pressure is very high, gravity load is neglected in the simulation.

Core and cover concrete in the beam are modeled by the Johnson Holmquist concrete material model (MAT_111) with two different material properties so that the model can simulate confinement effects from ties. As discussed in Chapter 4, the JSC material model is capable of simulating large strains, high strain rates and high pressures on concrete subject to blast loads. Steel rebars in the beam are modeled as beam elements using Plastic Kinematic material model (MAT_3), assuming that a perfect bond exists between concrete and rebar at the shared nodes. Note that beam elements instead of truss elements are used to model rebars to simulate lateral confinement effects on mechanical performance of concrete because of rebars. Many investigators have investigated stress-strain relationship of reinforced concrete at high strain rates and have shown experimentally that ultimate strain values are almost constant [Army (1990); Fu et al. (1991); Malvar (1998)]. Table 5.12 shows values of ultimate strain used in the simulation of beams. Elements at supports are assigned a bigger ultimate strain capacity to avoid local stress concentration. The FEM model of beams in LS-DYNA is shown in in Figure 5.13.

Table 5.12 Ultimate strain in the simulation

	Failure strain
Steel rebar	0.23
Core concrete	0.005
Cover concrete	0.002

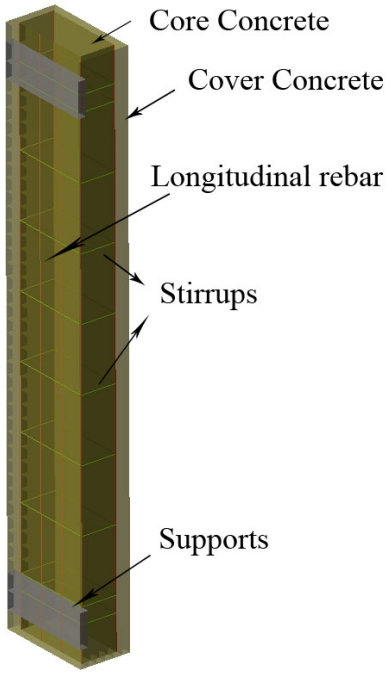

Figure 5.13: FEM Model of the Beam.

5.4.1 Ductile Failure of the Beam

Figure 5.14 shows the simulation of beam B100 subject to blast loads at different time instants. Figure 5.14 (a) shows spalling of beam at time instant of t = 2.4 seconds. At t = 3.75 seconds, tensile concrete in the region of maximum moment cracks. Failure in the beam is initiated by a yielding of the steel while the strains in the concrete are relatively low and with crack climbing up to compression region. At time t = 5.1 milliseconds, longitudinal rebars are severed. Finally, at time t = 5.2 milliseconds, concrete in the compression zone is crushed completely following the severance of rebars, leading to a complete failure of the beam.

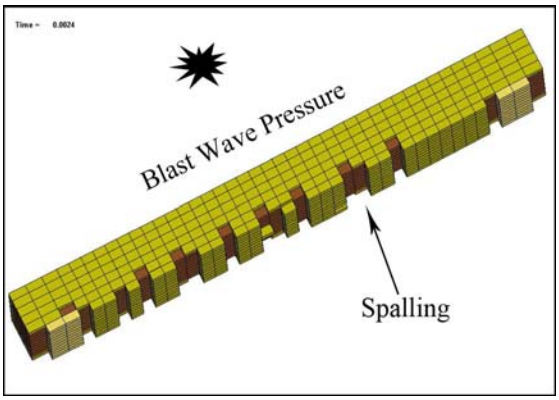

(a) t= 2.4

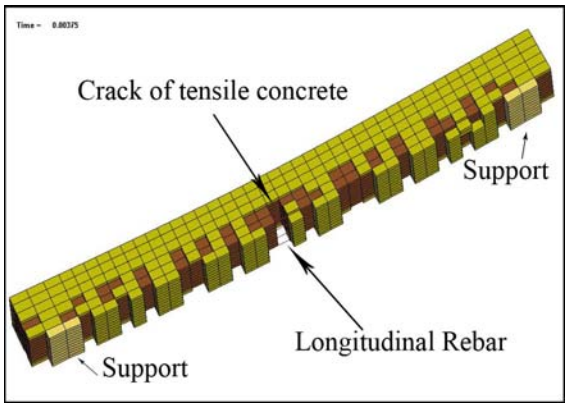

(b) t=3.75

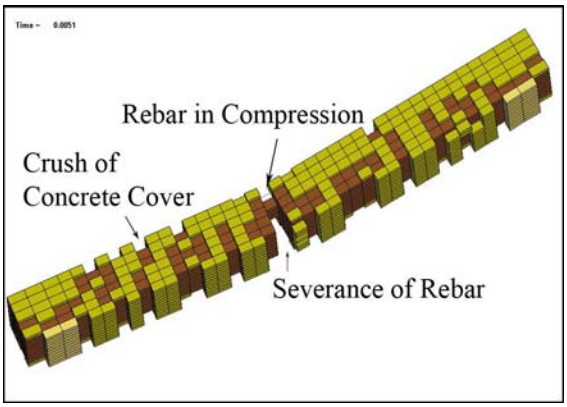

(c) t = 5.1 ms

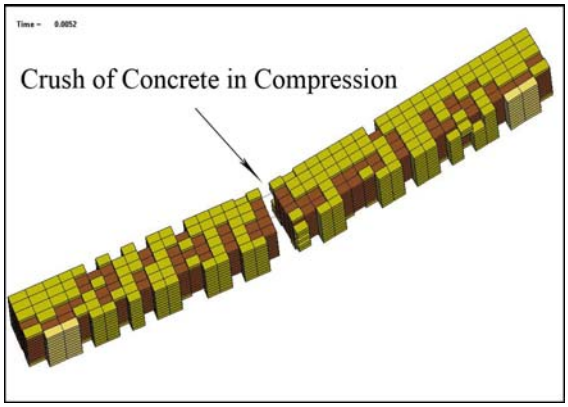

(d) t = 5.2 ms

Figure 5.14 Effects of blast loads on under-reinforced beam B100 in Section 5.1.

The final stage of failure, i.e., crushing of concrete following severance of rebars, is similar to that observed during experiments by Magnusson and Hallgren (2004). In the simulation, failure time is considered at the instant when the severance of longitudinal rebar occurs, as shown in Figure 5.14(c). The beam B100 in Figure 5.14 demonstrates ductile failure because of its under-reinforced design.

5.4.2 Brittle failure of the beam

Figure 5.15 shows the simulation of over-reinforced beam B40 in Section 5.1 subject

to blast loads. In this beam, failure is initiated by crushing of the concrete followed by a sudden disintegration of the compression zone while the stress in the relatively large area of steel has not reached its yield point. By using finite element meshing parameters of B100 beam, the deformation predicted by the FEM model in LS-DYNA matches well that from the experimental data. Table 5.13 shows some of the results of simulation for the B40 beam.

It has been observed that the identification of failure time and its corresponding deflection is difficult during blast loads on over-reinforced beam, whose failure mode essentially behaves as brittle failure. For example, crush of concrete in compression zone initiate at t = 4.2 ms with the deflection of 0.559 inch. However, the failure process continued until 8.52 ms with deflection of 1.95 inch. In order to identify the failure instant, we plot time history of kinetic energy of the beam, as shown in Figure 5.16. It is observed from Figure 5.16 that the system kinetic energy jumps up and reached the maximum value at time instant t = 4.58 milliseconds. Hence, the time instant of 4.58 milliseconds can be considered as the instant of brittle failure of the beam B40.

Table 5.13: Parameters and simulated deflection for beam B40

ITEM	Value
Failure strain of core concrete	0.005
Failure strain of cover concrete	0.002
Failure strain of steel rebar	0.23
Element size (in.)	1.12
Deflection (in.)	0.6869

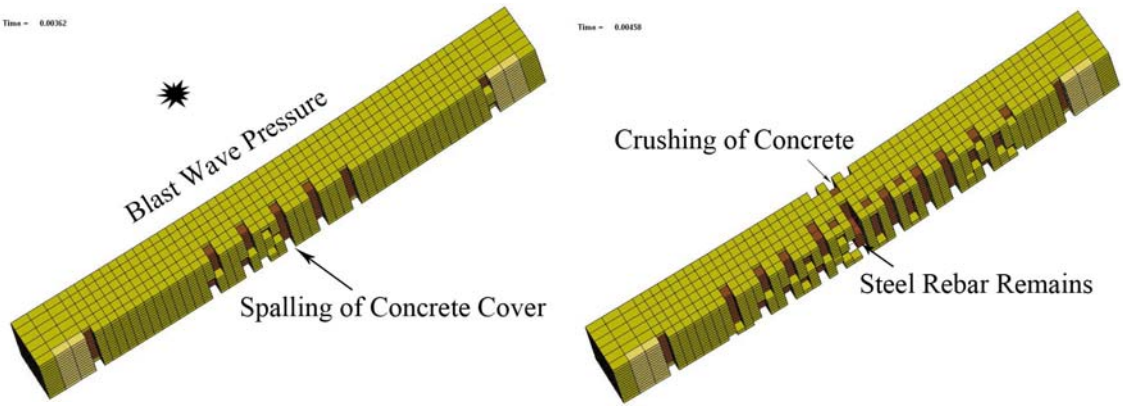

(a) t = 3.62 ms (b) t = 4.58 ms

Figure 5.15: Effects of blast loads on over-reinforced beam B100 in Section 5.1.

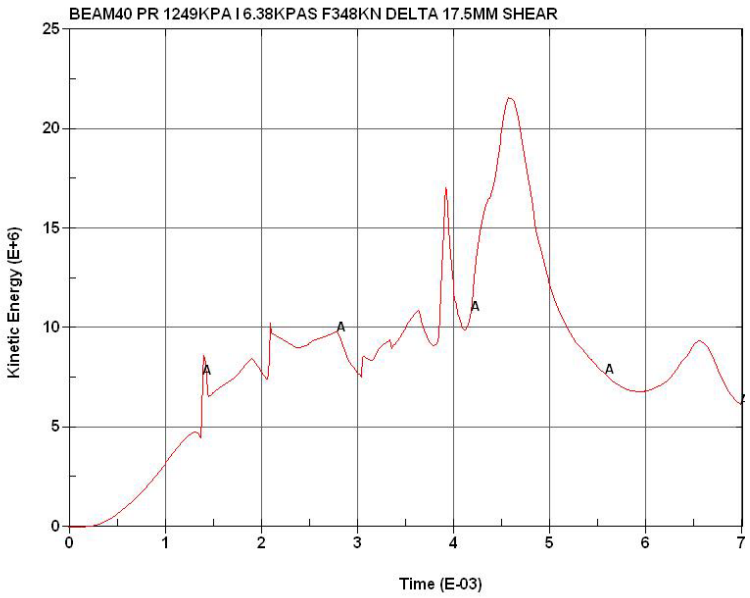

Figure 5.16 Kinetic energy time history of beam B40.

5.5 BLAST LOAD EFFECTS ON A REINFORCED CONCRETE COLUMN

On February 7, 2003, a 200-kilo car bomb exploded near Club El Nogal in Columbia, killing 25 and wounding 120. Figure 4.19 shows a column of the club building, 10 ft away from the bomb (square column on the left side of the picture) that survived after the attack. Parameters of the column are shown in Table 5.14. FEM model of the column is shown in Figure 5.18. In the finite element model of the column, size of solid element (i.e., mesh size) is taken as 1.0 inch.

Figure 5.19 shows the simulation of the column subject to blast loads. It is observed from Figure 5.19 that only the concrete cover got spalled and the core concrete remained intact. The maximum midpoint deflection of the column is approximately 0.12 in. It has been observed that the simulation results match very well with those observed at the blast site.

Figure 5.20 shows comparison between midpoint deflections ofb the FEM models of the column with mesh sizes 1.0 and 1.5 inches. It is observed from Figure 5.20 that the maximum difference between deflections using mesh sizes 1.0 and 1.5 inches is less than 2%. This implies that a coarser mesh may be sufficient in simulating blast loads if the observed damage is not severe.

Table 5.14 Parameters of column in Club El Nogal [CE676 2003]

Item	Value
Height	3.15 m (124 in.)
Width	0.9 m ×0.9 m (35.4 in. × 35.4 in.)
Concrete Strength	20.68 MP (3000 psi)
Reinforcement Ratio	1.44%
Charge weight	440 lb ANFO
Element # of fine mesh	165148
Element # of coarse mesh	25955

Figure 5.17: Damaged Club El Nogal Site. Undamaged column is pointed by an arrow.

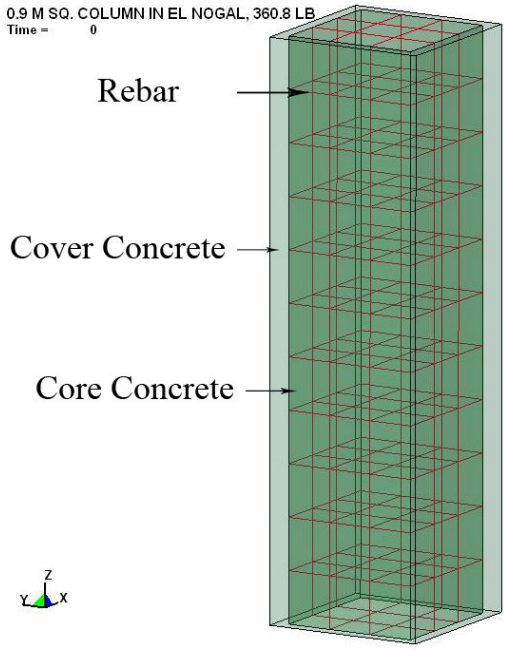

Figure 5.18 FEM Model of the Column in Club El Nogal.

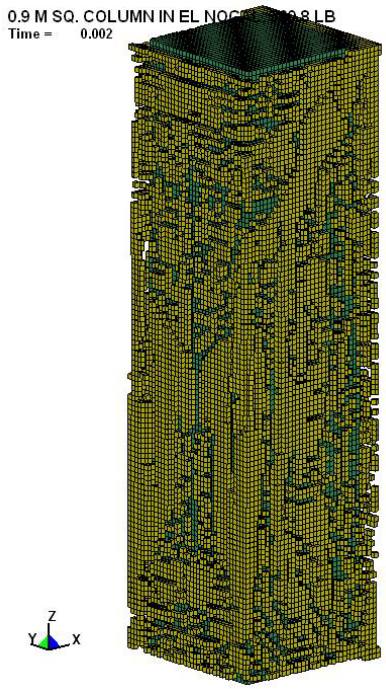

Figure 5.19: Simulation of Blast Load Effects on Column in Club El Nogal.

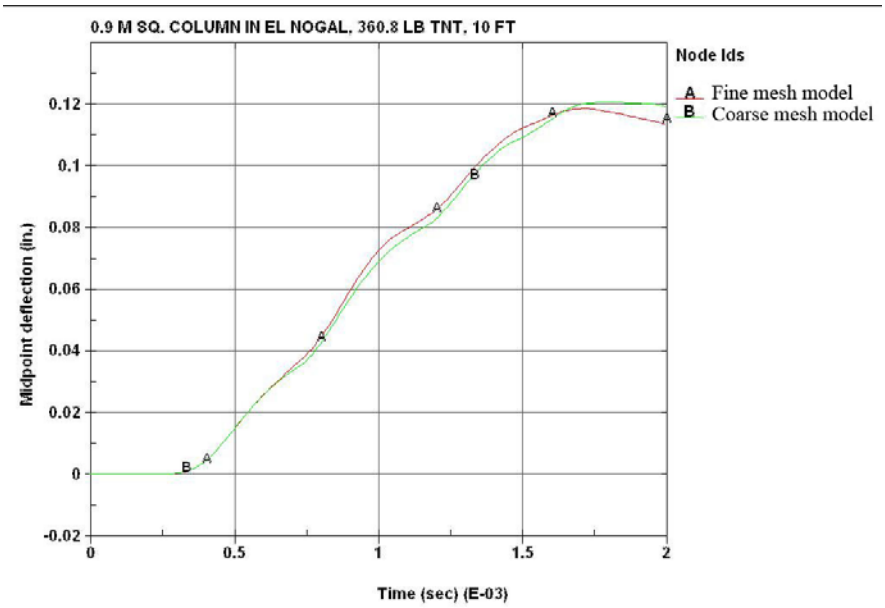

Figure 5.20: Comparison of Midpoint Deflection Between Model with 1.0 and 1.5 Inches Mesh Sizes.

CHAPTER 6 BLAST LOAD EFFECTS AND BLAST-SEISMIC CORRELATIONS FOR HIGHWAY BRIDGES

6.1 INTRODUCTION

According to the Blue Ribbon Panel set up to further study the issue of blast loads on bridges [BRP (2003)], substantial causalities, economic disruptions and other societal ramifications would result from isolated attacks on 1000 of 600,000 bridges in the country. The need to better understand the mechanism of blast loads on highway bridges and the approaches for damage mitigation has become more prominent because of increased terrorist threats to civil infrastructures since the collapse of the World Trade Center (WTC) in New York City on September 11, 2001. In fact, a workshop on applications of seismic rehabilitation technologies to mitigate blast-induced progressive collapse was organized on September 10, 2001 through the sponsorship of the National Institute of Standards and Technology (NIST) and General Services Administration (GSA) [Carino and Lew (2001)]. The workshop identified similarities and differences between seismic and blast loadings, applicability of several seismic rehabilitation/strengthening technologies, and recommended to develop guidelines for blast resistant design of structures, including progressive collapse mitigation. Since then, significant progress has been made on the development of design guidelines for mitigating progressive collapse of buildings and other framed structures [ASCE (2005); Canada (1995); DOD (2003); Ettouney et al. (1996); GSA (2003); ISC (2001)]. However, the guidelines for multi-hazard design of bridges are not yet available.

A brief review on state-of-the-art and state-of-the-practice in blast and progressive

collapse design of reinforced concrete structures has been presented by Munshi (2004). For a typical 8-story commercial building, Ettouney et al (1996) have discussed the design of floor slabs, columns, facades, atrium areas, and windows and the prevention of progressive collapse in the blast environment. For reinforced concrete structures, concrete columns and walls retrofitted with steel jackets and FRP wraps have been found to be effective in resisting explosive loads [Morrill et al. (2004)]. The behavior of steel structures subject to blast loadings is discussed in Shipe and Carter (2004) and Rittenhouse et al (2001). Simplified methods and models for blast analysis are presented in Sunshine et al (2004). Muszynski and Purcell (2003) have investigated the applications of two types of materials: (1) an autoclave-cured, three-ply, carbon fiber-epoxy laminate; and (2) a knitted biaxial E-glass fabric, for protection against blasts. A full-scale testing using a blast from 860 kg of TNT on a wall retrofitted with above two materials showed that the walls didn't suffer any damage due to the blasts. Effects of blasts on CMU walls have been investigated through field testing by Dennis et al (2002). Blast damage to Murrah building in Oklahoma has been investigated by Mlakar et al (1998). Blast loading on petrochemical facilities has been investigated by Forbes (1999).

All above references discuss the behavior of only buildings under blast loads. There is very limited information available on the behavior of bridges during blast loads. Effect of blast on highway bridge superstructures has recently been addressed in a preliminary study by Marchand et al (2004) for a two-span bridge model subject to under-deck blasts. They show that breaching failure of the concrete governs in cases of large truck bombs with limited standoff or for counterforce charges. Williamson and Winget (2005, 2006) and Winget et al. (2005a) have presented some analysis results and

design recommendations for bridge under blast load based on SDOF analysis. Progressive collapse of highway bridges has been investigated by Ghali and Tadros (1997) for the 12,910 m long bridge on Northumberland strait in Canada to propose a modified design where a drop-in span will just separate from rest of the bridge during local damage to the bridge deck, leaving the remaining bridge system vibrating freely due to dynamic loads created during local damage process to improve the performance of the bridge system.

In this research, we investigate the effects of blast loads on a 3-span simply supported bridge that has been designed for seismic loads in New York, California and two times requirements of California using the specifications in AASHTO (2002). A high-precision 3-D model of the bridge has been developed in LS-DYNA computer program, which is a general purpose explicit finite element code which is widely used by researchers on explosion and impacts. It has parallel computation capabilities on multi-CPU machines and has approximately one-hundred built-in constitutive models to simulate soil properties and the cracking and spalling of concrete [LSTC (2003)]. LS-DYNA allows different domains such as structures, gases and explosives to be simulated using different FEM scheme such as Lagrangian and Eulerian. Then these different domains are coupled together in space and time for an interactive simulation of these different domains to effectively simulate an actual event. In this research, we have developed a detailed finite element model of the bridge and have dipped the entire bridge in to the air mesh to identify damage mechanisms of all affected elements of the bridge.

The 3-span non-continuous highway bridge with concrete piers and steel stringers considered in this research has been selected on the basis of statistical analysis of 687,347

bridges in the country as described in Chapter 3. Blast loads on the components of this bridge have been simulated through a vehicle bomb under the middle span, 10 feet away from one of the piers. The maximum weight of charge considered is a typical value that is likely to occur and is comparable to the value recommended by the ASCE [ASCE (1999)], and is significantly smaller than the charge during the Oklahoma bombing in 1995 [Mlakar et al. (1998)]. Blast loads have been generated by the approach presented in Chapter 3. Ground vibrations induced by blast loads have not been considered in the simulations since the effects of direct blast loads have been found to be significantly more dominant.

6.2 DESIGN OF SEISMIC BRIDGES AND BLAST LOAD CASES

The bridge considered for FEM modeling is a 3-span non-continuous bridge. Plan and elevation of the bridge are shown in Figure 6.1 below. Key parameters of the bridge geometry and design load are shown in Table 6.1. We have chosen non-continuous bridge so that prominent damage mechanisms only because of blast loads can be investigated, since continuous bridge subject to blast loads are also likely to undergo global collapse because of progressive collapse mechanism.

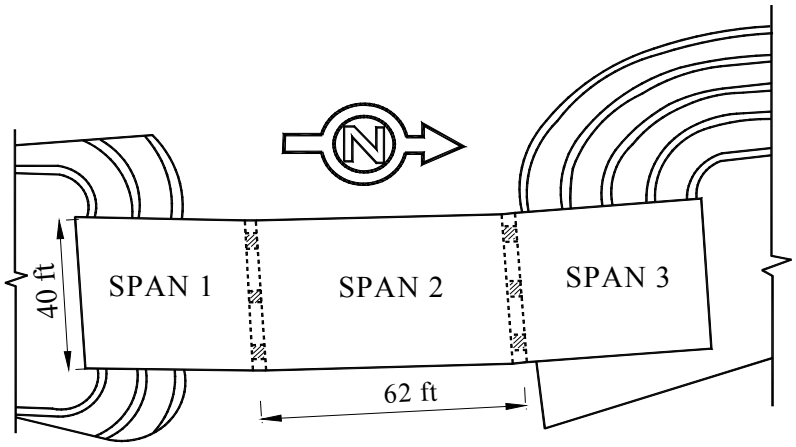

PLAN

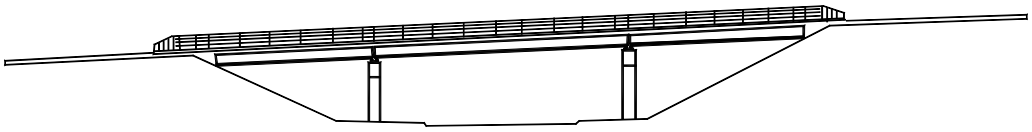

ELEVATION

Figure 6.1: Plan and Elevation of the Typical Highway Bridge.

Table 6.1 Parameters of the Typical Bridge in Figure 6.1.

ITEM	VALUE
Redundancy	Non-continuous
Length of Maximum Span	62 ft
Number of Spans in Main Unit	3
Design Load	MS 18 or HS 20
Deck Width	40 ft
Deck Thickness	13 in.
Lanes on Structure	2
Height of Pier	16 ft
Number of Piers	3×(2 group) = 6
Pier section	Rectangular 3.0 ft × 3.0 ft
Material / Design Type	RC concrete pier & deck, steel stringer

Design of Bridges for Blast-Seismic Correlations

The seismic safety of highway bridges can be improved through the following four approaches:

1. Increasing the load level such as acceleration coefficient which usually results in larger pier section size and materials with higher strength.
2. Imposing more stringent displacement requirement to prevent superstructure from sliding away from pier cap.
3. Utilizing a better design detailing to guarantee ductility of bridge members and the full use of material strength.
4. Applying supplemental damping systems to dissipate energy.

The bridge model in Figure 6.1 is based on an existing bridge and is designed to satisfy AASHTO bridge service loads. Following the 2002 AASHTO Guide Specifications for Seismic Design of Highway Bridges [AASHTO (2002)], three sample bridges have been designed to meet seismic requirements in New York, California and Over-design for California (two times of usual requirements). These example bridges will be referred to as NY, CA and 2CA, respectively. Table 6.2 presents detailed data on the capacities of the three bridges designed for different seismic capacities.

Table 6.2: Seismic Capacities of Sample Bridges.

		NY	CA	2CA
Pier parameter	Pier size (ft)	3.0	3.5	4.5
	Concrete strength (ksi)	3.0	3.0	3.0
	Acceleration Coefficient A (g)	0.2	0.8	1.6
Design Load	Moment (kip-ft) $1.0L^{*}+0.3T^{**}$	816.96	8169.6	16339.2
	Shear (kips) 0.3L+1.0T	35.52	355.20	710.4
	Axial force P (kips)	147.3	166.9	188.2
	Displacement Requirement (ft)	2.12	3.22	4.32
Elastic Capacity	Moment (kip-ft)	929.2	1115.0	1375.83
	Shear (kips)	1869	2544	4205
	Axial force (kips)	4212	5733	9477

* Longitudinal. ** Transverse

According to AASHTO LRFD Design Specifications, bridges are essentially designed to be elastic during small to moderate earthquakes. During more severe earthquakes, the intent is to accept structural damages while avoiding collapse. This means that the stresses due to seismic loads will exceed the yield strength of some of the structural members and inelastic deformations, such as plastic hinges, will form during such earthquakes (Buckle, et al, 1987). Among NY, CA and 2CA bridges in Table 6.2, NY bridge is designed to resist earthquake with 0.2g peak ground earthquake elastically. On the other hand, both CA and 2CA bridges are designed to behave inelastically during design earthquakes with 0.80g and 1.60g PGAs. In order to investigate the correlations between seismic and blast load effects, the three bridges (NY, CA and 2CA) have been designed by varying their pier sizes, while keeping the amount of steel reinforcement exactly the same in the piers of the three bridges. Table 6.2 shows detailed description of seismic capacities of the three bridges. In addition to this, unconfined strength of concrete in bridge piers has been varied from 3000 psi to 10,000 psi to investigate effects of concrete strength on blast resistance.

Seismic capacity of bridge piers can be quantified in terms of the ductility factor defined as (Chopra, 2001),

$$\mu = \frac{u_m}{u_y} \tag{6.1}$$

where u_m is the peak inelastic deformation and u_y is the deformation at the yield point. The yield strength f_y can be related to f_0, which is defined as the minimum strength required for the structure to remain linearly elastic during the ground motion, through a yield strength reduction factor R_y as

$$R_y = \frac{f_0}{f_y} = \frac{u_0}{u_y} \tag{6.2}$$

Figure 6.2 illustrates the concept of ductility factor and strength reduction factor for a typical structure possessing elastic-perfectly plastic behavior.

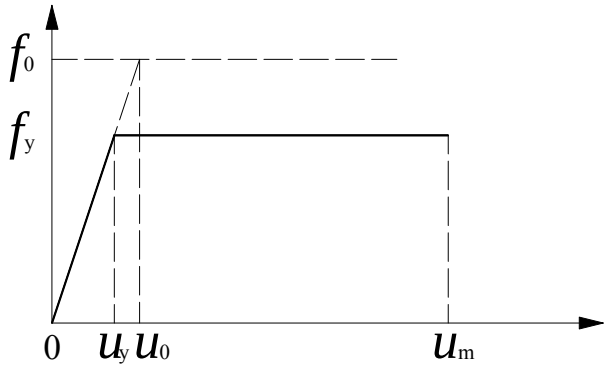

Figure 6.2: Strength Versus Ductility in Seismic Design of Structures.

To calculate the ductility factor, moment curvature curves for bridge pier sections have been calculated by a computer program called BIAX [Wallace (1992), Wallace and Ibrahim (1996)]. The capabilities of BIAX Program include the calculation of section properties, interaction diagrams and moment-curvature relations for bridge piers. In order

to calculate moment-curvature relationship of bridge piers in this study using BIAX, bilinear material model for steel reinforcement and modified Kent-Park model for stress-strain relations of confined and unconfined concrete [Kent and Park (1971), Park et al. (1982)] have been used. The rebar detailing shown in Figure 4.4 has been used for piers of NY, CA and 2CA bridges of sizes in Table 6.2. Figures 6.3 to 6.5 show moment curvature curves of NY, CA and 2CA bridge piers, respectively, with concrete strengths 3000 psi, 5000 psi and 10,000 psi. It is observed from Figures 6.3 to 6.5 that the moment capacities increase with increase in the section size. On the other hand, the maximum available curvature decreases with increase in pier size.

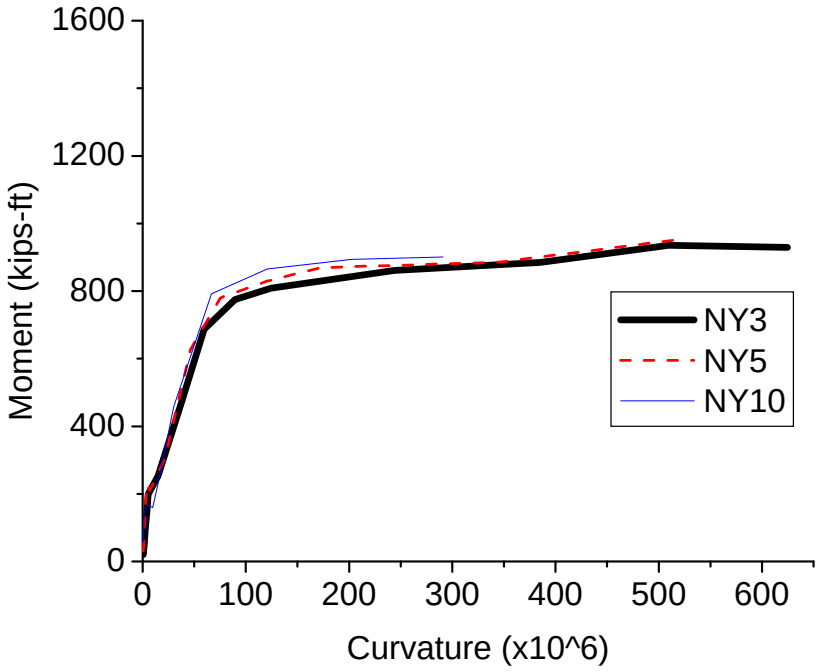

Figure 6.3: Moment Curvature Plot for the New York Bridge.

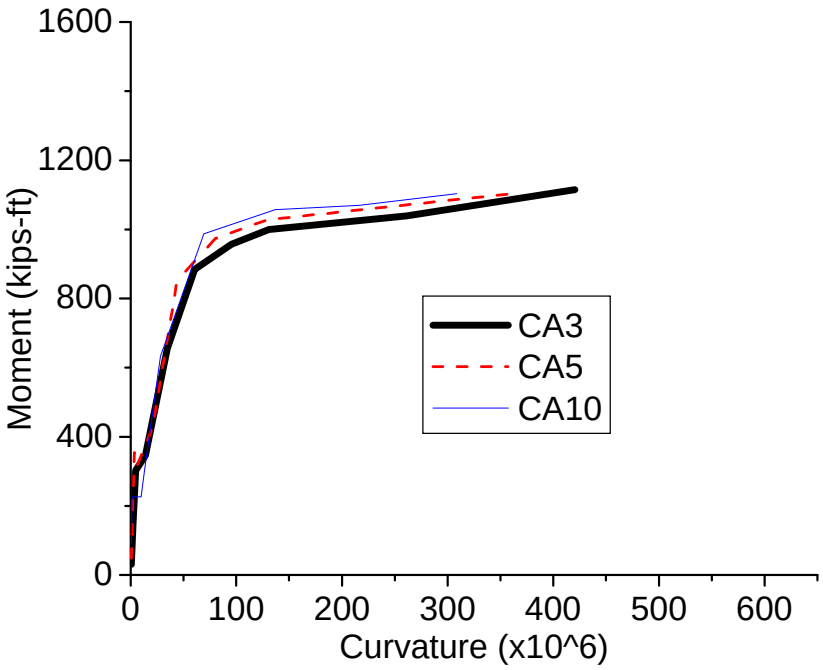

Figure 6.4: Moment Curvature Plot for the California Bridge.

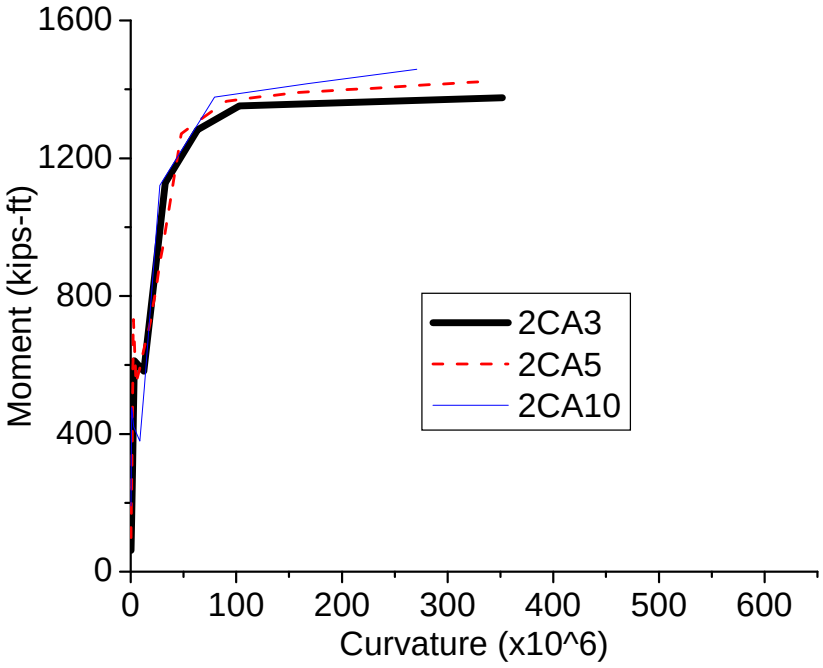

Figure 6.5: Moment Curvature Plot for 2CA bridges.

Moment curvature curves in Figures 6.3 to 6.5 have been used as nonlinear hinge properties to carry out pushover analysis by SAP2000 program (CSI 2007) to obtain force-deflection curves shown in Figures 6.6 to 6.8.

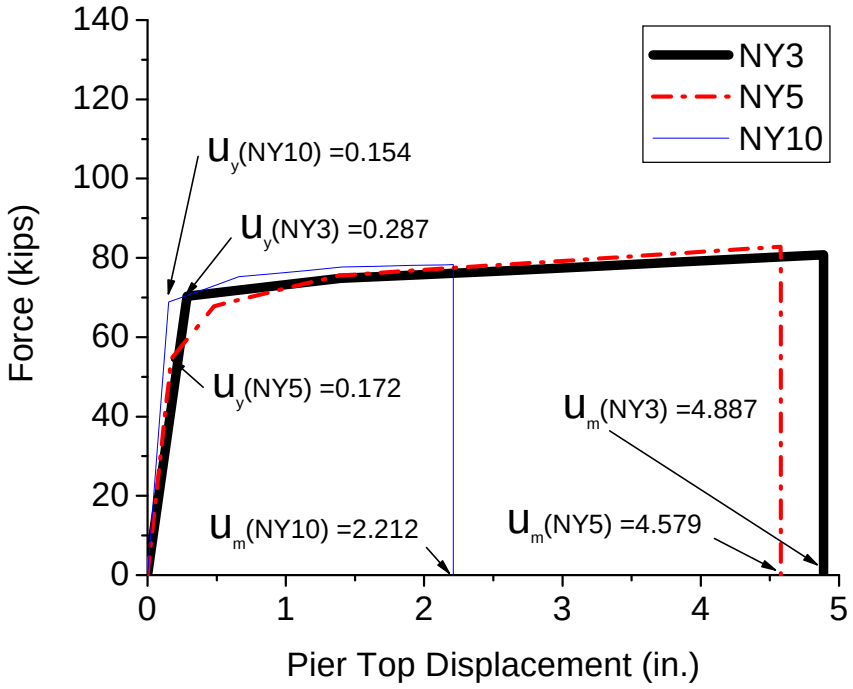

Figure 6.6: Force-Deflection Curve Pier of New York Bridge.

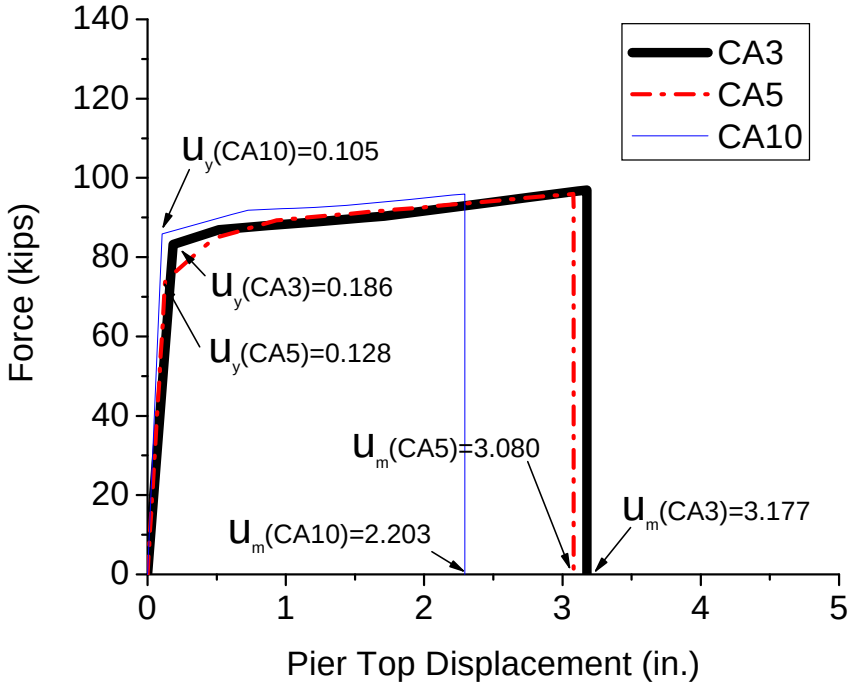

Figure 6.7: Force-Deflection Curve of Pier California Bridge.

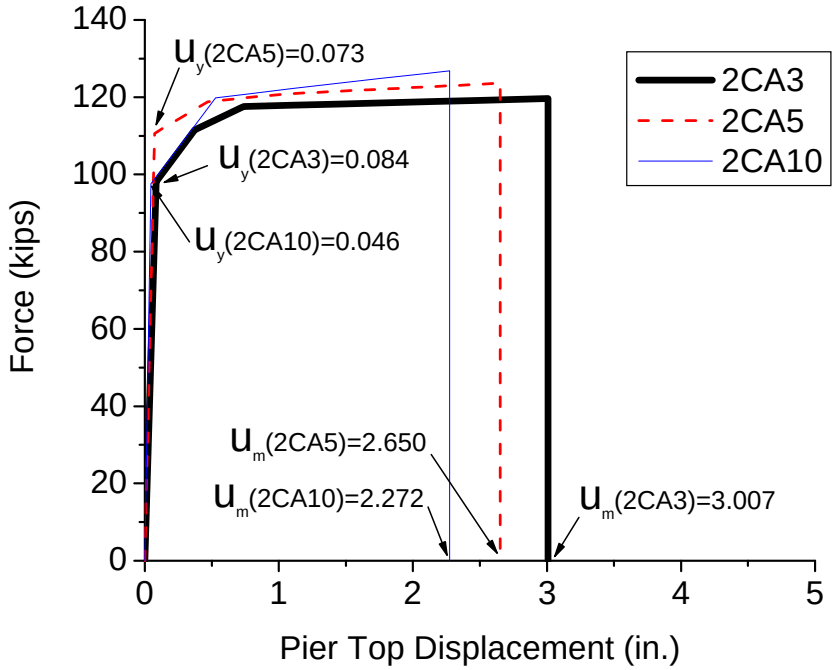

Figure 6.8: Force-Deflection Curve of Pier 2CA Bridge.

Using equations (6.1) & (6.2), we can calculate the yield strength factor R_y and ductility factor μ for three bridge piers in Figures 6.6 to 6.8. For example, for New York bridge with f_c'=3000 psi, the yield strength factor R_y = 0.505 and ductility factor μ = 17.1 are calculated by considering 0.2 g seismic load. This implies that the bridge is in elastic range to resist the seismic load. For California bridge with f_c'=3000 psi, the yield strength factor R_y and ductility factor μ are calculated to be 4.27 and 17.07, respectively, for a seismic load of 0.8g.

In order to compare the ductility factor of all bridge piers, R_y and μ are calculated by considering 0.8 g seismic load for piers of NY, CA and 2CA bridges. Table 6.3 shows values of R_y, μ and μ/R_y for NY, CA and 2CA bridges. In Table 6.3, subscripts to NY, CA and 2CA unconfined strength of concrete in ksi.

Table 6.3. Ductility factor of bridges considering 0.8g seismic load

	u_y (in.)	um (in.)	Ry	μ	μ/R_y
$f_c' = 3{,}000$ psi					
NY3	0.287	4.887	5.053	17.05	3.4
CA3	0.186	3.177	4.270	17.07	4.0
2CA3	0.084	3.007	3.620	35.96	9.9
$f_c' = 5{,}000$ psi					
NY5	0.172	4.579	6.512	26.59	4.1
CA5	0.128	3.080	4.796	24.00	5.0
2CA5	0.073	2.650	3.210	36.28	11.3
$f_c' = 10{,}000$ psi					
NY10	0.154	2.212	5.158	14.39	2.8
CA10	0.105	2.203	4.136	20.94	5.1
2CA10	0.046	2.272	3.642	49.92	13.7

For bridges with 3000 psi concrete strength, it is observed that μ is the same for NY3 and CA3 bridge piers and it increases to approximately 36 for 2CA3 bridge pier. On the other hand, the strength reduction factor, R_y, decreases as the bridge design changes from NY3 to CA3 to 2CA3. The ratio $\mu/R_y = u_m/u_0$ can be defined as the ratio of maximum inelastic displacement and the elastic displacement during the ground motion (if the structure didn't yield). This ratio can be considered as a quantitative measure of ductile capacity of the bridge piers with respect to equivalent elastic system. It is observed from Table 6.3 that the ratio μ/R_y increases from 3.4 to 9.9 for three bridges with concrete strength of 3000 psi. For concrete strength 5000 psi and 10,000 psi, this ratio increases from 4.1 to 11.3 and 2.8 to 13.7 respectively.

Three levels of blast loads have been applied on the bridge to investigate correlations between blast loads and seismic strengths. These levels of loads are categorized as "Low", "Medium" and "High" loads. The amount of TNT charge for these levels of blast loads is not mentioned because of sensitivity of the information. Hence, all together, 27 cases of blast load simulations, as shown in Table 6.4, have been considered.

Table 6.4: Load Cases for Blast Load Simulations on the Bridge.

Load Case	Seismic Capacity	Pier size (ft)	Concrete strength (psi)	Blast load level
1	NY	3	3,000	Low
2	NY	3	3,000	Medium
3	NY	3	3,000	High
4	CA	3.5	3,000	Low
5	CA	3.5	3,000	Medium
6	CA	3.5	3,000	High
7	2CA	4.5	3,000	Low
8	2CA	4.5	3,000	Medium
9	2CA	4.5	3,000	High
10	NY	3	5,000	Low
11	NY	3	5,000	Medium
12	NY	3	5,000	High
13	CA	3.5	5,000	Low
14	CA	3.5	5,000	Medium
15	CA	3.5	5,000	High
16	2CA	4.5	5,000	Low
17	2CA	4.5	5,000	Medium
18	2CA	4.5	5,000	High
19	NY	3	10,000	Low
20	NY	3	10,000	Medium
21	NY	3	10,000	High
22	CA	3.5	10,000	Low
23	CA	3.5	10,000	Medium
24	CA	3.5	10,000	High
25	2CA	4.5	10,000	Low
26	2CA	4.5	10,000	Medium
27	2CA	4.5	10,000	High

6.3 BLAST LOAD ANALYSIS AND OBSERVED FALIURE MECHANISMS

Numerical simulations have been carried out by developing FEM models for each of the 27 load cases in Table 6.4, The FEM model has 500,000 to 700,000 DOFs and typically require approximately 12 days to finish one simulation on a Quard-Core Pentium computer with 3 GB RAM. Using the simulation results for first 9 load cases, various failure mechanism of bridge components of subject to blast loads have been identified. Description of these failure mechanisms is presented in the following.

6.3.1 Failure mechanisms

A. Failure of Pier / Abutment: Six types of failure mechanisms described below have been identified for pier through FEM simulation of the bridge subject to blast loads. These mechanisms, labeled as A1 to A6, are discussed in the following..

Damage Mechanism A1. Eroding of pier bottom concrete: It has been observed that the concrete near the bottom section of piers close to blast loads get eroded, as shown in Figure 6.9. Strength of pier material and rebar detailing in the bottom portion of the pier are the key factors affecting this damage mechanisms.

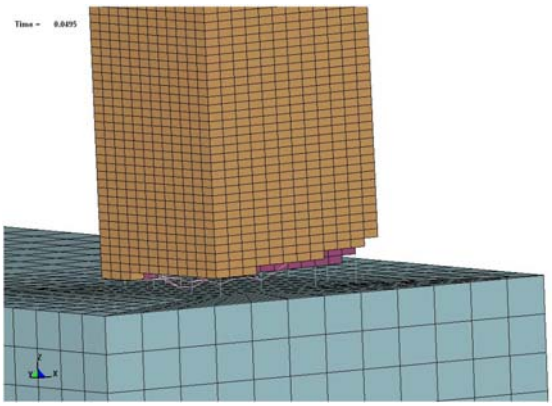

Figure 6.9 Damage Mechanism A1: Eroding of pier bottom concrete

Damage Mechanism A2. Shearing of a Pier from the footing: Blast pressure on a pier and horizontal force transferred from pier cap to a pier can cause the shearing failure at the bottom of a pier, as shown in Figure 6.10. A circle section of pier can be effective in reducing this kind of failure.

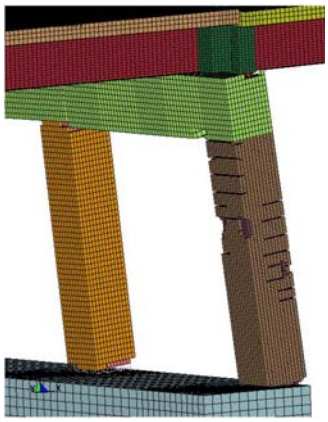

Figure 6.10 Damage Mechanism A2: Shearing of the Pier from the Footing

Although there are limited experimental data on blast tests, damage mechanisms A1 and A2 can be observed from some explosion tests, as shown in Figure 6.11 [Odwald (2005)]. Figure 6.11 clearly shows the tendency of steel and concrete columns to shear away and damage near the bottom section of concrete column.

Figure 6.11. Column failure mechanisms in explosive tests [Oswald (2005)]

Damage Mechanism A3. Rebar severance: If pier is tied well to the pier cap, the pier will tend to be pulled out from the footing because of the concentration of stress induced by section change between the pier cap and a pier. This can cause severance of longitudinal rebars, as shown in Figure 6.12, in affected bridge piers.

Stirrups fail at the connection of pier and footing, as shown in Figure 6.12. This mechanism can also be observed in Figure 6.12. Denser detailing of stirrups may prevent occurrence of this type of mechanism.

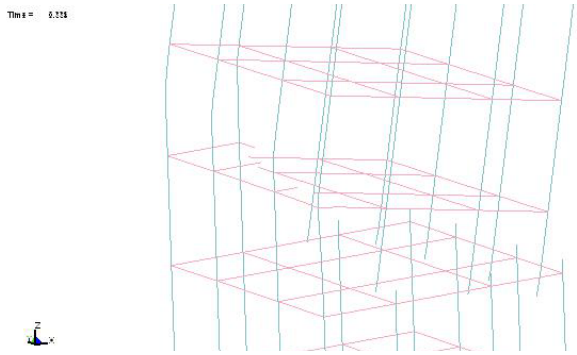

Figure 6.12: Severance of Rebars in the Pier Steel Cage.

Matthews et. al. has presented damage of steel rebar cage in column in a progressive collapse test completed in Taiwan in August 2006 [Matthews et al. (2007)]. His test results show the observed longitudinal rebar severance mechanism shown in Figure 6.13, which is similar to the mechanism in Figure 6.12 observed by numerical simulations.

Figure 6.13: Severance of longitudinal rebars during a test by Matthews et al. (2007).

Damage Mechanism A4. Breakage of pier: Pier breaks because of flexural failure or shear failure, as shown in Figure 6.14. This mechanism will lead to bridge collapse inevitably.

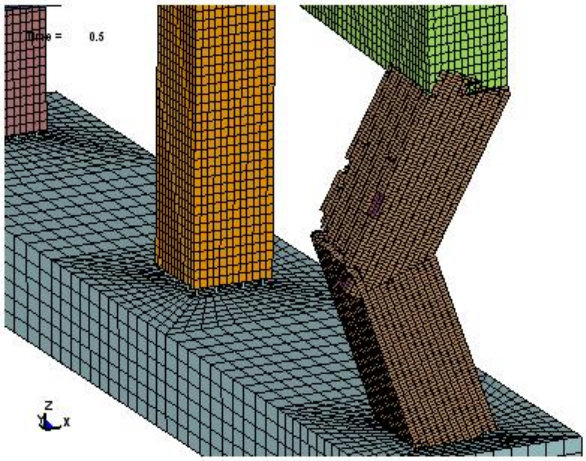

Figure 6.14: Breakage of Pier

Damage Mechanism A5. Spalling of concrete surface: Concrete surfaces undergo significantly amount of spalling under blast wave loads. During the application of blast loads on concrete surface of a pier, some of the blast waves are reflected back from the pier

surface. This causes a tensile wave effect on the back surface of the pier, which causes spalling of concrete, see Figure 6.15. Hence, spalling of concrete is usually more severe on the back surfaceof a puier than on the front surface facing the explosive.

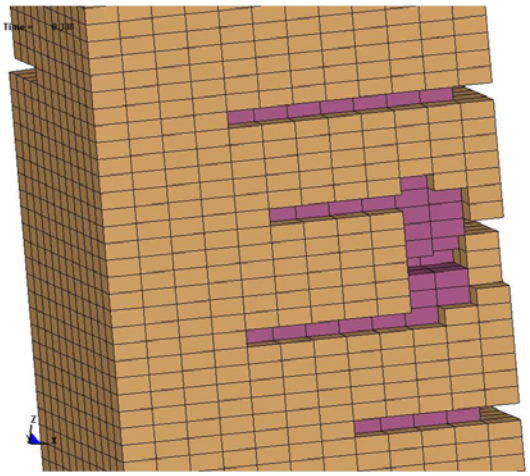

Figure 6.15: Spalling of Concrete Surface and Damage of Pier Concrete Core.

Damage Mechanism A6. Plastic Hinge Formation: Concrete core of piers is crushed under the impact of high blast loads, resulting in the formation of plastic hinge in piers at locations of high blast loads, as shown in Figure crushes. It means that a plastic hinge forms at the middle of pier. In extreme case, the column breaks in the middle, as shown in Fig 6.16. Plastic hinges in columns can also be observed in explosion tests carried out by Oswald (2005). Recently, Bruneau et al. (2006) have also carried out blast tests on scaled models of steel piers. Their test results also show the formation of plastic hinges in steel piers, as shown in Figure 6.17.

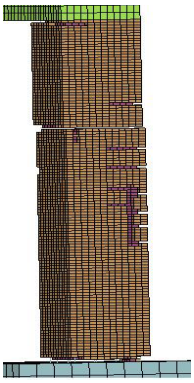

Figure 6.16: Formation of Plastic Hinge in the middle of a Pier.

Figure 6.17: Plastic Hinge Formation in a Pier During Blast Test by Bruneau et al. (2006).

Damage Mechanisms for the Bent Beam: Bent beam has been observed to be failing through mechanisms B1, B2 and B3 shown in Figures 6.18.

Damage Mechanism B1. Local Failure of Concrete Under Bearings. Bridge bearings can sustain pressure load up to 12 ksi, which is much higher than 3000 psi compressive strength of concrete. As a result of this, the bent concrete under a bridge bearing may be damaged by crushing. Improved detailing under bearings or the use of higher compressive strength concrete can be helpful in preventing or minimizing this type of damage mechanism.

B2. Crush of Concrete. Concrete near the connection between bent and pier may be crushed because of stress concentration.

B3. Shear failure of bent. Deck may be lifted during the explosion. When the deck falls back on bents, shear failure of bents may occur. This mode of failure can be prevented by improved detailing in the bents and by the use of uplift restrained bearings to prevent lifting up of the deck. An example of similar type of bent beam failure has been observed in transfer girder of Alfred Murrah Building, Oklahoma City in 1995 [Osteraas (2006)], as shown in Figure 6.19.

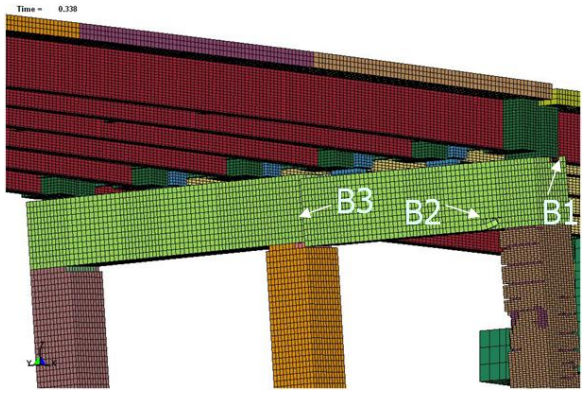

Figure 6.18: Damage Mechanisms for the Failure of the Bent Beam.

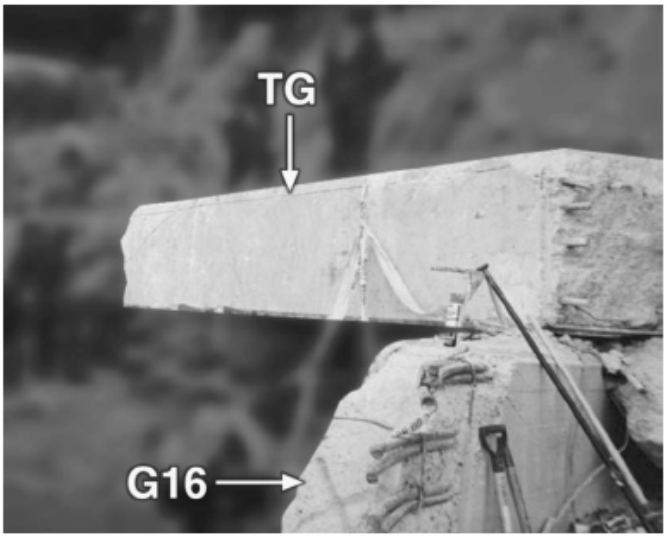

Figure 6.19: Failure of Connection Between Transfer Girder and Column in Alfred Murrah Building. [Osteraas (2006)]

C. Damage Mechanisms For the Failure of Stringers: Two mechanisms, C1 and C2, have been observed to be responsible for causing failure of stringers during blast load simulations on highway bridge.

Damage Mechanism C1. Collapse: The most prominent mechanism for the failure of stringers is the loss of pier support because of blast load. It has been observed during numerical simulations that piers are likely to be blown away, particularly during high blast loads.

C2. Yielding of steel material: The yield stree of steel in steel stringers is 36 ksi. Hence, steel stringers are likely to be damaged by yielding if the maximum stress exceeds 36 ksi. For example, Figure 6.20 shows stress time history of steel stringers under blast loads. It is observed that the maximum stress in a stringer reaches 37,558 psi, which is higher than the 36 ksi yield stress 36 ksi. Hence, stress in steel stringers becomes saturated at 36 ksi, implying that the stringer is undergoing yielding.

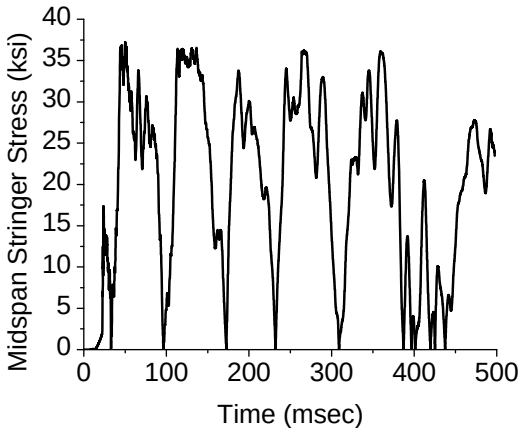

Figure 6.20: Stress Time History of Stringer Under Blast Load.

D. Damage Mechanisms for Failure of Deck: The bridge deck has been seen to be failing in the three mechanisms described below.

Damage Mechanism D1. Being Crushed Under High Pressure: Fig. 6.21 shows the damage mechanism where the bridge deck is crushed under high pressure blast load.

Damage Mechanism D2. Being lifted up by the blast wave: Deck can be lifted up if it is not well tied to the bridge substructure. Figure 6.21 shows this mechanism of bridge deck being lifted up by blast wave pressure.

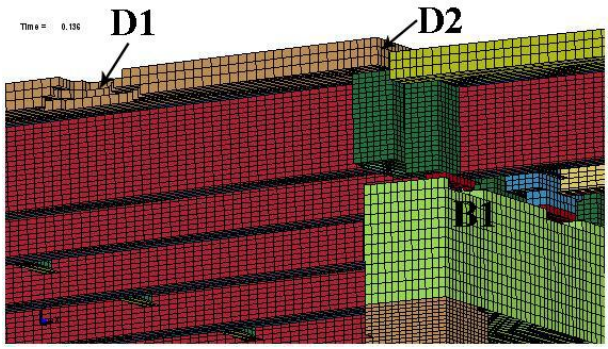

Figure 6.21: Bridge Deck Damage Mechanisms.

Damage Mechanism D3. Collapse Because of Loss of Support: The kinetic force of the

bridge deck falling back can cause the stringer failure mechanism C1. The bridge deck can lose support and collapse after the failure of substructure. The bridge deck can also collapse because of excessive later movement at the top of bridge piers. Figure 6.22 shows this mode of failure of the bridge deck.

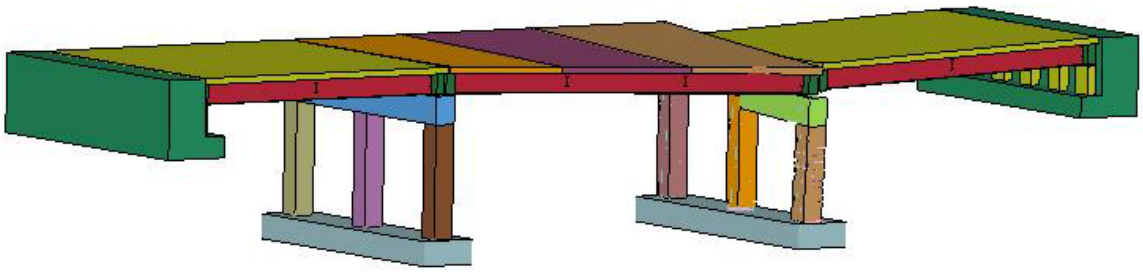

Figure 6.22 Deck collapse

6.3.2 Failure Mechanisms during Whole Bridge Simulation

Failure mechanisms described above have been identified from numerous bridge response simulations. Hence, not all failure mechanisms may appear during blast load simulation of a particular bridge. In fact, presence of a particular failure mechanism depends on bridge geometry, magnitude of blast loads, distance of blast charge from bridge components, and surrounding environment. Figures 6.23 to 6.49 shows different failure mechanisms observed during different cases of whole bridge simulation cases in Table 6.4.

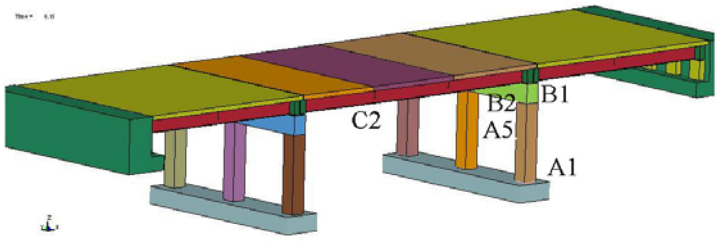

Figure 6.23: Damage Mechanisms during Bridge with New York Seismic Capacity and Subjected to Low Level Blast Loads.

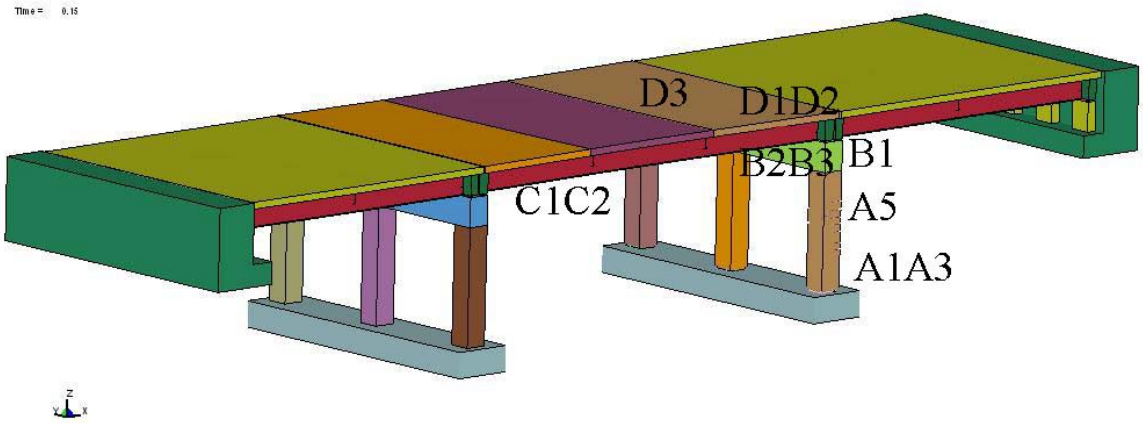

Figure 6.24: Damage Mechanisms during Bridge with New York Seismic Capacity and Subjected to Medium Level Blast Loads.

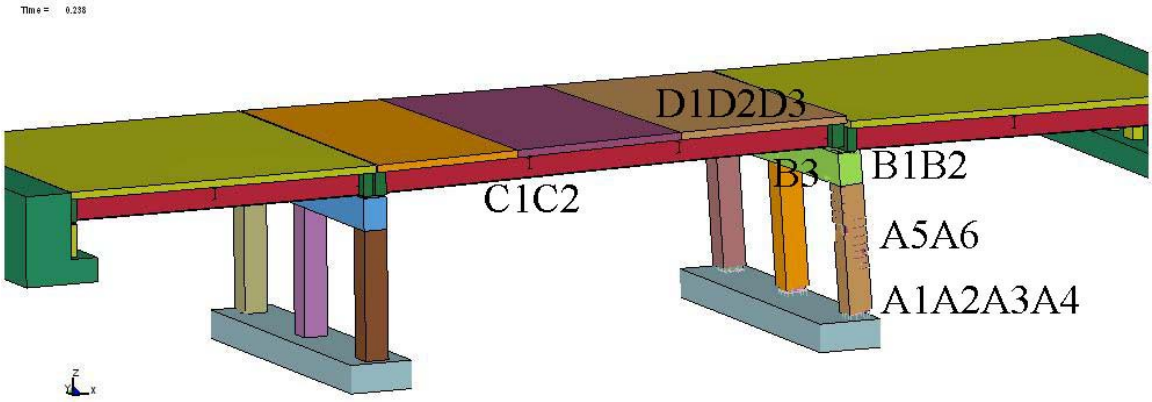

Figure 6.25: Damage Mechanisms during Bridge with New York Seismic Capacity and Subjected to High Level Blast Loads.

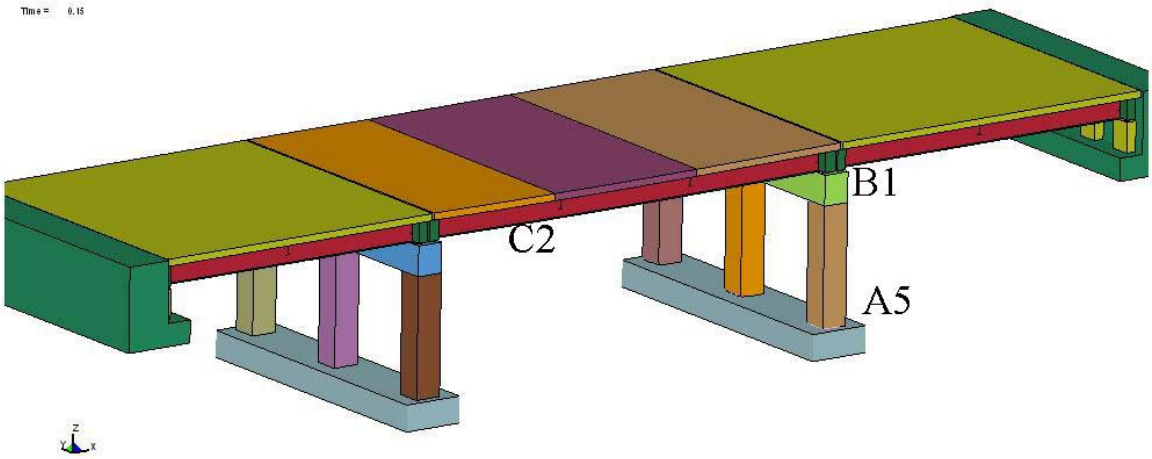

Figure 6.26: Damage Mechanisms during Bridge with California Seismic Capacity and Subjected to Low Level Blast Loads.

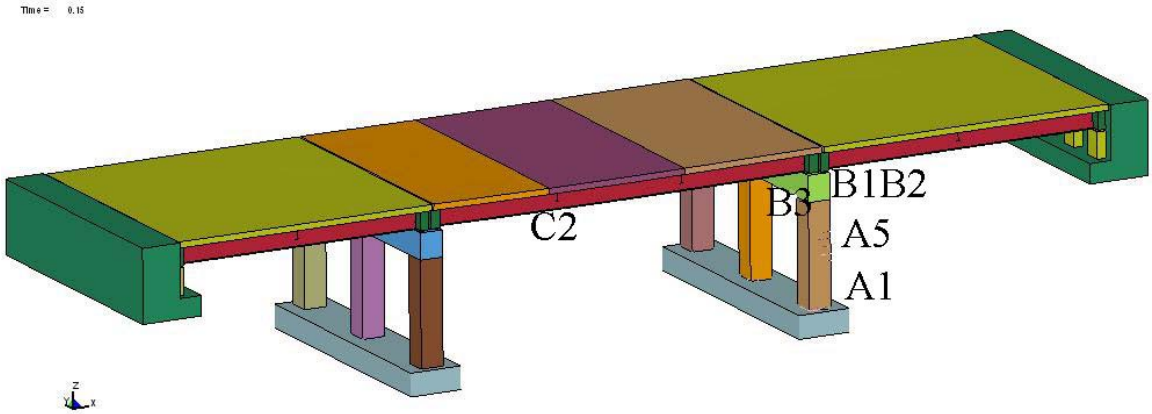

Figure 6.27: Damage Mechanisms during Bridge with California Seismic Capacity and Subjected to Medium Level Blast Loads.

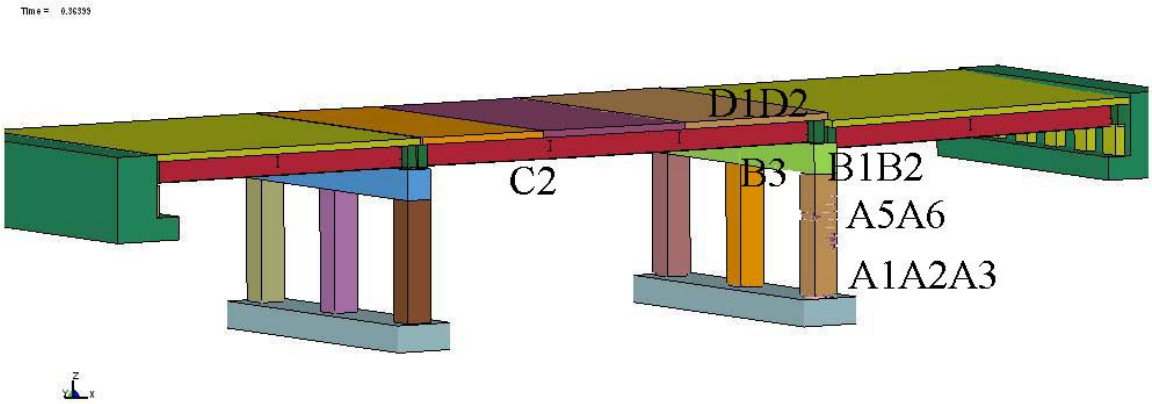

Figure 6.28: Damage Mechanisms during Bridge with California Seismic Capacity and Subjected to High Level Blast Loads.

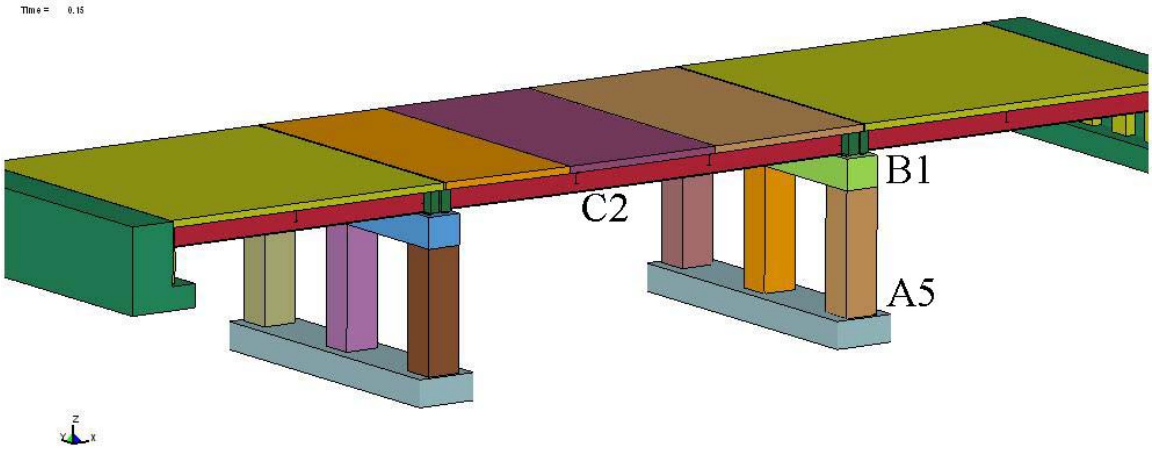

Figure 6.29: Damage Mechanisms during Bridge with Double of California Seismic Capacity and Subjected to Low Level Blast Loads.

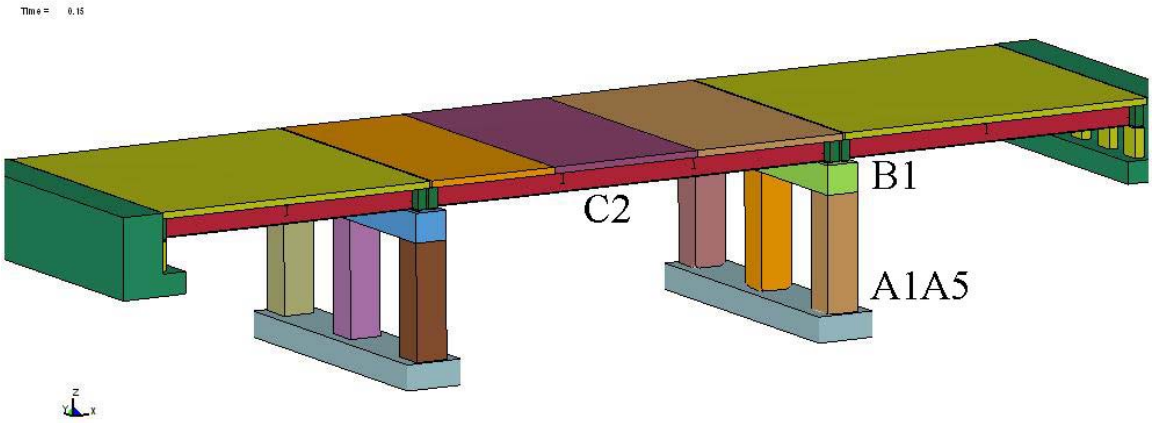

Figure 6.30: Damage Mechanisms during Bridge with Double of California Seismic Capacity and Subjected to Medium Level Blast Loads.

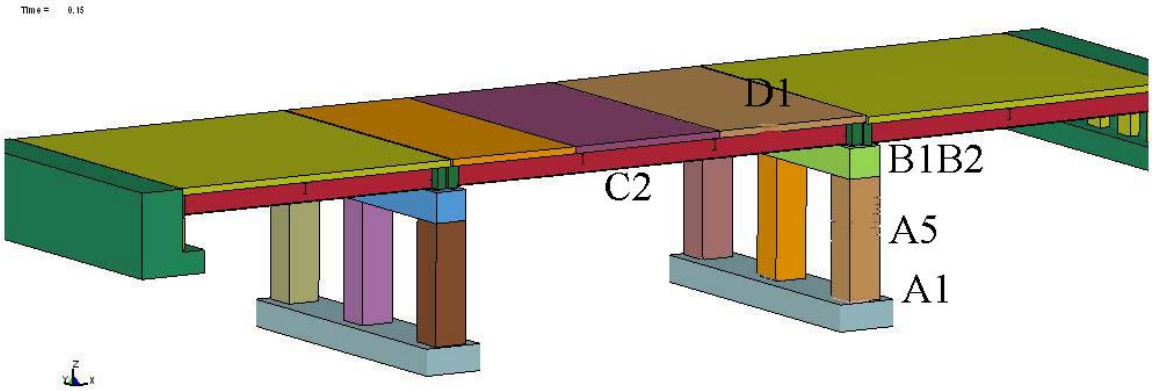

Figure 6.31: Damage Mechanisms during Bridge with Double of California Seismic Capacity and Subjected to High Level Blast Loads.

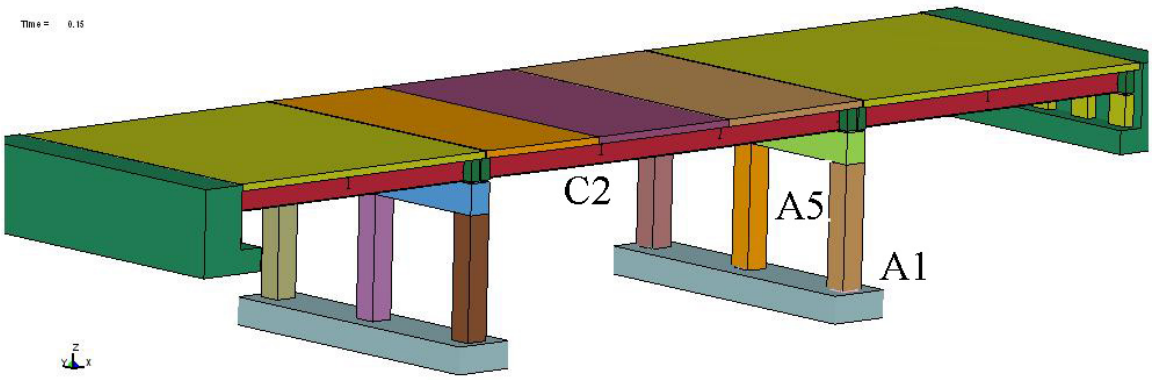

Figure 6.32: Damage Mechanisms during Bridge with 5000 psi Concrete, New York Seismic Capacity and Subjected to Low Level Blast Loads.

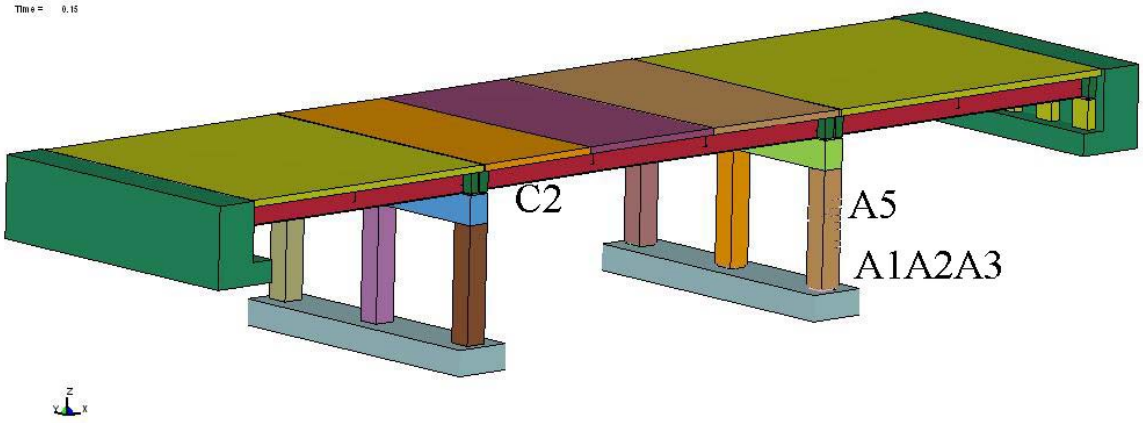

Figure 6.33: Damage Mechanisms during Bridge with 5000 psi Concrete, New York Seismic Capacity and Subjected to Medium Level Blast Loads.

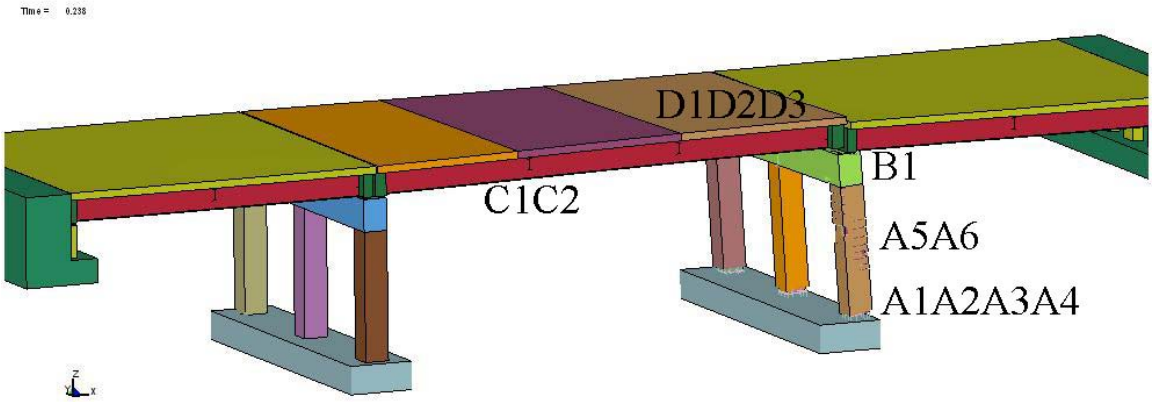

Figure 6.34: Damage Mechanisms during Bridge with 5000 psi Concrete, New York Seismic Capacity and Subjected to High Level Blast Loads.

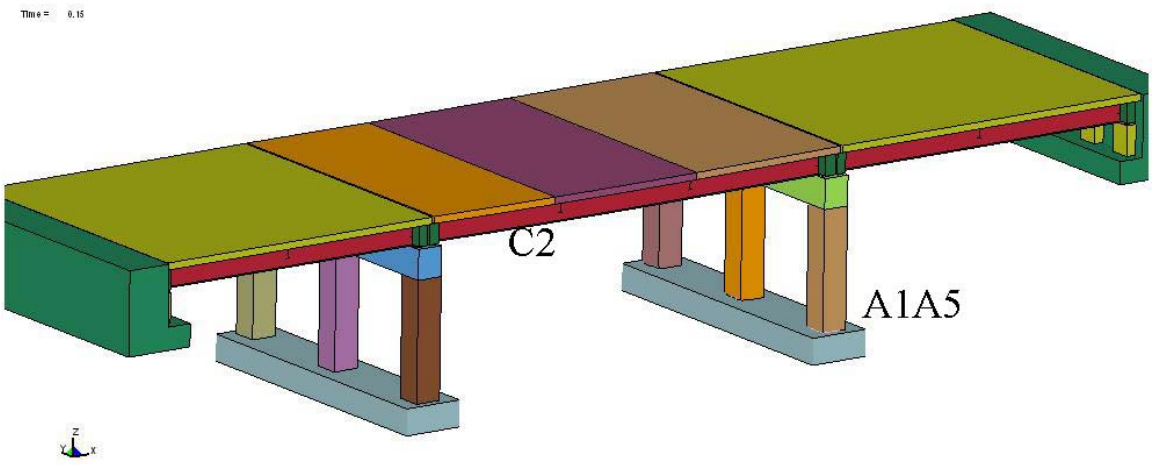

Figure 6.35: Damage Mechanisms during Bridge with 5000 psi Concrete, California Seismic Capacity and Subjected to Low Level Blast Loads.

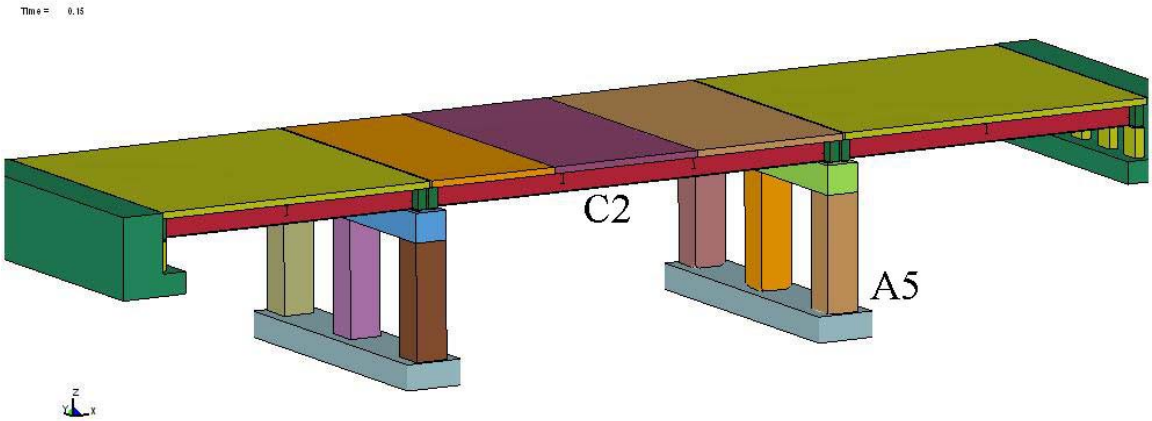

Figure 6.36: Damage Mechanisms during Bridge with 5000 psi Concrete, California Seismic Capacity and Subjected to Medium Level Blast Loads.

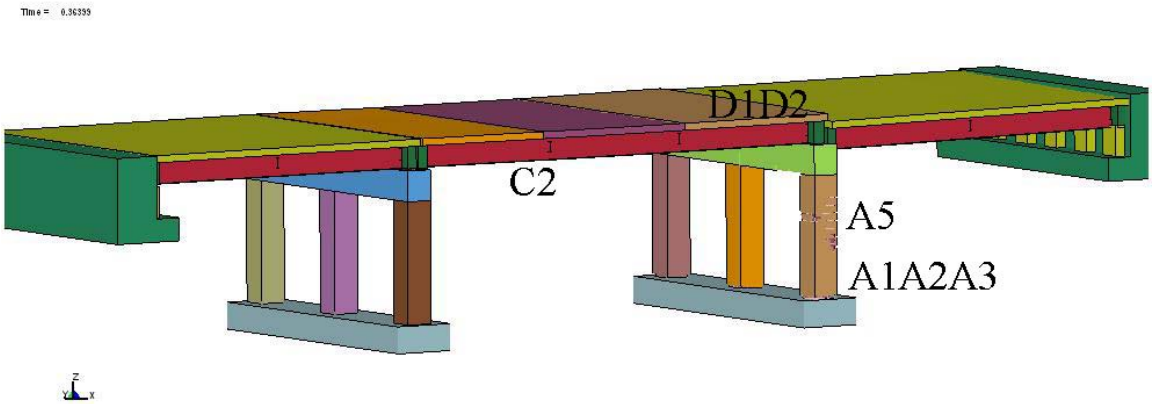

Figure 6.37: Damage Mechanisms during Bridge with 5000 psi Concrete, California Seismic Capacity and Subjected to High Level Blast Loads.

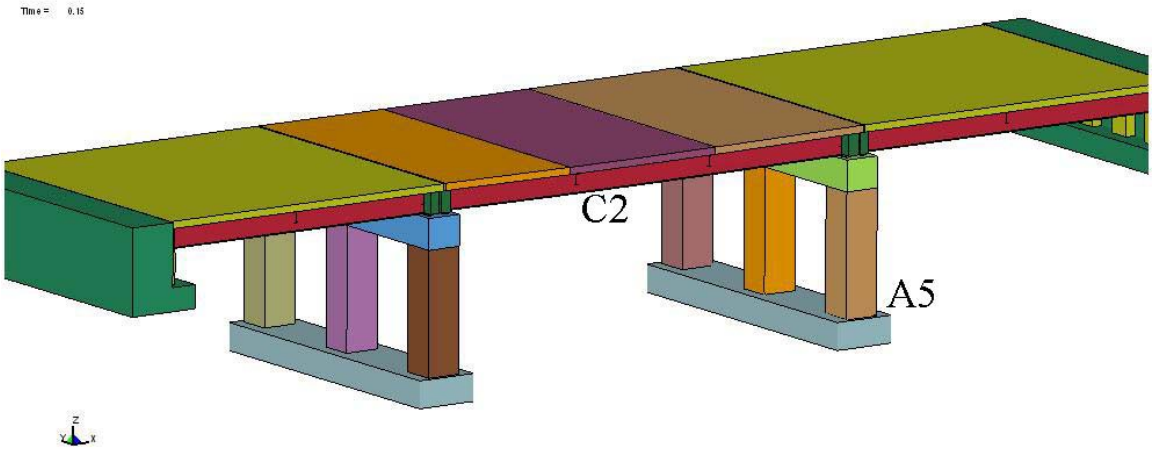

Figure 6.38: Damage Mechanisms during Bridge with 5000 psi Concrete, Double of California Seismic Capacity and Subjected to Low Level Blast Loads.

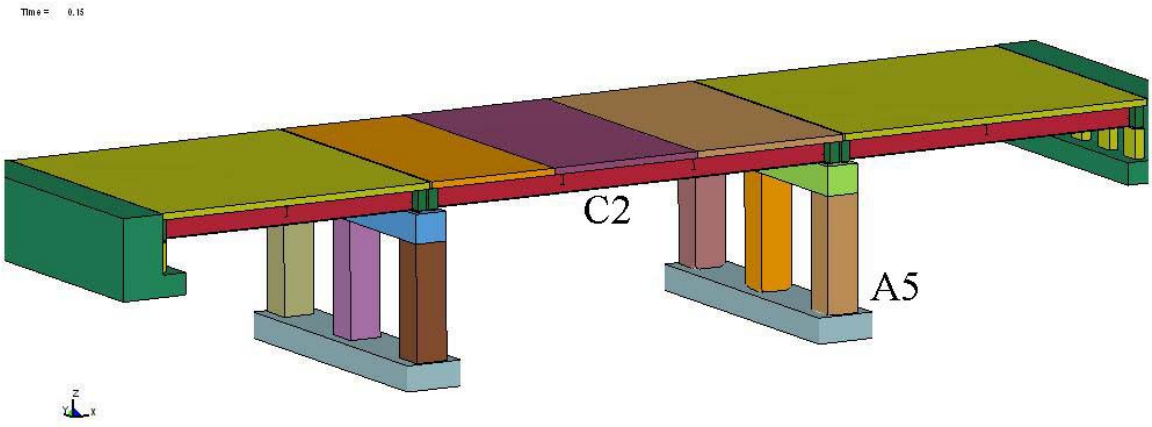

Figure 6.39: Damage Mechanisms during Bridge with 5000 psi Concrete, Double of California Seismic Capacity and Subjected to Medium Level Blast Loads.

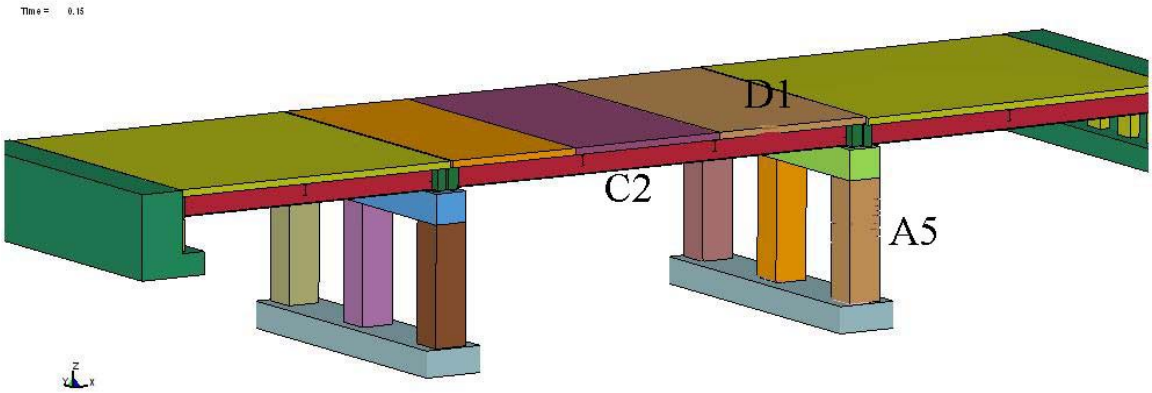

Figure 6.40: Damage Mechanisms during Bridge with 5000 psi Concrete, Double of California Seismic Capacity and Subjected to High Level Blast Loads.

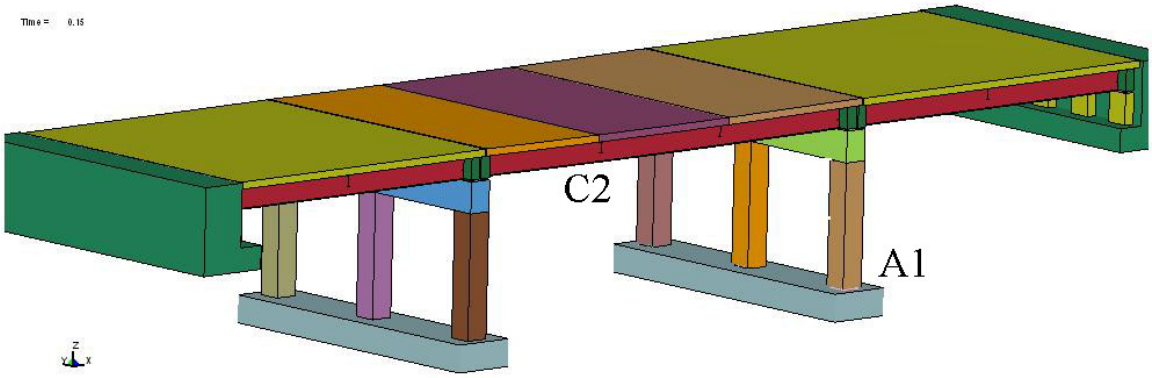

Figure 6.41: Damage Mechanisms during Bridge with 10,000 psi Concrete, New York Seismic Capacity and Subjected to Low Level Blast Loads.

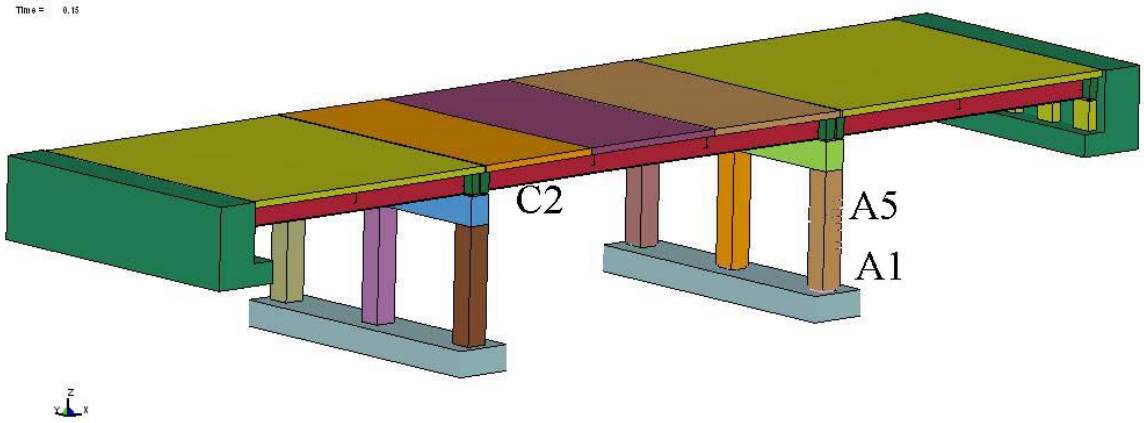

Figure 6.42: Damage Mechanisms during Bridge with 10,000 psi Concrete, New York Seismic Capacity and Subjected to Medium Level Blast Loads.

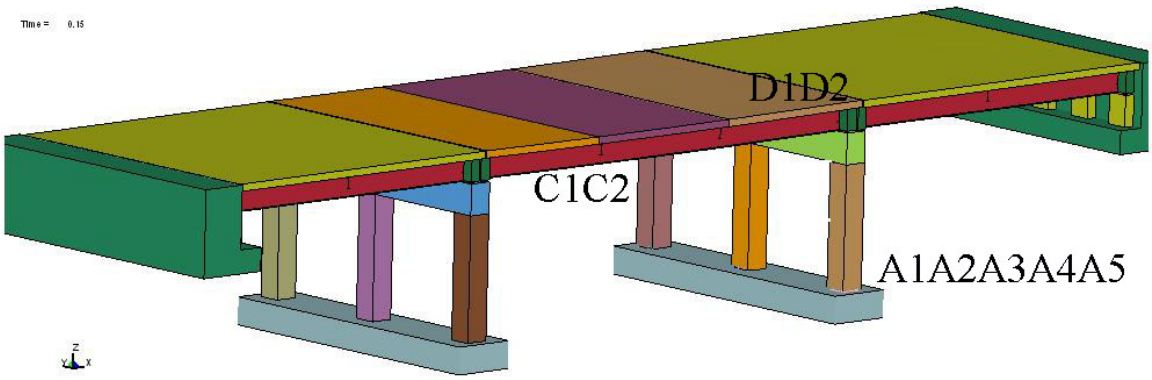

Figure 6.43: Damage Mechanisms during Bridge with 10,000 psi Concrete, New York Seismic Capacity and Subjected to High Level Blast Loads.

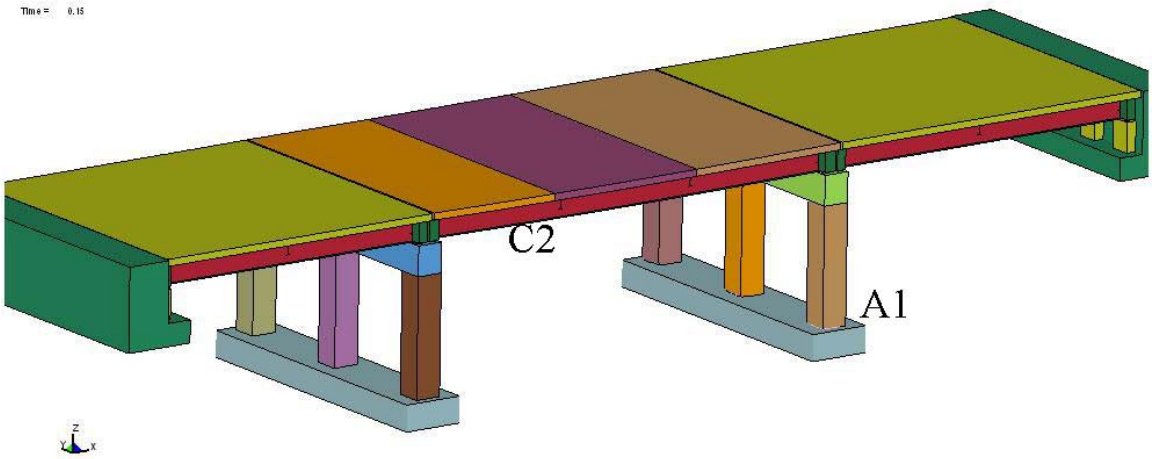

Figure 6.44: Damage Mechanisms during Bridge with 10,000 psi Concrete, California Seismic Capacity and Subjected to Low Level Blast Loads.

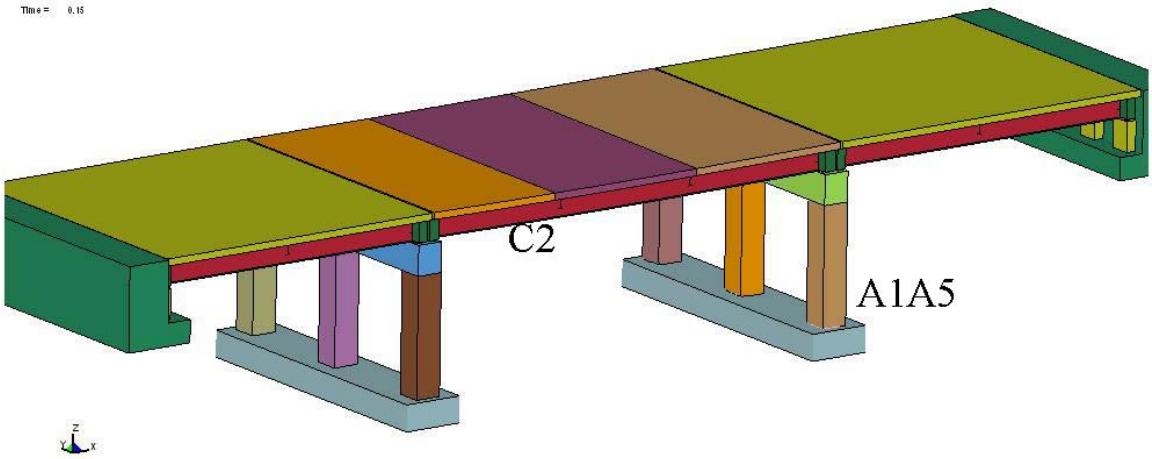

Figure 6.45: Damage Mechanisms during Bridge with 10,000 psi Concrete, California Seismic Capacity and Subjected to Medium Level Blast Loads.

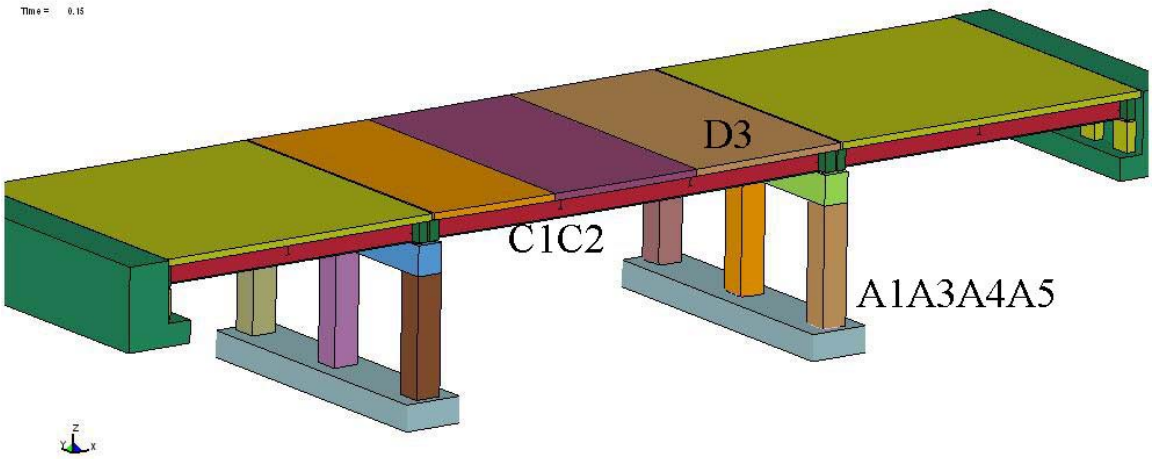

Figure 6.46: Damage Mechanisms during Bridge with 10,000 psi Concrete, California Seismic Capacity and Subjected to High Level Blast Loads.

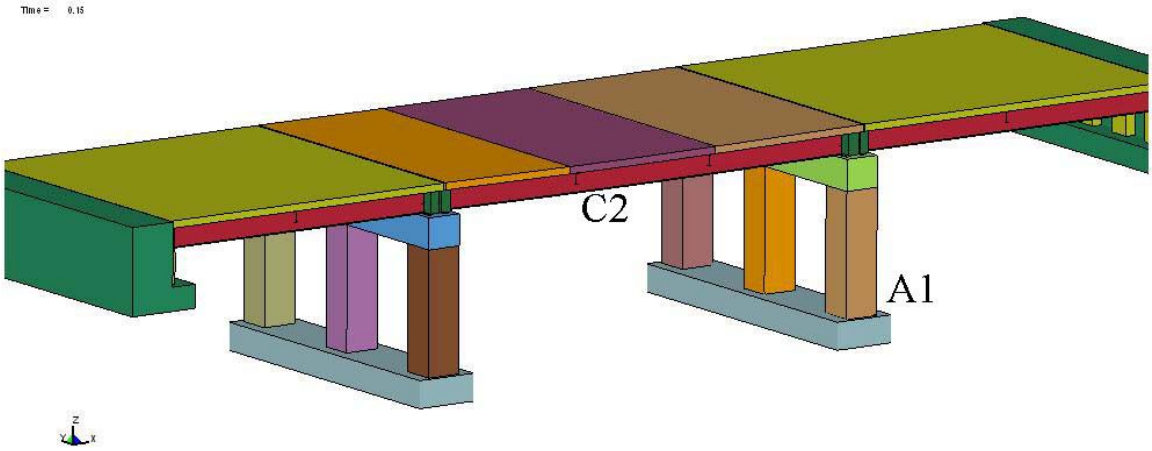

Figure 6.47: Damage Mechanisms during Bridge with 10,000 psi Concrete, Double of California Seismic Capacity and Subjected to Low Level Blast Loads.

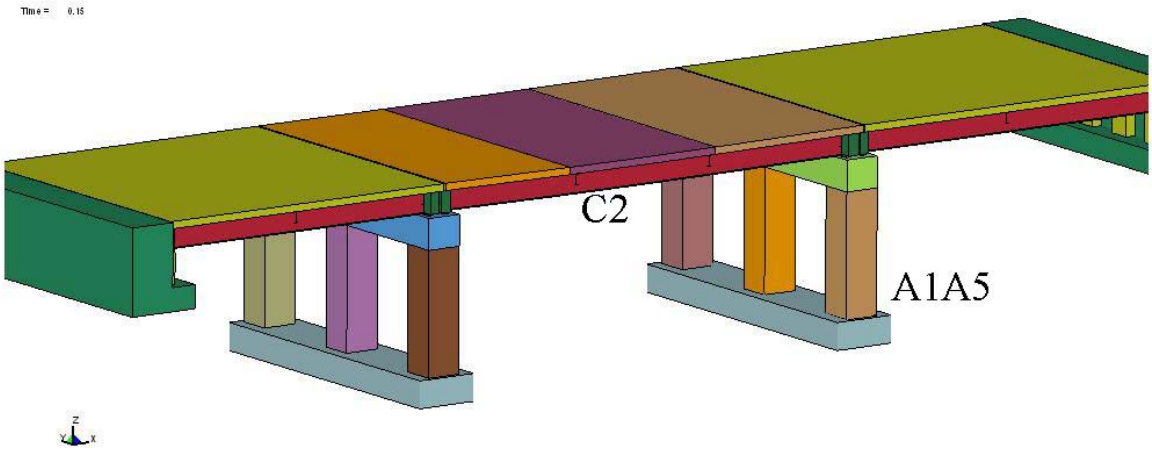

Figure 6.48: Damage Mechanisms during Bridge with 10,000 psi Concrete, Double of California Seismic Capacity and Subjected to Medium Level Blast Loads.

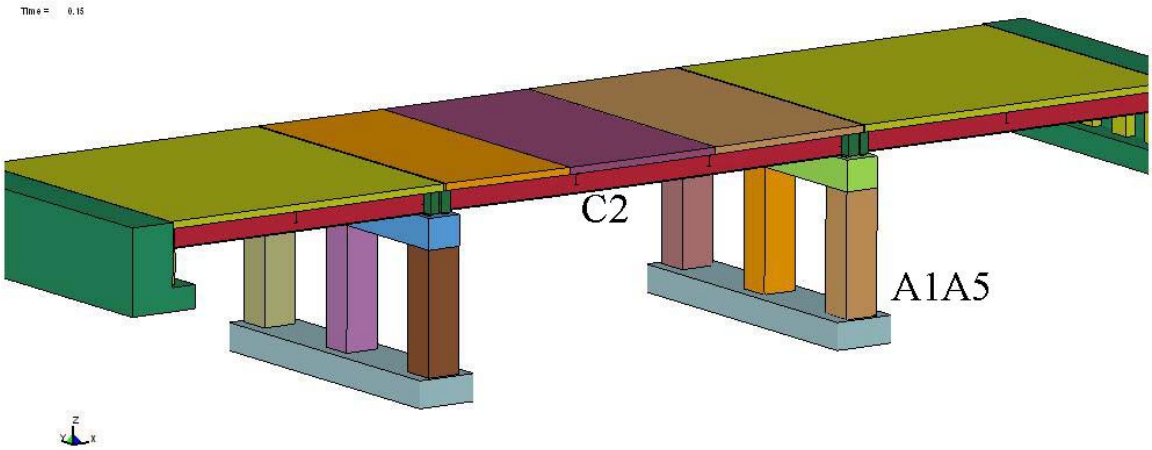

Figure 6.49: Damage Mechanisms during Bridge with 10,000 psi Concrete, Double of California Seismic Capacity and Subjected to High Level Blast Loads.

Based on damage mechanisms for various blast load levels, concrete compressive strength and bridge seismic resistance presented above, we can make the following observations.

Influence of blast load level. Generally, fewer number of damage mechanisms have been observed in a particular bridge simulation for a lower level of blast load. With an increase

in blast load on a particular bridge, number of damage mechanisms is also seen to increase. For example, for bridges in New York seismic zone with concrete compressive strength of 3000 psi, the bridge has all 14 failure mechanisms under high level blast load, 11 mechanisms under medium level blast load and 5 in case of low level blast load.

Influence of pier size. Bridges with higher seismic capacities (i.e., bridges with larger pier sizes) have been observed to have a lesser level of damages. For example, bridges designed for New York (3 ft pier size), California (3.5 ft pier size) and Double of California (4.5 ft pier size) have been observed to have all 14 damage mechanisms, 6 damage mechanisms and only 3 failure mechanisms, respectively, under a high level of blast load. Hence, higher level of seismic resistance of bridge components has direct correlations with higher level of blast resistance.

Relationship between Different failure mechanisms. Some damage mechanisms, such as collapse of stringer and deck, are combined together. The occurrence of one will definitely lead to the occurrence of the other. On the other hand, damage mechanisms such as pier spalling and deck crushing, have no intrinsic relationship to each other.

Key damage mechanisms. Damage mechanisms, such as deck collapse and eroding of piers, are critical to the service performance of the bridge and should be prevented through multi-hazard blast resistant design. Damage mechanisms, such as spalling of pier and yielding of stringer, will occur under any level of blast load and don't pose serious restrictions to service level performance of the bridge. Multi-hazard blast level design should be carried out to minimize the impact of these mechanisms only during very high levels of blast loads.

Degree of Damages during a Damage Mechanism: It has been observed that the same type of damage mechanism may have different degrees of damages, depending on the blast load level, and bridge and material characteristics. For example, we observe pier eroding in cases 1-6 under different levels of blast load. However, the degree of damage in this mechanism varies significantly in cases 1 to 6. This is illustrated through Figure 6.50 which shows spalling of piers in New York Bridge subject to low, medium and high level blast loads. It is observed from Figure 6.50(c) that while entire pier bottom is eroded (which eventually leads to the collapse of the bridge) during high blast load, only a part of pier section is eroded during medium blast load. In fact, eroding of piers during medium level of blast load doesn't lead to collapse of the bridge. Only a minor spalling of concrete occurs in case of low level of blast load, as can be seen from Figure 6.50(a).

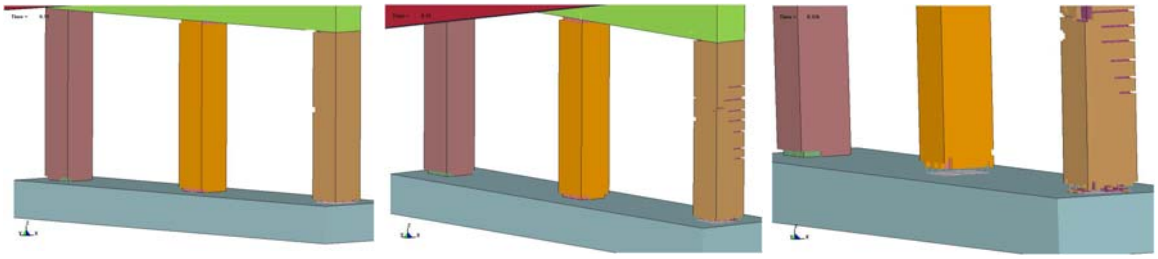

(a) Low Level Blast load (b) Medium Level Blast Load (c) High Level Blast

Figure 6.50: Degrees of Damage in Pier Eroding Damage Mechanism during Different Levels of Blast Loads.

6.3.3 Seismic Versus Blast Correlations

Figures 6.23 to 6.49 show different damage mechanisms observed in bridges with different levels of seismic resistance and subject to three different levels of blast loads. These damage mechanisms have been populated into Tables 6.5 to 6.7 for concrete

compressive strength of 3000 psi, 5000 psi and 10,000 psi, respectively, to investigate multi-hazard seismic-blast correlations. In these tables, "X" indicates the presence of a damage mechanism for a particular blast load case in Table 6.4.

For a particular value of compressive strength of concrete, Tables 6.5 to 6.7 show presence of damages mechanisms in a bridge with different levels of seismic resistance (i.e., NY, CA and 2CA bridges) and blast loads. It is observed from Table 6.5 that all bridges survive the low level blast load. Under high level blast load, both NY and CA bridges collapse and 2CA bridge survives, although it is severely damaged. As the seismic capacity of bridge components is increased from NY to 2CA, lesser damage mechanisms are observed to appear for a particular bridge. For example, NY bridge under high blast load exhibits 14 mechanisms and it exhibits 5 under low blast load. In comparison to this, the "2CA" bridge under low blast load exhibits only 3 mechanisms. These damage mechanisms contribute differently towards the failure of the bridge, as discussed previously. Mechanisms such as breakage of pier and crushing of bent, will lead to a definite collapse of the bridge. Hence, these mechanisms should be specially addressed in the multi-hazard design. Other mechanisms, such as spalling of pier and yielding of stringer, exist in all simulation cases, indicating that they cannot be prevented by increasing seismic design level, although their degree of severity can be reduced.

Table 6.6 shows damage mechanisms for bridges with concrete compression strength of f_c' = 5 ksi (5000 psi). Although the trend in Table 6.6 is similar to that in Table 6.5, fewer mechanisms are seen to be appearing because of increased concrete strength. For example, 12 mechanisms are observed in NY bridge under high blast load, as compared to 14 in Table 6.5 using 3000 psi concrete. Likewise, only 2 mechanisms are

observed in case of "2CA" bridge under low blast load as compared to 3 in Table 6.5 using 3000 psi results. Overall, it has been observed that the collapse is prevented in all cases of bridge simulations in Table 6.6 except for the NY bridge under high blast load.

Table 6.7 shows damage mechanisms for bridges with concrete compressive strength of f_c' = 10 ksi (10,000 psi). It is observed from Table 6.7 that the number of failure mechanisms increase with an increase in blast loads. The number of failure mechanisms decrease with an increase in section size of piers.

Although bridges with 10 ksi concrete exhibit lesser number of failure mechanisms than bridges with 5 ksi, they have exhibit brittle failure mechanisms during simulations. This can be explained by ductility factor in Table 6.3. Since we maintain the same steel reinforcement details for all bridges, ductility of bridge piers decreases with increase in concrete strength. In order to resist blast loads, bridge piers should be designed to resist both "local" effects and "global" effects. Local effects have been observed to control the bridge with 3 ksi concrete. Consequently, numerous failure mechanisms that result from direct action of blast loads have been observed in case bridges with 3 ksi concrete. Global effects control the behavior of the bridges in case of 10 ksi concrete. In this case, dynamic forces transferred from deck will push the pier into damage, which is similar to seismic mechanisms. Failure modes observed in case of 10 ksi concrete bridges have been observed to be caused by this process. Lesser number of failures are observed in case of bridges with 5 ksi concrete strengths because of a compromise (although not optimal) between "local" and "global" resistance capacities.

In order to investigate the influence of concrete strength, results are reorganized for

NY, CA and 2CA bridges for two levels of concrete compressive strength and are presented in Tables 6.8 to 6.10, respectively. It is clearly observed that the number of damage mechanisms in a particular simulation case decreases with increase in compressive strength of concrete from 3000 psi to 5000 psi, e,g., 14 to 12 for NY bridge, 13 to 7 for CA bridge and 6 to 3 for 2CA bridge under high blast load. NY bridge is too weak to sustain blast load. Hence, increased concrete strength cannot prevent it from collapsing. 2CA bridge is already strong (because of larger pier size) and it doesn't have many of the mechanisms even for 3000 psi concrete. However, increase in compressive strength of concrete plays a significant role in improving its blast resistance; number of damage mechanisms has been reduced from 13 to 7 because of increase in the compressive strength of concrete from 3000 psi to 5000 psi. Among these 7 mechanisms in 2CA bridges with 5000 psi concrete strength, 3 mechanisms (pier eroding, spalling of pier and yielding of stringers) are present even in case of low level blast load and these mechanisms don't pose serious threat to the safety of the bridge. The severity of remaining 4 mechanisms (shear at footing, rebar severance, crushing of deck and lifting up of deck) can be reduced by designing detailing and measures specific to these mechanisms. For example, crushing of deck can be reduced by measures such as improving the detailing, higher strength concrete and the use of composite panels, such as CFRP. Likewise, uplift of the deck can be eliminated by the uplift restrained bearings. These results clearly show that an effective multi-hazard design of bridge can be achieved by optimizing the design of bridge components to sustain different extreme events.

Tables 6.5 to 6.10 are essentially blast-seismic multi-hazard tables that can be used to modify existing seismic detailing guidelines to improve the performance of bridge

components during blast load events. For example, Table 6.9 can be used to improve the blast resistance of a bridge in California with 3000 psi concrete and a design blast load level of "Low" by identifying prominent damage mechanisms (e.g., spalling of pier, local failure of bent below bearings and the yielding of stringer) and designing appropriate countermeasures to resist these mechanisms. Although these countermeasures can be designed based on general engineering principles, a more detailing research on effective countermeasures is a topic of successive report.

Table 6.5: Blast –Seismic Muti-hazard Correlations for Bridges with 3000 psi Compressive Strength Concrete.

Failure Mechanism			Blast loads level on bridges (Low, Medium or High)								
			New York			California			2 CA		
	Item	Description	Low	Medium	High	Low	Medium	High	Low	Medium	High
Pier	A1	Pier eroding	X	X	X		X	X		X	X
	A2	Shear at footing			X			X			
	A3	Rebar severance		X	X			X			
	A4	Breakage of pier			X						
	A5	Spalling of pier	X	X	X	X	X	X	X	X	X
	A6	Plastic hinge			X			X			
Bent	B1	Local failure	X	X	X	X	X	X	X	X	X
	B2	Crush of bent	X	X	X		X	X			X
	B3	Shear failure		X	X		X	X			
Stringer	C1	Collapse		X	X			X			
	C2	Yielding	X	X	X	X	X	X	X	X	X
Deck	D1	Crush		X	X			X			X
	D2	Lift up		X	X			X			
	D3	Collapse		X	X			X			

X : Failure mechanism is observed in the specific bridge blast simulation.

Table 6.6: Blast –Seismic Muti-hazard Correlations for Bridges with 5000 psi Compressive Strength Concrete.

Failure Mechanism			Blast loads level on bridges (Low, Medium or High)								
			New York			California			2 CA		
	Item	Description	Low	Medium	High	Low	Medium	High	Low	Medium	High
Pier	A1	Pier eroding	X	X	X	X	X	X			
	A2	Shear at footing		X	X			X			
	A3	Rebar severance		X	X			X			
	A4	Breakage of pier			X						
	A5	Spalling of pier	X	X	X	X	X	X	X	X	X
	A6	Plastic hinge			X						
Bent	B1	Local failure			X						
	B2	Crush of bent									
	B3	Shear failure									
Stringer	C1	Collapse			X						
	C2	Yielding	X	X	X	X	X	X	X	X	X
Deck	D1	Crush			X			X			X
	D2	Lift up			X			X			
	D3	Collapse			X						

X : Failure mechanism is observed in the specific bridge blast simulation.

Table 6.7: Blast –Seismic Muti-hazard Correlations for Bridges with 10,000 psi Compressive Strength Concrete.

Failure Mechanism			Blast loads level on bridges (Low, Medium or High)								
			New York			California			Over-design		
	Item	Description	Low	Medium	High	Low	Medium	High	Low	Medium	High
Pier	A1	Pier eroding	X	X	X	X	X	X	X	X	X
	A2	Shear at footing			X						
	A3	Rebar severance			X			X			
	A4	Breakage of pier			X			X			
	A5	Spalling of pier		X	X		X	X		X	X
	A6	Plastic hinge									
Bent	B1	Local failure									
	B2	Crush of bent									
	B3	Shear failure									
Stringer	C1	Collapse			X			X			
	C2	Yielding	X	X	X	X	X	X	X	X	X
Deck	D1	Crush									
	D2	Lift up			X						
	D3	Collapse			X			X			

X : Failure mechanism is observed in the specific bridge blast simulation.

Table 6.8: Effects of Compressive Strength of Concrete on Blast Resistance of Bridges in New York.

Failure Mechanism			Blast loads level on bridges (Low, Medium or High)								
			$f_c' = 3000\,psi$			$f_c' = 5{,}000\,psi$			$f_c' = 10{,}000\,psi$		
	Item	Description	Low	Medium	High	Low	Medium	High	Low	Medium	High
Pier	A1	Pier eroding	X	X	X	X	X	X	X	X	X
	A2	Shear at footing			X		X	X			X
	A3	Rebar severance		X	X		X	X			X
	A4	Breakage of pier			X			X			X
	A5	Spalling of pier	X	X	X	X	X	X		X	X
	A6	Plastic hinge			X			X			
Bent	B1	Local failure	X	X	X			X			
	B2	Crush of bent	X	X	X						
	B3	Shear failure		X	X						
Stringer	C1	Collapse		X	X			X			X
	C2	Yielding	X	X	X	X	X	X	X	X	X
Deck	D1	Crush		X	X			X			
	D2	Lift up		X	X			X			X
	D3	Collapse		X	X			X			X

X : Failure mechanism is observed in the specific bridge blast simulation.

174

Table 6.9: Effects of Compressive Strength of Concrete on Blast Resistance of Bridges in California.

Failure Mechanism			Blast loads level on bridges (Low, Medium or High)								
			$f_c' = 3000\,psi$			$f_c' = 5{,}000\,psi$			$f_c' = 10{,}000\,psi$		
	Item	Description	Low	Medium	High	Low	Medium	High	Low	Medium	High
Pier	A1	Pier eroding		X	X	X	X	X	X	X	X
	A2	Shear at footing			X			X			
	A3	Rebar severance			X			X			X
	A4	Breakage of pier									X
	A5	Spalling of pier	X	X	X	X	X	X		X	X
	A6	Plastic hinge			X						
Bent	B1	Local failure	X	X	X						
	B2	Crush of bent		X	X						
	B3	Shear failure		X	X						
Stringer	C1	Collapse			X						X
	C2	Yielding	X	X	X	X	X	X	X	X	X
Deck	D1	Crush			X			X			
	D2	Lift up			X			X			
	D3	Collapse			X						X

X : Failure mechanism is observed in the specific bridge blast simulation.

Table 6.10: Effects of Compressive Strength of Concrete on Blast Resistance of Bridges With Double of California Seismic Resistance.

Failure Mechanism			Blast loads level on bridges (Low, Medium or High)								
			$f_c' = 3000\,psi$			$f_c' = 5{,}000\,psi$			$f_c' = 10{,}000\,psi$		
	Item	Description	Low	Medium	High	Low	Medium	High	Low	Medium	High
Pier	A1	Pier eroding		X	X				X	X	X
	A2	Shear at footing									
	A3	Rebar severance									
	A4	Breakage of pier									
	A5	Spalling of pier	X	X	X	X	X	X		X	X
	A6	Plastic hinge									
Bent	B1	Local failure	X	X	X						
	B2	Crush of bent			X						
	B3	Shear failure									
Stringer	C1	Collapse									
	C2	Yielding	X	X	X	X	X	X	X	X	X
Deck	D1	Crush			X			X			
	D2	Lift up									
	D3	Collapse									

X : Failure mechanism is observed in the specific bridge blast simulation.

6.4 PERFORMANCE BASED MULTI-HAZARD APPROACH

6.4.1 Blast Versus Seismic Damage Mechanisms

In order to develop a blast-seismic multi-hazard approach, we further compare 14 damage mechanisms that occur during blast loads with those observed during seismic loads on bridges. Table 6.11 shows comparisons between damage mechanisms occurring during seismic and blast loads. It is observed that nine damage mechanisms can be observed during both seismic and blast loads. However, there are five damage mechanisms that occur during blast events only.

Blast load originates from one point and spreads radially. As a result, local structural members undergo high level of blast force during first few milliseconds, which is further transferred to the whole structure. Hence, local damage occurs during first few milliseconds. For example, concrete material in pier, bent and deck is crushed under the compressive blast wave, whereas spalling of concrete on the back surface of piers occurs because of reflected tension wave. Following this, blast load is transferred to the entire structural system and can cause damages to critical sections such as bottom of pier, which can be considered as “global” damage.

Since the blast load spreads radially for the charge center, even though its magnitude decreases with distance, it will be applied over a larger area of the structure at larger distance. Hence, total force applied on structural members even at larger distances can be considerable and it can be applied in the direction opposite to those of conventional forces, causing uncommon damage mechanisms such as lifting of the deck. After the blast wave passed, the response of the structure may be magnified if there is any resonance. If the bridge deck undergoes uplifting, the impact force because of the deck dropping back can

result in damage mechanism such as shear failure of the bent beam, which is not observed during seismic loads.

Table 6.11 Comparison of failure mechanisms in blast and seismic hazards

	Item	Description	Blast Load	Seismic Load
Pier	A1	Pier eroding	Yes	Yes
	A2	Shear at footing	Yes	Yes
	A3	Rebar severance	Yes	Yes
	A4	Breakage of pier	Yes	Yes (different mechanism)
	A5	Spalling of pier	Yes	No
	A6	Plastic hinge	Yes	Yes
Bent	B1	Local failure	Yes	Yes (different mechanism)
	B2	Crush of bent	Yes	No
	B3	Shear failure	Yes	No
Stringer	C1	Collapse	Yes	Yes
	C2	Yielding	Yes (local)	Yes (global)
Deck	D1	Crush	Yes	Rarely
	D2	Lift up	Yes	No
	D3	Collapse	Yes	Yes

Seismic load is applied as a global force proportional to the mass and it is transferred to the local members. Usually horizontal force controls damage modes during seismic loads. Hence, lateral shear resistance capacity is emphasized in seismic design. It has been observed from Table 6.11 that 9 damage mechanisms are common to seismic and blast loads and 5 are specific to blast loads only. Hence, countermeasures for seismic design should also be effective in reducing damages because of 9 common damage mechanisms during blast loads. However, 5 damage mechanisms specific to blast loads are primarily related to local damages/failures and should be addressed separately.

An optimized blast-seismic design approach is a challenging approach because of

conflicting requirements of seismic and blast loads. For example, a massive structure has more blast resistant capacity; however, it is more vulnerable to seismic damages because of larger mass. Another example is the strong-column/weak-beam rule in seismic design. The weak beam is more vulnerable to damages during blast loads. Hence, an optimized multi-hazard seismic-blast design will require multi-objective optimization of structural geometry, material strength and mechanisms and is a topic of future research.

6.4.2 Performance Based Blast Resistant Design Approach

Ngo (2005) and Mezzi (2006) have discussed performance based blast resistant design concepts for buildings. Using their approach, results in multi-hazard Table 6.5 can be used to develop performance based criteria for blast loads.

The performance of highway bridges can be categorized into 8 levels: operational, local damage, life safety, few-limit posting, few-pass posting, closing, partial collapse and total collapse. The first 3 levels (operational, local damage, and life safety) are in based on serviceability requirements and may require minor repairs to maintain the performance of the bridge after a blast event. "Life Safety" performance means the bridge ductility meet AASHTO requirements.

Further damage to the bridge may require load posting actions to limit traffic on the bridge. Posting level depends on the damage degree of the bridge and can be quantified in terms of Load Rating Factor [AASHTO (2003)]. The last two performance levels, "Partial collapse" and "Collapse", indicate failure and irreparable damages to the bridge.

Based on the definitions of different performance levels above, Table 6.5 can be used to obtain performance based interpretation of results as shown in Figure 6.51. It is

observed that the performance of a particular bridge decreases with an increase in blast load level. The bridge in New York is severely impaired when the blast load is slightly higher than the "Low" level blast load. There exists a capacity value for bridge to resist a particular blast load level. This capacity level essentially depends on the size of the pier.

With an increase in seismic design level, blast resistant performance of the bridge also increases. For example, increasing seismic design level from 0.2 g PGA (i.e., New York bridge) to 0.8g PGA (i.e., California level), the blast performance level is improved by 1+2+1=4 levels. Further increasing the seismic performance level from 0.8g PGA (i.e., California level) to to 1.6g PGA (double of California level), blast performance level of the bridge improves by 1+1+1=3 levels. Further hypothetical increase in seismic performance may result in lesser improvement in blast performance because of presence of damage mechanisms specific to blast loads only.

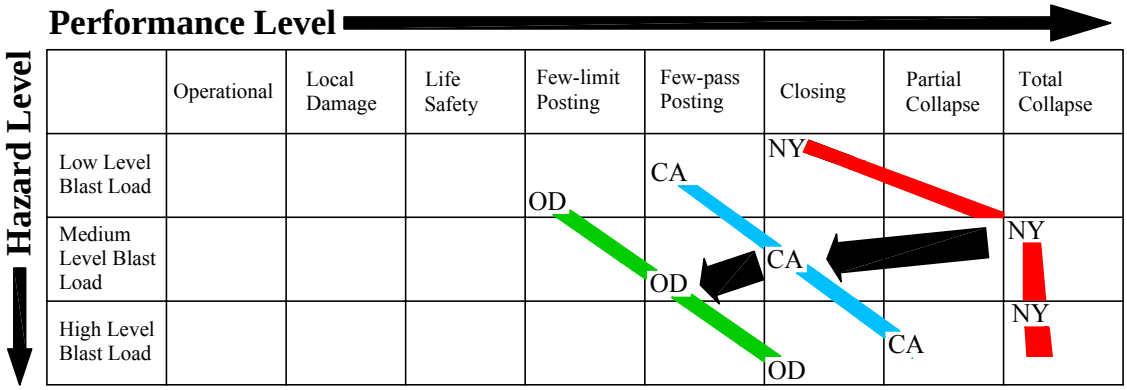

Figure 6.51: Performance Based Blast-Seismic Multi-Hazard Correlations using 3000 psi Concrete.

Figure 6.52 shows performance based multi-hazard interpretation of results using 5000 psi compressive strength of concrete. Bridges with 5000 psi compressive strength of

concrete have a trend similar to those of 3000 psi in terms of multi-hazard performance. It is observed from Figure 6.52 that the blast performance level improves 0+1+1=2 levels by increasing seismic design level from 02g (New York) to 0.8g (California) and it improves by 0+1+1=2 levels by improving seismic design level from 0.8g (California) to 1.6g (Double of California).

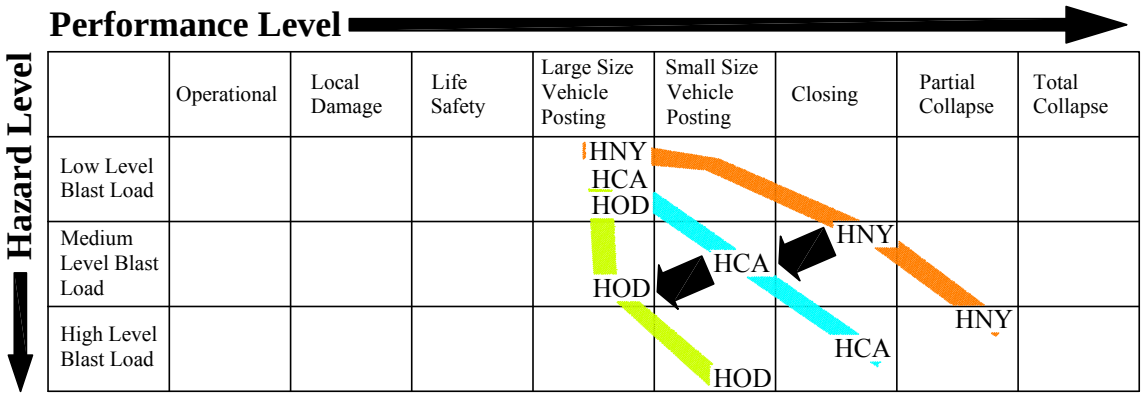

Figure 6.52: Performance Based Blast-Seismic Multi-Hazard Correlations using 5000 psi Concrete.

An assessment of influence of compressive strength of concrete can be made by plotting performance levels in Figures 6.45 and 6.46 together, as shown in Figure 6.53. It is observed from Figure 6.53 that the blast performance level of New York (NY), California (CA) and Double of California (2CA) bridges improves by 2+2+1=5 , 1+1+1=3 and 0+1+1=2 because of increase in compressive strength of concrete from 3000 psi to 5000 psi. It is also observed from Figure 6.53 that the improvement in blast performance by increasing seismic design capacity is less when original capacity of the bridge is high, as in case of the bridge with 5000 psi concrete. Likewise, improvement in blast performance by increasing concrete strength is less effective for a bridge with higher seismic capacity.

Comparing seismic versus concrete strength, it is observed from Figure 6.53 that the

improvement in performance levels by seismic upgrade from New York to California (change in pier size section from 3.0 ft to 3.5 ft) and California to Double of California (change in pier size section from 3.5 ft to 4.5 ft) are 1+2+1=4 and 1+1+1 = 3, respectively. This change in performance level by increasing concrete strength from 3000 psi to 5000 psi are 2+2+1=5 and 1+1+1 = 3 for New York and California bridges, respectively. Hence, increasing compressive strength of concrete is more significant for a bridge design for low seismic region. On the other hand, both concrete strength and seismic capacity are equally effective for bridges in high seismic regions. It should be noted that the limitation in improvement of performance because of increase in concrete strength can also be limited by the capacity of bridge superstructures, which has been designed as "weak" following the strong-column/weak-beam rule in seismic design.

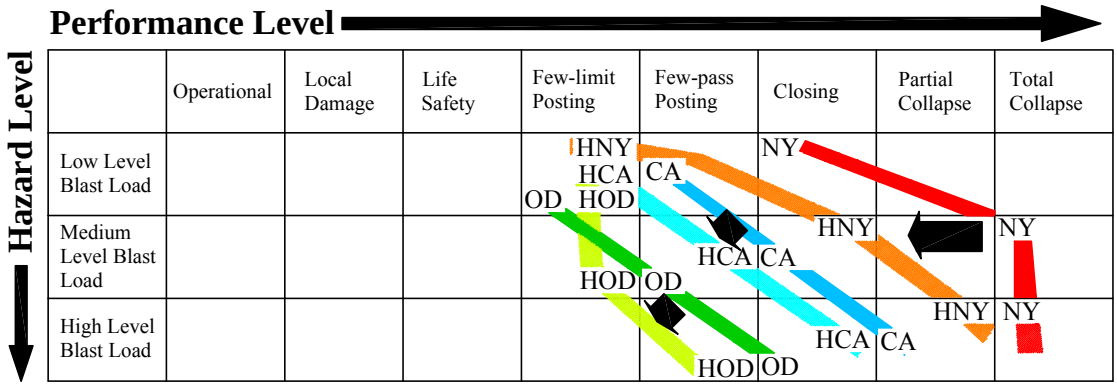

Figure 6.53: Comparison Between Performance Based Blast-Seismic Multi-Hazard Correlations using 3000 psi and 5000 psi Concrete.

6.5 PIER TOP DISPLACEMENT TIME HISTORIES

Longitudinal displacement at the top of the pier nearest to the explosive charge can be used to investigate blast performance of the bridge macroscopically. Pier top displacement can also characterize local behavior of the pier. Figure 6.54 shows pier tip

displacement time histories for New York, CA and 2CA bridges with 3000 psi concrete. It is observed that the pier top displacement of the New York bridge decreases drastically as it is seismically upgraded to CA conditions. Further reduction in peak displacement as the bridge is upgraded to 2CA (double of California) is much lesser.

It is observed that the peak displacements are reached after 50 milliseconds, although air blast wave passed the bridge in about 50 milliseconds. This indicates that the dynamic effect is very important in analysis of bridges subject to blast loads. Vibration cycles for NY and CA bridges become longer with respect to the natural period of the bridge because of formation of plastic hinge in piers. In fact, the NY bridge shows an elasto-plastic type of displacement curve and bent fails because of impact of falling deck after it has been uplifted by the blast wave.

Figure 6.55 shows pier top displacement histories for bridges with 5000 psi compressive strength concrete. Table 6.12 shows maximum pier top displacements in Figures 6.54 and 6.55. It is observed that the peak displacement with 5000 psi concrete are much smaller than those using 3000 psi concrete. However, unlike failure because of shearing of bent in case of 3000 psi concrete, NY bridges with 5000 psi fails because of brittle failure of the pier.

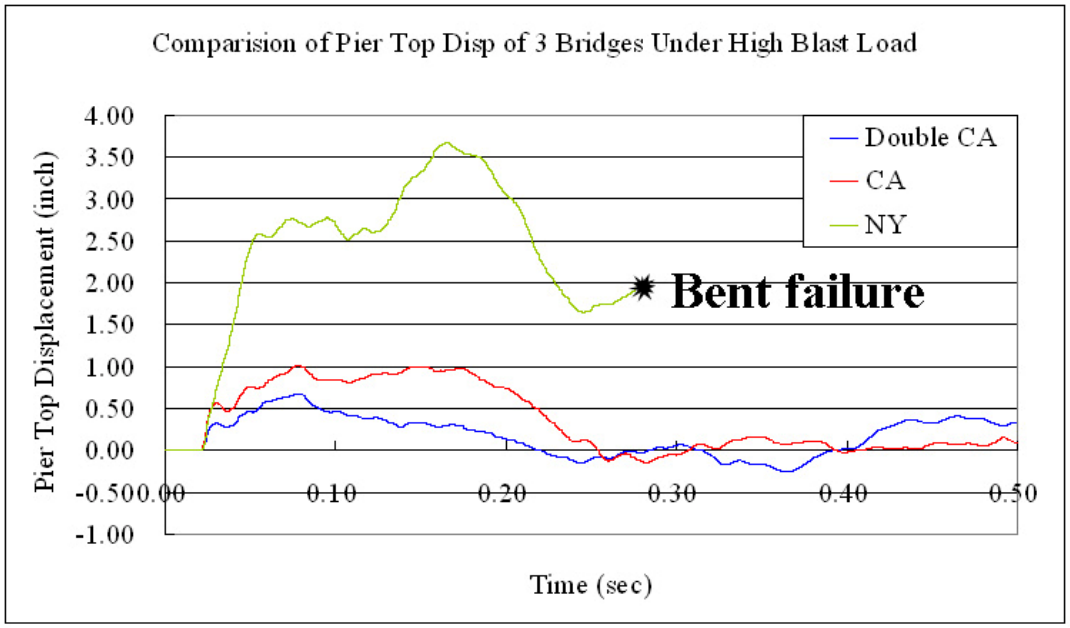

Figure 6.54: Pier Top Displacement Time Histories for Bridges with 3000 psi Concrete.

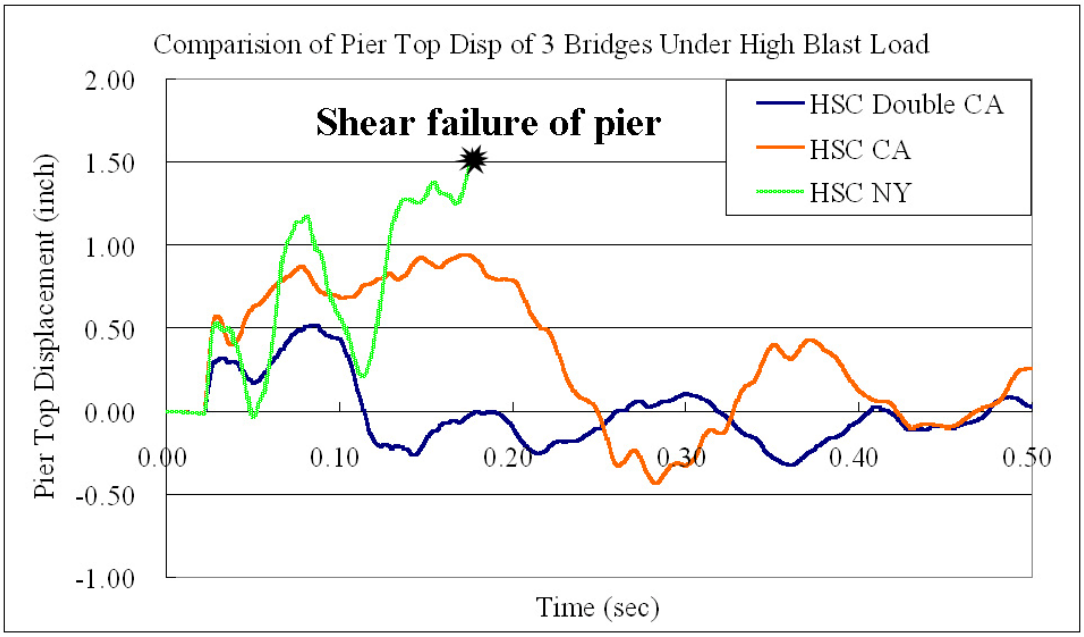

Figure 6.55: Pier Top Displacement Time Histories for Bridges with 5000 psi Concrete.

Table 6.12 Maximum Displacement of Pier Top (unit: inch)

Bridge	f_c' = 3 ksi	f_c' = 5 ksi
New York (PGA=0.2g)	3.66 (collapse)	1.48 (collapse)
California (PGA=0.8g)	1.03 (collapse)	0.94
Over-design (PGA=1.6g)	0.67	0.52

Figures 6.56 to 6.58 show comparison between pier top displacement time histories of NY, CA ands 2CA bridges, respectively, with 3000 psi, 5000 psi and 10,000 psi concrete strengths. It is observed that the peak pier top displacement is much smaller in case of 5000 psi concrete. This is because bridge piers with 3000 psi concrete develop elasto-plastic behavior under blast load while those with 5000 psi concrete fail after fully developing plastic behavior. The rebar detailing and the amount of rebars play a critical role in ensuring sufficient ductility capacity for the bridge pier. For the CA bridges, reduction in the peak pier top displacement because of increased concrete strength is not significant and rebars have been observed to be severed in both cases. Hence, increasing the concrete strength doesn't reduce peak pier top displacement during a blast event. For the 2CA bridge, increase in concrete strength improves the behavior of the bridge in elastic range, which is efficient and successful in resisting effects of blast loads.

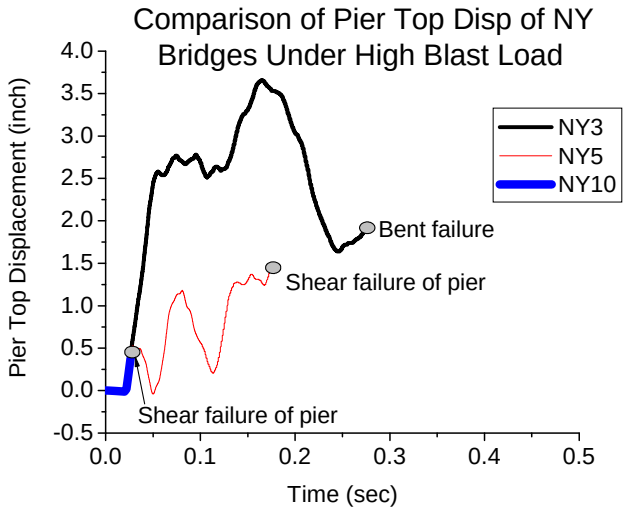

Figure 6.56: Influence of Concrete Strength on Pier Top Displacement; NY bridge.

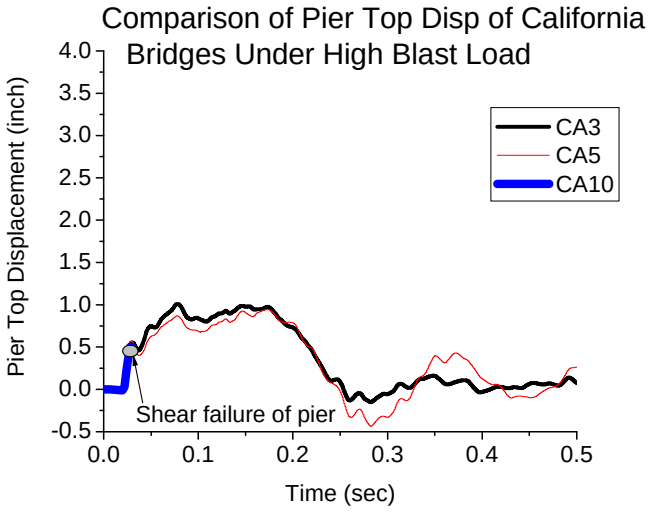

Figure 6.57: Influence of Concrete Strength on Pier Top Displacement; CA bridge.

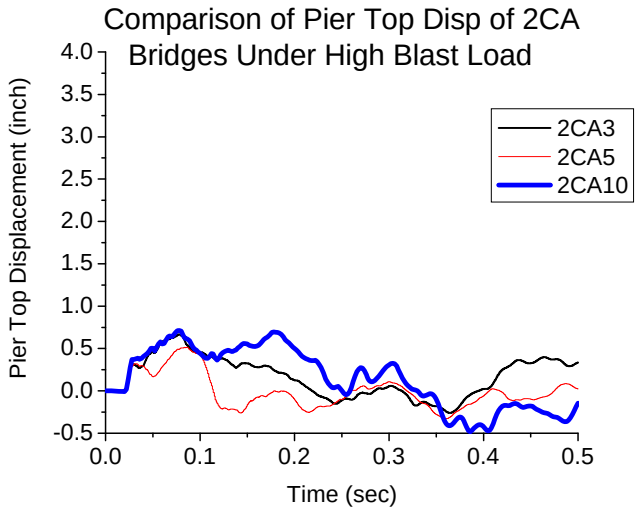

Figure 6.58: Influence of Concrete Strength on Pier Top Displacement; 2CA bridge.

Figure 6.59 shows the plot of peak values of pier top displacements in Figures 6.56 to 6.58 as a function of μ/R_y ratio in Table 6.3 for nine cases of high blast loads. It is observed that the value of peak pier top displacement is reduced drastically and all failure modes are avoided as μ/R_y ratio is increased beyond 6 for all bridges. For μ/R_y ratio less than 6, shear failure and bent failure are observed in bridges with concrete strengths of 3, 5 and 10 ksi.

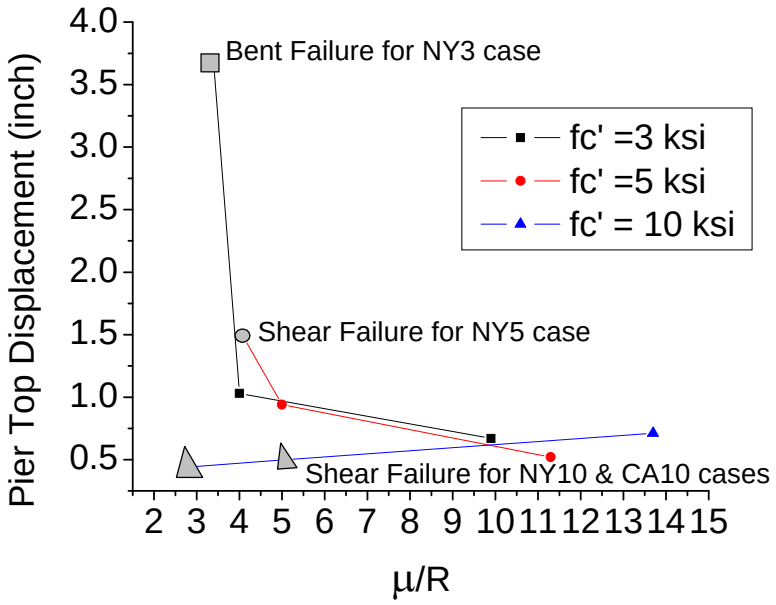

Figure 6.59: Plots of Peak Pier Top Displacement versus μ/R_y Ratio for Bridge Piers Subjected to High Blast Loads.

CHAPTER 7 CONCLUSIONS AND FUTURE RESEARCH

The number and intensity of domestic and international terrorist activities, including the September 11, 2001 attack on World Trade Center towers in New York, have heightened our concerns towards the safety of our infrastructure systems. Terrorists attack targets where human casualties and economic consequences are likely to be substantial. Transportation infrastructures have been considered attractive targets because of their accessibility and potential impacts on human lives and economic activity. Duwadi and Chase (2006) and Duwadi and Lwin (2006) have noted that bridges are vulnerable to physical, biological, chemical and radiological attack in addition to natural hazards and FHWA must prepare for the next generation of bridges and tunnels that are redundant and resilient to withstand unforeseen events. The focus of this report has been to investigate blast load effects on a typical highway bridge and multi-hazard seismic blast correlations. This objective has been achieved by developing a high fidelity finite element model of a highway bridge in LS-DYNA. Important conclusions of the study are the following:

1. Although several tools (e.g., blastX) exists for generating blast loads on building components, no such approach exists for applying blast loads on bridge components. We have proposed a new approach to simulate loads on structural elements similar to that by ConWep. In this approach, ConWep pressure generated for a specific charge weight is transferred to an air layer near structural element. The blast wave front propagates through the surrounding air layer. The air mesh interacts with Lagrangian structure element to apply the load on structural elements. It produces correct pressure field with the same arriving time of blast wave as ConWep and can simulate wave reflection and diffraction. When simulation involves complex geometry or non-air

blast waves such as inter-explosion in box girder and air pressure near deck, other experimental data or program such as BlastX are necessary to calibrate the load effect parameters. It has been observed from simulation results that the blast pressure is transmitted accurately to structural elements when air density of surrounding air layers is 1/10 of normal air density.

2. In order to investigate blast load effects of highway bridges, a typical three span simply supported bridge has been selected as a case study. A high fidelity three dimensional finite element model of the bridge with approximately 1 million degrees of freedom has been developed. The finite element model of the bridge models each component of the bridges as on the construction drawing. For example, rebars are modeled as beam elements; elastomeric bearings are modeled as a block consisting of layers of steel shims and elastomers. A detailed review of the literature has been carried out to select most appropriate models of materials in the bridge, e.g., concrete, steel and elastomers. These material models have the capability to deal with high strain, high strain rates, high pressures, and damages. Parameters of the material models have been selected on the basis of parametric studies and data based on experimental results available in literature.

3. Numerical simulation of blast loads on structural components is highly nonlinear process because of high strain and high strain rates and eroding of damaged elements. This nonlinear behavior leads to numerical problems because of damages and rebar-concrete bonding issues. We have carried out any extensive study and literature review and propose an approach to resolve numerical problems by calibrating mesh size using experimental displacement data. However, this leads to the dependence of

constitutive equations on element size. It has been observed that, unlike elastic simulation where finer element sizes give better results, there is a characteristics element size for reinforced concrete members in case of inelastic behavior which gives best correlation with test results. This element size depends on bonding between concrete and rebars and nonlinear material model. In this report, we have determined this characteristic element size for reinforced concrete members by correlations between FEM results and test data on reinforced concrete members in a shock tube. It has been observed that a characteristics size of 1 inch for reinforce concrete members is the most appropriate.

4. In order to investigate effects of time step on air blast load predictions, numerical simulations have been carried out using several time steps. It is observed that, compared to a time step of 5.0×10^{-9}, maximum error introduced in the prediction of air blast because of a time step of 2.0×10^{-6} is only 2.59%.

5. Through the simulation of elastic response of a beam, it has been observed that the maximum contact pressure increases with a decrease in time step size and contact pressure is nearly reciprocal to time step size. In the simulation, PFAC factor can be adjusted to obtain the same maximum contact pressure for a value of time step size. However, when the blast load is large enough to push concrete material into nonlinear range, the mechanism of contact is different since the elastic modulus of structure material is equal to or only a little bit bigger than zero, which makes the interaction between air and structure more like interaction between two fluid materials. In this case, the contact pressure is relatively insensitive to both time step and penalty factor.

6. Blast load effects on the three-span reinforced concrete bridge have been investigated

by three levels of blast loads: low, medium and high. Numerical values of charge size presenting these load levels are kept confidential because of security reasons. In order to investigate correlations between seismic detailing and blast effects, models of three span bridge have been generated by designing the bridge for different seismic egions: New York, California and a hypothetical double of California. These three models correspond to 0.2g, 0.8g and 1.6g peak ground accelerations during an earthquake. Unconfined compressive strength of concrete has been varied in these models from 3000 psi to 5000 psi to investigate the effects of concrete compressive strength on blast load effects. Hence, altogether 18 cases of blast loads on bridges have been simulated. Based on these simulation results, 14 damage mechanisms prominent during blast load effects on bridges have been identified and have been correlated with seismic damage mechanisms.

7. It has been observed from simulation results that seismic capacities and blast load effects are strongly correlated. Better seismic capacity directly implies better blast load resistance. However, there are several damage mechanisms that are not present during seismic loadings and protection of bridge components from failure because of these mechanisms needs to be considered by improved detailing of components and optimization for multi-hazard seismic blast designs.

8. Based on simulation results, we have also presented a framework for performance based multi-hazard blast-seismic design approach. Different performance levels for bridge components subject to blast loads have been defined. Considering bridges designed for different seismic capacities, performance matrices have been developed to demonstrate the limitation of seismic detailing in dealing with blast loads. These

performance matrices can be fully developed by considering different performance levels during multi-hazard seismic-blast loads in future research.

Although a detailed study on blast effects of a highway bridge has been carried out in this reports, the research presented in this report lays basic foundation of more detailed study of blast effects and multi-hazard seismic-blast correlations for highway bridges. Some of the future needs in this area are described in the following.

1. The material models for concrete, steel and elastomer are based on limited data presented in the literature. Very few data on blast effects to calibrate material model have been found. In order to improve reliability of the finite element simulation, it is necessary to calibrate material models using blast tests on typical bridge components, e.g., concrete, reinforce concrete, stringers, elastomeric bearings, etc.

2. In this study, we have considered only one bridge type, which is a typical bridge. However, in order to fully understand the dynamics of bridge components during blast loads, and develop guidelines, there is a need to investigate different variations of bridge components, e.g., wall type piers, circular piers, continuous bridges, detailings at footings and in piers, etc.

3. In this report, we have identified several damage mechanisms that appear predominantly during blast loads. Research on modified detailing to minimize impact of these mechanisms and optimization of bridge detailing and components is needed to develop effective multi-hazard design guidelines for highway bridges.

4. We have presented a preliminary approach on performance based multi-hazard seismic blast guidelines. Definitions of different performance levels arte based on current

knowledge on seismic design of bridges. There is a need to develop detailed knowledge and guidelines on performance based multi-hazard seismic-blast design of bridge components.

REFERENCES

AASHTO. (2002). *Standard Specifications for Highway Bridges*, American Association of State Highway and Transportation Officials, Washingtong, D.C.

AASHTO. (2003). "GUIDE MANUAL FOR CONDITION EVALUATION AND LOAD AND RESISTANCE FACTOR RATING (LRFR) OF HIGHWAY BRIDGES." AASHTO, 448.

AASHTO. (2008). "AASHTO LRFD Bridge Design Specifications, Customary U.S. Units."

Army, D. o. t. (1990). *Structures to Resist the Effects of Accidental Explosions*, Army Technical Manual 5-1300/Navy Publication NAVFAC P-397/Air Force Manual (AFM) 88-22 (TM 5-1300), Washington, D.C.

Army, U. S. D. o. t. (1998). "Design and analysis of hardened structures to conventional weapons effects." *TM 5-855-1*, Headquarters, U.S. Department of the Army, Washington, DC.

ASCE. (1985). "Design of Structures to Resist Nuclear Weapons Effects. Manual 42." American Society of Civil Engineers, Washington, D.C.

ASCE. (1999). "Structural Design for Physical Security: State of the Practice." the Structural Engineering Institute Task Committee, American Society of Civil Engineers.

ASCE. (2005). "Minimum design loads for buildings and other structures." *ASCE/SEI 7-05*, American Society of Civil Engineers, Reston, Virginia.

Ash, C., Schwartz, J., Aschheim, M., Hawkins, N., and Gamble, B. (2002). "Evaluation of Elastomeric Bridge Bearings for Seismic Design." *ITRC FR 99-4*, Department of Civil and Environmental Engineering, University of Illinois at Urbana-Champaign.

ASI. (2005). "Extreme loading for structures." Applied Science International, LLC, Raleigh, NC.

Baker, W. E., Cox, P. A., Westine, P. S., Kulesz, J. J., and Strehlow, R. A. (1983). *Explosion hazards and evaluation*, Elsevier, London.

Bangash, M. Y. H. (1993). *Impact and Explosion-Analysis and Design*, CRC Press., Boca Raton, Florida.

Batsanov, S. S. (1994). *Effects of Explosions on Materials*, Springer-Verlag, New York.

Baylot, J. T., Ray, J. C., and Hall, R. L. (2003). "Prediction Method for Response of Steel Bridge Beams and Girders to Blast and Fragment Loads." *Transportation Research Record*, 1827(0361-1981), 69-74.

Bazant, Z. P. (2002). *Scaling of Structural Strength*, Hermes Penton Science,

London.

Bazant, Z. P., and Belytschko, T. B. (1985). "WAVE PROPAGATION IN A STRAIN-SOFTENING BAR: EXACT SOLUTION." *Journal of Engineering Mechanics*, 111(3), 381.

Bazant, Z. P., and Verdure, M. (2007). "Mechanics of progressive collapse: Learning from World Trade Center and building demolitions." *Journal of Engineering Mechanics*, 133(3), 308.

Belytschko, T., Liu, W. K., and Moran, B. (2000). *Nonlinear Finite Elements for Continua and Structures*, John Wiley & Sons Ltd., West Sussex.

Boyd, S. D. (2000). "Acceleration of a Plate Subject to Explosive Blast Loading - Trial Results." *DSTO-TN-0270*, Maritime Platforms Division, Aeronautical and Maritime Research Laboratory, Australia Department of Defense, Melbourne, Australia.

Brode, H. L. (1955). "Numerical solution of spherical blast waves." *J. App. Phys.*, No. 6.

BRP. (2003). *Recommendations for Bridge and Tunnel Security*, The American Association of State Highway and Transportation Officials (AASHTO) Transportation Security Task Force.

Bruneau, M., Lopez-Garcia, D., and Fujikura, S. "Multihazard-resistant highway bridge bent." St. Louis, MO, United States, 30.

Buckle, I.G., Mayes, R.L., and Button, M.R. (1987). Seismic Design and Retrofit Manual for Highway Bridges, Prepared for Federal Highway Administration, FHWA-IP-87-6.

Canada, N. R. C. o. (1995). *National Building Code of Canada*, Canada.

Carino, N. J., and Lew, H. S. "Summary of NIST/GSA Workshop on Application of Seismic Rehabilitation Technologies to Mitigate Blast-Induced Progressive Collapse." Oakland, CA.

CE676. (2003). "El Nogal Files." http://cobweb.ecn.purdue.edu/~ce676/, Purdue University.

Chen, G. (2007). "Wood Pier Bridge Blast Experiments of UMR." Rolla, MO.

Chen, G., and Baker, G. (2003). "Influence of bond slip on crack spacing in numerical modeling of reinforced concrete." *Journal of Structural Engineering*, 129(11), 1514.

Chopra, A. K. (2001). *Dynamics of Structures: theory and applications to earthquake engineering*, Prentice Hall, Upper Saddle River.

Constantinou, M. C. (2006). "Seismic Protective Systems - Seismic Isolation and Damping Systems." *The City College of New York: Bruce Podwal Seminar Series*, New York.

Crawford, E. R., Higgins, C. J., and Bultmann, E. H. (1974). "The Air Force Manual for Design and Analysis of Hardened Structures." *AFWL-TR-74-102*, Air Force Weapons Laboratory, Kirtland Air Force Base, New Mexico.

CSI (2007). SAP2000 User Manual.

Dang, X., and Chan, P. C. (2006). "Design and test of a blast shield for boeing 737 overhead compartment." *Shock and Vibration*, 13(6), 629.

DDESB. (2004). "DoD Ammunition and Explosives Safety Standards." *DoD 6055.9-STD, Revision 5*, Department of Defense Explosives Safety Board, Alexandria, VA.

De Nardin, S., Almeida Filho, F. M., Oliveira Filho, J., Haach, V. G., and El Debs, A. L. H. C. "Non-linear analisys of the bond strength behavior on the steel-concrete interface by numerical models and pull-out tests." New York, NY, United States, 1077.

Dennis, S. T., Baylot, J. T., and Woodson, S. C. (2002). "Response of 1/4-scale concrete masonry unit (CMU) walls to blast." *Journal of Engineering Mechanics*, 128(2), 134.

DOD. (2003). "Uniform Facilities Criteria: Department of Defense Minimum Antiterrorism Standard for Buildings." *UFC 4-010-01*, Department of Denfence.

DoD. (2005). "UNIFIED FACILITIES CRITERIA (UFC): DESIGN OF BUILDINGS TO RESIST PROGRESSIVE COLLAPSE." *UFC 4-023-03*, Department of Denfence, Washington, D.C.

DOD. (2007). "UNIFIED FACILITIES CRITERIA (UFC): DoD Minimum Antiterrorism Standoff Distances for Buildings." *UFC 4-010-02*, Department of Defence, Washington, D.C.

Drake, J. L., Twisdale, L. A., Frank, R. A., Dass, W. C., Rochefort, M. A., Walker, R. E., Britt, J. R., Mruphy, C. E., Slawson, T. R., and Sues, R. H. (1989). "Protective Construction Design Manual." *ESL-TR-87-57*, Air Force Engineering & Services Center, Tyndall Air Force Base, Florida.

Drysdale, W., and Zak, A. (1985). "Mechanics of materials and structural theories, a theory for rate-dependent plasticity." *Computers & Structures*, 20(1-3), 259-264.

DTRA. (1997). *Design and analysis of hardened structures to conventional weapons effects*, Defense Threat Reduction Agency (distribution restricted to U.S. Government agencies and their contractors), Washington, D.C.

Dusenberry, D. O. "Review of Existing Guidelines and Provisions Related to Progressive Collapse." *PREVENTION OF PROGRESSIVE COLLAPSE: THE JULY 2002 NATIONAL WORKSHOP AND RECOMMENDATIONS FOR FUTURE EFFORTS*, the Gateway Sheraton Suites O'Hare Hotel in Rosemont, Illinois.

Duwadi, S. R., and Chase, S. B. (2006). "Multiyear Plan for Bridge and Tunnel Security Research, Development, and Deployment." *FHWA-HRT-06-072*, Office of Infrastructure Research and Development, Federal Highway Administration, Springfield, VA.

Duwadi, S. R., and Lwin, M. "Securing the highway infrastructure - An R and D program." St. Louis, MO, United States, 177.

Ellingwood, B., and Leyendecker, E. V. (1978). "APPROACHES FOR DESIGN

AGAINST PROGRESSIVE COLLAPSE." 104(3), 413.

English, B. A., Klingner, R. E., and Yura, J. A. (1994). "Elastomeric Bearings: Background Information and Field Study." *Research Report 1304-1*, The University of Texas at Austin.

Ettouney, M. (2004). "Development of a Progressive Collapse Analysis Method and the PROCAT Computer Program." *Counter Terrorism Technology Support Office Technical Support Working Group (CTTSO/TSWG)*.

Ettouney, M., Hansen, E., Hapij, A., Lawver, D., Tang, M., Tennant, D., Vaughan, D., and Xie, M. (2004). "Development of a Progressive Collapse Tool." *WA-0403*, Arlington, VA.

Ettouney, M., Smilowitz, R., and Rittenhouse, T. (1996). "Blast resistant design of commercial buildings." *Practice Periodical on Structural Design and Construction*, 1(1), 31-39.

Ettouney, M., Smilowitz, R., Tang, M., and Hapij, A. (2006). "Global system considerations for progressive collapse with extensions to other natural and man-made hazards." *Journal of Performance of Constructed Facilities*, 20(4), 403.

Fickett, W. (1985). *Introduction to Detonation Theory*, University of California Press., Berkeley.

Forbes, D. J. (1999). "Blast loading on petrochemical buildings." *Journal of Energy Engineering*, 125(3), 94.

Fu, H. C., Erki, M. A., and Seckin, M. (1991). "Review of effects of loading rate on reinforced concrete." *Journal of Structural Engineering*, 117(12), 3660.

Ghali, A., and Tadros, G. (1997). "Bridge progressive collapse vulnerability." *Journal of Structural Engineering*, 123(2), 227.

Glasstone, S., and Dolan, P. J. (1977). *The Effects of Nuclear Weapons, 3rd edition*, U.S. Department of Defense and U.S. Department of Energy, Washington, D.C.

Gong, M. (2006). "Mutual Interactions between Shock Waves and Structures," City University of New York, New York.

GSA. (2003). *ISC Security Design Criteria for New Federal Office Buildings and Major Modernization Projects*, U.S. General Services Administration.

GSA. (2006). "AT-Blast 2.2." U.S. General Services Administration.

Hallquist, J. O. (1998). *LS-DYNA Theoretical Manual*, Livermore Software Technology Corporation, Livemore, California.

Han, Z., and Yin, X. (1993). *Shock Dynamics*, Kluwer Academic Publishers, Boston, Massachusetts.

Hansen, E., Wong, F., Lawver, D., Oneto, R., Tennant, D., and Ettouney, M. "Development of an analytical database to support a fast running progressive collapse assessment tool." New York, NY, United States, 2095.

Hillerborg, A., Modeer, M., and Peterson, P. (1976). "Analysis of crack formation

and crack growth in concrete by means of fracture mechanics and finite elements." *Cement Concrete Res.*, 6, 773-782.

Holmquist, T. J., Johnson, G. R., and Cook, W. H. "A Computational Constitutive Model for concrete Subjected to Large Strains, High Strain Rates, and High Pressures." *Proceedings 14th International Symposium on Ballistics, 1993*, Quebec, Canada, 591-600.

HooFatt, M. S., and Ouyang, X. "The behavior of elastomers at high strain rates." *Structures Under Shock and Impact IX*, Wessex Institute of Technology, 97-106.

Hyde, D. (2005). *ConWep 2.1.0.8 - Application of TM 5-855-1*, Vicksburg, MS.

ISC. (2001). *ISC Security Design Criteria for New Federal Office Buildings and Major Modernization Projects*, Washington, D.C., General Services Administration, Interagency Security Committee.

John, A. G. (2005). "STUDY OF BLAST WAVE IMPACT ON CONCRETE," THE UNIVERSITY OF TEXAS AT ARLINGTON, Ann Arbor.

Jones, N. (1989). *Structural Impact*, Cambridge University Press, Cambridge.

Kent, D. C., and Park, R. (1971). "Flexural Members with Confined Concrete." Journal of the Structural Division, ASCE, 97(7), 1969-1990.

Krauthammer, T., and Otani, R. K. (1997). "Mesh, gravity and load effects on finite element simulations of blast loaded reinforced concrete structures." *Computers and Structures*, 63(6), 1113.

Lew, H. S. "Overview of Fedral and International Progressive Collapse Guidelines." *Progressive Collapse Workshops*, New York City.

Li, Q. M., and Meng, H. (2002). "Pressure-impulse diagram for blast loads based on dimensional analysis and single-degree-of-freedom model." *Journal of Engineering Mechanics*, 128(1), 87.

Liepmann, H. W., and Roshko, A. (1957). *Elements of Gas Dynamics*, John Wiley, New York.

Limkatanyu, S., and Spacone, E. (2002a). "Reinforced concrete frame element with bond interfaces. I: Displacement-based, force-based, and mixed formulations." *Journal of Structural Engineering*, 128(3), 346.

Limkatanyu, S., and Spacone, E. (2002b). "Reinforced concrete frame element with bond interfaces. II: State determinations and numerical validation." *Journal of Structural Engineering*, 128(3), 356.

Lowes, L. N. (1999). "Finite element modeling of reinforced concrete beam-column bridge connections," University of California, Berkeley.

LSTC. (2003). *LS-DYNA keyword user's manual*, Livermore Software Technology Corporation, Livermore.

Luccioni, B., Ambrosini, D., and Danesi, R. (2006). "Blast load assessment using hydrocodes." *Engineering Structures*, 28(12), 1736.

Luccioni, B. M., Ambrosini, R. D., and Danesi, R. F. (2004). "Analysis of building

collapse under blast loads." *Engineering Structures*, 26(1), 63.

Magnusson, J., and Hallgren, M. "Reinforced high strength concrete beams subjected to air blast loading." *Structures Under Shock and Impact VIII*, Crete, Greece, 53-62.

Mahmadi, K., Aquelet, N., and Souli, M. "High Explosive Impact Analysis using LS-DYNA." Cleveland, OH, United States, 243.

Mair, H. U. (1999). "Review: hydrocodes for structural response to underwater explosions." *Shock and Vibration*, 6(2), 81.

Malvar, L. J. (1998). "Review of static and dynamic properties of steel reinforcing bars." *ACI Materials Journal*, 95(5), 609.

Marchand, K., Williamson, E. B., and Winget, D. G. (2004) "Analysis of blast loads on bridge substructures." Crete, Greece, 151.

Martineau, R., and Romero, C. "Response of a stainless steel cylinder with elliptical ends subjected to an off-center blast load." Montreal, Can, 37.

Matthews, T., Elwood, K. J., and Hwang, S.-J. "Explosive testing to evaluate dynamic amplification during gravity load redistribution for reinforced concrete frames." *Proceedings of the 2007 Structures Congress,Proceedings of the Research Frontiers Sessions of the 2007 Structures Congress, and Proceedings of the 2007 Forensic Engineering Track of the 2007 Structures Congress*, Long Beach, California.

Mays, G. C., and Smith, P. D. (1995). *Blast effects on buildings*, Thomas Telford.

McDonald, S. (2005). "Modeling of linear shaped charge performance using LS-Dyna." *SAFE Journal*, 33(1), 19.

McGraw-Hill. (1989). *McGraw-Hill Encyclopedia of Science and Technology*.

McGuire, W. "Prevention of Progressive Collapse." *Proceedings of the Regional Conference on Tall Buildings*, Bangkok, Thailand.

Mendola, L. L. (1997). "Cracking Analysis of RC Members by Using Coupled BE-FE Modeling." *Journal of Engineering Mechanics*, 123(7), 758-761.

Mezzi, M. "The Performance-Based Design of R/C Structures for the Reduction of Blast Damages." *Proceedings of the 2nd (fédération internationale du béton) fib International Congress*, Naples, Italy.

Mlakar, P. F., Sr., Corley, W. G., Sozen, M. A., and Thornton, C. H. (1998). "Oklahoma City bombing: Analysis of blast damage to the Murrah Building." *Journal of Performance of Constructed Facilities*, 12(3), 113.

MMC. "PREVENTION OF PROGRESSIVE COLLAPSE." *THE JULY 2002 NATIONAL WORKSHOP AND RECOMMENDATIONS FOR FUTURE EFFORTS*, Washington, D.C.

Morrill, K. B., Malvar, L. J., Crawford, J. E., and Ferritto, J. M. "Blast resistant design and retrofit of reinforced concrete columns and walls." Nashville, TN, United States, 1471.

Munshi, J. "State-of-the-art vs. State-of-the practice in Blast and Progressive Collapse Design of Reinforced Concrete Structures." *Structures 2004 - Building On The Past: Securing The Future, Proceedings Of The 2004 Structures Congress*, Nashville, Tennessee.

Muscarella, J. V., and Yura, J. A. (1995). "An Experimental Study of Elastomeric Bridge Bearings with Design Recommendations." *FHWA/TX-98/1304-3*, Center for Transportation Research, The University of Texas at Austin.

Muszynski, L. C., and Purcell, M. R. (2003). "Composite reinforcement to strengthen existing concrete structures against air blast." *Journal of Composites for Construction*, 7(2), 93.

Naito, C. J., and Wheaton, K. P. (2006). "Blast assessment of load-bearing reinforced concrete shear walls." *Practice Periodical on Structural Design and Construction*, 11(2), 112.

NBI, N. B. I. (2003). "Recording and Coding Guide for the Structure Inventory and Appraisal of the Nation's Bridges." *FHWA-PD-96-001*, U.S. Department of Transportation, Federal Highway Administration, Washington, D.C.

NCHRP. (2005). "Blast-Resistant Highway Bridges: Design and Detailing Guidelines, NCHRP 12-72." National Cooperative Highway Research Program (NCHRP).

NDRC. (1946). *Effects of Impact and Explosions*, Office of Scientific Research and Development, National Defense Research Committee, Washington, D.C.

Newmark, N. M., and Haltiwanger, J. D. (1962). "Air force Design Manual." *AFSWC-TDR-62-138*, Air Force Special Weapons Center, Kirland Air force Base, New Mexico.

Ngo, T. (2005). "Behaviour of high strength concrete subject to impulsive loading," University of Melbourne, Melbourne, Australia.

Ngo, T., Mendis, P., and Krauthammer, T. (2007). "Behavior of Ultrahigh-Strength Prestressed Concrete Panels Subjected to Blast Loading." *Journal of Structural Engineering, ASCE*, 133(11), 1582-1590.

NIST, and USDOC. (2006). "Best Practices for Reducing the Potential for Progressive Collapse in Buildings." *Draft*, National Institute of Standards and Technology.

O'Toole, B., Trabia, M. B., Thota, J., Wilcox, T., and Nakelswamy, K. K. (2006). "Structural response of blast loaded composite containment vessels." *SAMPE Journal*, 42(4), 6.

Osteraas, J. D. (2006). "Murrah building bombing revisited: A qualitative assessment of blast damage and collapse patterns." *Journal of Performance of Constructed Facilities*, 20(4), 330.

Oswald, C. J. "Prediction of injuries to building occupants from column failure and progressive collapse with the BICADS computer program." New York, NY, United States, 2065.

Park, R., Priestley, M. J. N., Gill, W. D. (1982). “Ductility of Square Confined

Concrete Columns." Journal of the Structural Division, ASCE, Vol. 108, No. ST4, 929-950.

PCI. (2004). "PCI's Architectural Precast Concrete Services Committee discusses items to consider in designing for blast resistance." PCI's Architectural Precast Concrete Services Committee.

PTI. (2001). "Recommendations for Stay Cable Design, Testing and Installation." Post-Tensioning Institute, Cable-Stayed Bridges Committee, Phoenix, Arizona.

Randers-Pehrson, G., and Bannister, K. A. (1997). "Airblast Loading Model for DYNA2D and DYNA3D." *Rept. ARL-TR-1310*, Army Research laboratory (publicly relearsed with unlimited distribuion).

Rankine, W. J. H. (1870). "On the Thermodynamic Theory of Waves of Finite Longitudinal Disturbance." *Phil. Trans. Roy. Soc.*, 160, 277-288.

Ray, J. C., Armstrong, B. J., and Slawson, T. R. (2003). "Airblast Enviornment Beneath a Bridge Overpass." *Transportation Research Record*, 1827, 63-68.

Rittenhouse, T., DiMaggio, P., and Ettouney, M. "Behavior of Steel Structures Subjected to Blast Loading." *Structures 2001 - A Structural Engineering Odyssey, Proceedings of the 2001 Structural Congress and Exposition*, Washington, D.C.

SAIC. (2006). "BlastX Version 6.4.2.2." Science Applications International Corporation, US Army Engineer Research and Development Center, Geotechnical and Structures laboratory and Air Force Research Laboratory, MNAL.

Salem, H. M., and Maekawa, K. (2004). "Pre- and postyield finite element method simulation of bond of ribbed reinforcing bars." *Journal of Structural Engineering*, 130(4), 671.

Sen, R., and Spillett, K. (1994). "Restraint Effect of Bearings - Phase I." *0510616*, Department of Civil Engineering and Mechanics, University of South Florida.

Shipe, J. A., and Carter, C. J. "Defensive design: Blast and progressive collapse resistance in steel buildings." Nashville, TN, United States, 1519.

Smilowitz, R. (2006a). "Fighting Terrorism Through Architecture." Seminar in the City College of New York, New York.

Smilowitz, R. (2006b). "Progressive collapse: Emerging challenges for the design professional." *Journal of Performance of Constructed Facilities*, 20(4), 307.

Smith, P. D., and Hetherington, J. G. (1994). *Blast and Ballistic Loading of Structures*, Butterworth Heinemann, Oxford.

Starossek, U. "Progressive Collapse of Bridges—Aspects of Analysis and Design." *Invited Lecture, International Symposium on Sea-Crossing Long-Span Bridges*, Mokpo, Korea.

Sun, M. (1998). "Numerical and Experimental Studies of Shock Wave Interaction with Bodies," Tohoku University.

Sunshine, D., Amini, A., and Swanson, M. "Overview of simplified methods and research for blast analysis." Nashville, TN, United States, 1479.

Symonds, P. S., and Mentel, T. J. (1958). "Impulsive loading of plastic beams with axial constraint." *J Mech Phys Solids*, 6, 186-202.

Timoshenko, S. (1962). *Elements of strength of materials*, D. Van Nostrand Company, INC.

TRB. (1977). "NCHRP Synthesis of Highway Practice 41: Bridge Bearings." *41*, American Association of State Highway and Transportation Officials in cooperation with the Federal Highway Administration, Washington, DC.

Tuler, F. R., and Butcher, B. M. (1968). "A Criterion for the Time Dependence of Dynamic Fracture." *The International Journal of Fracture Mechanics*, 4(4).

Turkmen, H. S., and Mecitoglu, Z. (1999). "Nonlinear Structural Response of Laminated Composite Plates Subjected to Blast Loading." *AIAA Journal*, 37(12), 1639.

TxDOT. (2002). "Literature Review and Work Plan, Executive Summary." *Project No. 0-4569, Phase I*, Texas Department of Transportation.

USAE Engineer Research & Development Center, G. S. L. (2005). "ConWep 2.1.0.8 - Application of TM 5-855-1." Vicksburg, MS.

USDOA. (1969). "Structures to Resist the Effects of Accidental Explosions." *Air Force Manual 88-22, Army Technical Manual 5-1300, and Navy Publication NAVFAC P-397*, Departments of the Air Force, Army, and Navy, Washington, DC.

USDOA. (1990). "Structures to Resist the Effects of Accidental Explosions." *Army Technical Manual 5-1300/Navy Publication NAVFAC P-397/Air Force Manual (AFM) 88-22 (TM 5-1300)*, U.S. Department of Army, Washington, D.C.

USDOA. (1992). "A Manual for the Prediction of Blast and Fragment Loading on Structures." *DOE/TIC-11268*, U.S. Department of the Army, U.S. Department of Energy., Washington, D.C.

USDOA. (1998). "Design and analysis of hardened structures to conventional weapons effects." *TM 5-855-1*, Headquarters, U.S. Department of the Army, Washington, DC.

Wallace, J. W. (1992). “BIAX, A Computer Program for the Analysis of Reinforced Concrete and Reinforced Masonry Sections.” Report No. CU/CEE-92/4, Department of Civil Engineering, Clarkson University, Potsdam, New York.

Wallace, J. W., and Ibrahim, Y. A. (1996). User’s manual for BIAX, “Strength analysis of reinforced concrete sections program.”

Wang, J. (2001). "Simulation of landmine explosion using LS-DYNA3D software: benchmark work of simulation of explosion in soil and air." *DSTO-TR-1168*, Weapons Systems Division, Aeronautical and Maritime Research Laboratory, Australia.

Warburton, G. B. (1976). *The dynamical behaviour of structures*, Pergamon Press, New York.

Williamson, E. B., and Marchand, K. A. "Recommendations for blast-resistant design and retrofit of typical highway bridges." St. Louis, MO, United States, 176.

Williamson, E. B., and Winget, D. G. (2005). "Risk management and design of

critical bridges for terrorist attacks." *Journal of Bridge Engineering*, 10(1), 96.

Winget, D. G., Marchand, K. A., and Williamson, E. B. (2005a). "Analysis and design of critical bridges subjected to blast loads." *Journal of Structural Engineering*, 131(8), 1243.

Winget, D. G., Williamson, E. B., Marchand, K. A., and Gannon, J. C. "Recommendations for blast design and retrofit of typical highway bridges." Boston, MA, United States, 1.

Wong, W. (2007). "Steel Bridge Blast Experiments of FHWA." Washington, D.C.

Yazdani, N., and Green, T. (2000). "Effects of boundary conditions on bridge performance." *WPI 0510843*, Tallahassee.

Yen, C. F. "Modeling of composite material behavior for blast and ballistic impact." Torino, Italy, 7.

Yi, Z., Agrawal, A. K., Ettouney, M., and Alampalli, S. "Finite Element Simulation of Blast Loads on Reinforced Concrete Structures using LS-DYNA." *2007 Structures Congress: New Horizons and Better Practices*, Long Beach, CA.

Zhang, X., Yang, X., Chen, Z., and Deng, G. (2006). "Explosion spalling of reinforced concrete slabs with contact detonations." *Qinghua Daxue Xuebao/Journal of Tsinghua University*, 46(6), 765.

Zukas, J. A. (1990). *High Velocity Impact Dynamics*, Wiley Interscience, New York.